CE-FBR-78-380
COO-2426-149

HOMOGENEOUS CARBIDE FUELED CORES FOR THE PROLIFERATION RESISTANT LMFBR CORE DESIGN STUDY

Prepared by

R. H. Klinetob
R. J. Calkins
M. R. Kulwich
V. Sehgal

COMBUSTION ENGINEERING
WINDSOR, CONNECTICUT

August 24, 1978

B

[redacted]

Table of Contents

Table of Contents (Cont.)

909 006

Table of Contents (Cont.)

Appendices

List of Figures

List of Figures (Cont.)

909 009

List of Tables

List of Tables (Cont.)

ABSTRACT

The performance of five, 1000 MWe, carbide-fueled, homogeneous core designs is presented. These designs fulfill various functions in a symbiotic, proliferation resistant, system of reactors. Three driver fuel types are included; U/Pu, U8/U3, and Th/Pu. The design of each core is based on limited parametric studies. A summary of these studies is presented. In addition, the economics of a symbiotic, proliferation resistant, system of reactors is presented.

1.0 Introduction and Summary

The Proliferation Resistant LMFBR Core Design Study (PRLCDS) was initiated to investigate various LMFBR fuel cycles which could be used in reactor systems resistant to nuclear weapons proliferation. Oxide, carbide and metal fuel types are included in the overall study as well as homogeneous and heterogeneous core configurations. Combustion Engineering carried out the carbide-fueled, homogeneous, core design effort.

1.1 Background

Nuclear weapons proliferation is of both national and international concern. In the first case, the problem is theft of fissile material (diversion) by subnational or radical groups. In the second case, the problem is a country with nuclear power plants, but no nuclear weapons, which can potentially divert the bred fissile material from power production to weapons production.

If present safeguards are not considered effective enough in preventing proliferation, then several alternatives are available. The denatured fuel cycle can be used in non-weapons countries. In denatured fuel, both the fertile and fissile components are isotopes of uranium and are not chemically separable. Fissile material in this form is not useable in a nuclear weapon if the U-233 concentration is less than 12%. Chemically separable fuel can be restricted to secure, internationally controlled, energy centers. The energy centers would include nuclear power plants as well as the fabrication and reprocessing facilities.

Another proliferation resistant fuel cycle is the "coprocessing" cycle. In this scheme, plutonium is never separated from uranium nor is there a capability to upgrade the plutonium concentration in the plutonium uranium mixture. Thus, weapons grade material is not normally produced in the fuel cycle; also the chemical reprocessing plant cannot be easily converted to produce weapons grade material.

1.2 Reactor Types and Objectives

Three general reactor types were studied by all the participants of the study. They are:

1. Reference - conventional uranium/plutonium fuel cycles
2. Denatured - U-238/U-233 fuel, various fertile materials
3. Transmuter - U-233 producer, plutonium burner

Reference fuel is included as a point of comparison for the other fuels. With thorium blankets, the Reference reactor can be used to breed U-233 within an energy center. The goals set for the homogeneous, carbide-fueled, Reference design are low cost and doubling time.

Denatured fuel is being studied to determine its effectiveness for use in LMFBR's located in non-weapons countries. To be an attractive system, the denatured LMFBR should compete economically with denatured light water reactors (LWR's) operating as U-233 burners. The homogeneous, carbide-fueled, Denatured design is optimized for low specific inventory and fuel cycle cost. In addition, the maximum fissile enrichment is held to less than 12%.

The Transmuter is being studied as a source of U-233. The fuel is chemically separable and must be used within an energy center. The Transmuter design must, therefore, compete with the Reference design with thorium blankets as an economic source of U-233. The homgeneous, carbide-fueled, Transmuter design is chosen to operate in the optimum range of cost and doubling time.

In addition to developing regular reactor designs using these three fuels, Combustion Engineering also investigated a fourth class of reactor, the Coprocessing concept. These reactors are designed to be used in conjunction with the reprocessing procedure, discussed previously in which fissile material is not separated. The core of these reactors is designed so that is produces at least enough fissile material to make up for decay and processing (fabrication and reprocessing) losses. This technique is called "self-regeneration". No fissile upgrading is required during reprocessing, but fertile material may be added for dilution. Fuel for a Coprocessing design can be either U/Pu or a combination of U/Pu and Th/U. Two reactor design variations are included in this study. One is optimized for low cost and fissile inventory. The other is optimized for low sodium void worth. A large spectrum of possibilities exists with the Coprocessing concept. Only two designs are presented because of time constraints. The low cost design uses U/Pu fuel only. The low void worth design uses both U/Pu and Th-232/U-233 fuel.

1.3 Design Choices

A limited parametric study of the design options shown in Table 1.1 was made of the Coprocessing, Denatured and Transmuter cores. The results of this study were used to select the final core designs in conjunction with three other criteria. They are:

1. Sodium void effect as low as possible and under $3.00 where attainable.

2. Assembly designs for all fuels would fit in the same reactor (convertibility).

3. The assemblies could operate with 316SS with their lifetimes reduced to two years.

1.3.1 Sodium Void Worth

Design parameters for all cores, except the Reference, were chosen to minimize sodium void worth. Direction given at the

Table 1.1

Design Parameters Studied for Coprocessing,

Denatured and Transmuter Concepts

Parameter	Coprocessing Low Cost	Coprocessing Low Void	Denatured	Transmuter
Pin Diameter	X		X	X
Core Height	X		X	
Fuel Life	X		X	
Sodium Void Worth		X		
Fissile Enrichment	X	X	X	
Reflector Replacing Blankets	X		X	
Fuel Shuffling	X			
Fuel Shims	X			

start of the study indicated that sodium void effect should not be considered in the design of the homogeneous Reference core. A target of \$3.00, given in the Ground Rules, was used for the other reactors.

A change in either the fertile or fissile isotope reduces the positive effect on reactivity of spectrum hardening. Spectrum hardening causes large increases in fertile fissions in U-238 due to the increase in the number of neutrons with energies above the high energy threshold for U-238 fission. It also causes an increase in the effect on reactivity of Pu-239 due to the sharp increase in neutrons per fission at high energies. The high energy threshold effect is not nearly as pronounced in Th-232 as in U-238. Also, the increase in neutrons per fission at high energies is much less in U-233 than in Pu-239. Substitution of either of these isotopes in a reactor (U-233 in the Denatured design and Th-232 in the Transmuter) reduces the sodium void effect below the \$3.00 limit. No further design changes are necessary in those two reactors. Th/U assemblies are included in the high worth regions of the low void worth Coprocessing design, with the result that sodium void worth in that reactor is reduced below \$3.00.

1.3.2 Pin Diameter

The pin diameter was varied for the Denatured, Transmuter and Coprocessing fuels in a parametric study to determine its effect on fuel cycle cost, doubling time, fissile inventory and enrichment. The pin diameter for the Reference design, 0.370" O.D., was selected based on previous studies[2,3,4].

The optimum fuel cycle cost for all fuels studied occurs in the range of 0.35" to 0.39" O.D. The doubling time minimizes beyond 0.470" O.D., but changes very little from 0.35" to 0.47" O.D. The largest pin diameter studied is 0.47" O.D. Designs with larger pin diameters show very little increase in fuel volume fraction. This phenomenon is discussed further in Section 4.0.

A 0.35" O.D. pin diameter was chosen for the Denatured design. It allows the lowest inventory for a design with a maximum fissile enrichment of less than 12%. A low inventory is required for a Denatured LMFBR to successfully compete against a Denatured LWR.

A 0.37" O.D. pin diameter was chosen for the Transmuter design as it has a minimum fuel cycle cost and a doubling time in the minimum range. The 0.37" O.D. pin diameter was also chosen for the low cost Coprocessing design for the same reason. In addition, it has only a small inventory penalty (7%), compared to the low inventory Coprocessing design (0.30" O.D.). A 0.30" pin diameter design requires a single enrichment zone and has excessively high radial peaking.

A 0.47" O.D. pin was chosen for the low sodium void worth Coprocessing design to maximize the number of Th/U assemblies in the core and thereby minimize sodium void worth. There is a maximum enrichment for each fuel type below which self-regeneration does not occur. The value is about 9.9% for U/Pu fuel and about 9.5% for Th/U fuel. The large pin diameter design requires the lowest average enrichment for criticality and therefore allows the largest number of Th/U assemblies.

1.3.3 Core Height

Results of the parametric study do not show a significant difference in performance between designs with core heights at 3' and 4'. This is due to the high sodium velocity (35 ft/sec). and large bundle pressure drop (90 psi) allowed by the Ground Rules. Parametric studies with oxide fuel do show that taller cores have better performance. To make these designs interchangable with oxide designs, a 42" core height was chosen for the Reference, Transmuter and Denatured design to match the height used in the Prototype Large Breeder Reactor (PLBR) studies[5]. A core height for the Coprocessing designs of 3' was chosen to help reduce the sodium void effect.

1.3.4 Fuel Residence Time

The fuel residence time for all five designs is based on duct/bundle interaction (DBI) limits. Preliminary studies of fuel pin stress histories were done by W-ARD[6]. They indicate that the sodium-bonded, carbide-fueled pins are not lifetime limiting at the temperatures and fluences found in this study. Helium-bonded pin designs are not included due to schedule limitations. (A discussion of performance of core designs using helium bonded pins is given in Section 4.0).

The lifetimes for all designs are based on the advanced alloy suggested by the Ground Rules. The fuel pin pitch/diameter (P/D) ratio (which dictates lifetime in a DBI limited design) was established for the Reference, Denatured and Transmuter designs, based on the performance of 316SS (1st core nominal properties) assuming a 2 year residence time. The lifetimes for the two Coprocessing designs were restricted to low burnups to achieve high smear density. The smallest allowable fuel pin P/D allowable under the Ground Rules (based on hydraulic considerations) was used in both designs.

1.3.5 Axial and Radial Blankets

The blanket material used in the Reference design is depleted UC. The blanket material used for all other designs is ThC. Due to a 25% lower density in ThC compared to UC, the thickness of the axial blankets with ThC is increased 25% from a

909 019

standard 14" to 18". The radial blanket thicknesses are increased from a standard 2 rows to 3 rows. The blanket thicknesses in the Reference design are the same for consistency.

1.4 Summary Final Design Description

The five final reactor designs, summarized in Table 1.2, are in the 1000 MWe class. They are designed using carbide fuel in a homogeneous configuration. With the exception of the Coprocessing design, they all have two driver enrichment zones to provide a flat radial flux. A flat flux is achieved in that design by evenly distributing the Th/U driver assemblies within the inner two-thirds of the core. The Th/U fuel has a depressing effect on the flux similar to that of internal blankets. Core layouts for the five designs are given in Appendix C.

1.4.1 Discussion of Design

The core volume is similar for the Reference, Denatured and Transmuter designs because they all have similar reactor powers, linear powers and pin diameters. To produce the same power as the other designs, the two Coprocessing designs require larger core sizes to allow the low enrichments required for self-regeneration. As discussed above, the core height for these two designs is shorter than that of the other designs to achieve a low sodium void worth.

The fuel residence times and assembly designs are based on preliminary physics results. The variation in residence time among the five designs is dependent on the fuel pin P/D ratio. This occurs because the lifetimes are limited by duct/bundle interaction constraints. The variation in fuel pin P/D ratio is caused by the various design requirements described previously and also on the preliminary flux estimates.

The number of pins/assembly and duct wall thicknesses were chosen to obtain similar lattice pitches for all designs. With small adjustments in the pin diameter, all the assembly designs are interchangeable in the same reactor.

The pin diameters were chosen based on the parametric studies described in Section 3.0. The cladding thicknesses were chosen based on the thickness/diameter ratio (0.015/0.370) specified in Reference 7. Only one bond type was studied due to time constraints. Helium bonded design performance is discussed further in Section 4.0. The smear density was calculated based on a 2.7% $\Delta V/V/(MWD/kg)$ swelling rate and the design lifetime for each design.

1.4.2 Discussion of Performance

The performance of the five designs summarized in Table 1.2 is based on detailed neutronic and thermal calculations. Detailed thermal, hydraulic and mechanical results and calculational methods are discussed further in Sections 6.0 and 7.0. Neutronic results and methods are discussed further in Section 5.0.

The linear powers of all five designs were held to within 5% of the design peak of 125 kW/m (38 kW/ft, 3σ + 15% O.P.). The low cost Coprocessing design linear power exceeds the limit slightly and will be reduced in future iterations.

The 2σ cladding midwall temperatures at end of life are below the maximum set for carbide fuel of $677^{o}C$ ($1250^{o}F$). The designs are orificed for equal end of life 2σ cladding mid-wall temperatures.

The breakdown of fissile inventory by isotope chain shows the diversity in the combinations of fuel used for the various designs. The fissile inventory is important in

909 021

Table 1.2

Summary Core Design Description

	Reference		Coprocessing		Denatured	Transmuter
	UC Blankets	ThC Blankets	Low Void	Low Cost		
General						
Reactor Power, MWt	3000	2850	3000	2740	2880	3000
Core Volume, 10^3 L	11.1		14.4	11.1	11.2	11.6
Core Height, cm	106.7		91.4	91.4	106.7	106.7
Fuel Residence Time, yrs	2.4		3.0	2.2	2.9	2.7
Driver Assembly						
Pins/Assembly	169		127	169	169	169
Pin Pitch/Diameter Ratio	1.20		1.11	1.17	1.24	1.24
Lattice Pitch, cm	16.51		16.58	16.21	16.21	17.09
Duct Wall Thickness, mm	3.81		3.56	3.81	3.81	4.06
Pin Diameter, mm	9.40		11.94	9.40	8.89	9.40
Cladding Thickness, mm	0.38		0.48	0.38	0.36	0.38
Bond Type	sodium		sodium	sodium	sodium	sodium
Smear Density, % T.D.	77		87	83	78	78
Performance						
Peak Linear Power (3σ + 15% OP), kW/m	120	----	124	130	126	123
Peak Cladding Temperature, EOL (2σ midwall), ^oC	658	----	668	----	637	663
Fissile Inventory (BOEC, kg)						
U_{fiss}	----	271	1840	294	2556	915
Pu_{fiss}	3155	2764	2843	2949	434	2721
Total	3155	3035	4683	3243	2990	3636
Fissile Production/Destruction, kg/yr						
U_{fiss}	----	304	276	267	-248	693
Pu_{fiss}	321	-20	11	43	398	-576
Total	321	284	287	310	150	117
Fuel Cycle Cost, mills/kWh	7.5	8.3	12.1	9.6	8.4	11.3
Symbiotic System Doubling Time, yrs	----	13.2	----	14	16	25
Sodium Void Worth (EOEC), $	5.02	----	2.00	4.63	0.67	1.35

determining both the doubling time and the fuel cycle cost of a reactor. It also dictates how fast a closed system of reactors can grow if it is short of fissile material. The Reference design requires the largest plutonium fissile inventory, while the Denatured design requires the largest uranium fissile inventory. The low void worth Coprocessing design requires the largest total fissile inventory due to its large size and large heavy metal mass. The Denatured design has the lowest total fissile inventory due to the large amount of high worth U-233 (relative to Pu-239) in the core. The Transmuter has a large fissile inventory compared to the Reference design due to the large leakage allowed by the low density thorium fuel and its low fission rate.

The fissile gain is a good indicator of the breeding performance of these designs. It is important in determining the doubling time and fuel cycle cost. The Denatured design has the largest plutonium gain, while the Transmuter has the largest uranium gain. The small plutonium fissile gain in the low void worth Coprocessing design is just sufficient to make up decay and process losses. The gain in the low cost Coprocessing design is large enough to cause some doubling. If the pin diameter or core size were increased sufficiently in that design, core doubling times of 30 to 40 years could be obtained.

The Reference design has the largest total fissile gain. The low cost Coprocessing design has a smaller total gain due, primarily, to its 10% smaller power output. The Transmuter design has the smallest gain because of the poor breeding performance of thorium in the reactor core. Thorium in the radial and axial blankets does not cause a significant loss of breeding. This is illustrated by a comparison of the low cost Coprocessing and Reference designs.

The total power cost of a reactor is made up primarily of capital and fuel cycle costs. In this study, the capital costs of the designs are essentially equal so that fuel cycle cost is a good indicator of the relative costs. Fuel cycle cost is dependent on assembly design, heavy metal mass, linear power, fissile inventory, residence time and fissile gain.

The Reference and Denatured designs have the lowest fuel cycle cost. The fact that the cost of the Denatured design is as low as that for the Reference design is due to its depleting U-233; a lower priced fissile isotope relative to Pu-239. The cost of the Denatured design as well as the costs of the Coprocessing and Transmuter designs would be lower if UC blankets were used due to the difference in fissile values.

The low cost Coprocessing design has a 28% larger fuel cycle cost than the Reference design. The difference is due, in part, to the ThC blankets and, in part, to the higher fabrication cost caused by the larger number of assemblies required to produce the same power. The low void worth Coprocessing design has a 61% higher cost than the Reference design. The larger fissile inventory and lower fissile gain account for a large part of the difference. The increased number of assemblies and larger fabrication cost of the Th/U assemblies account for the remainder of the difference. The Transmuter design has a 51% higher cost than the Reference design. The primary reasons for the high cost are the combination of low fissile gain and depleting a high priced fissile isotope and replacing it with a lower priced isotope.

The symbiotic system doubling time (SSDT) is a measure of how fast a system of symbiotic reactors can grow. The partner reactors are specified by the Ground Rules. The SSDT is dependent on residence time, fissile inventory and fissile gain. Fissile losses and out of reactor times, which also affect the SSDT, are fixed for this study. The SSDT is not calculated for the Reference design with UC blankets because the design is not intended for a symbiotic system. If thorium fuel is used as blanket material, the SSDT for the Reference design is 13 years. The SSDT is slightly higher in the low cost Coprocessing design due to a shorter residence time and somewhat larger fissile mass. The Denatured design shows only a small increase in SSDT even with much poorer breeding performance and a higher inventory.

It is clear that the growth rate would be much lower in a symbiotic system containing Transmuters compared to one containing either Reference cores with thorium blankets or low cost Coprocessing designs. Also, the cost of the system using Transmuters would be much larger compared to one using the Reference design with thorium blankets.

The sodium void worth of a reactor is important in determining its response during a core disruptive accident. A previous study[8] has indicated that designs with sodium void worths under $3.00 may have some licensing advantages. The Reference design has a large positive sodium void worth due to the presence of both U-238 and Pu-239. The low cost Coprocessing design also has a large positive sodium void worth. It is slightly lower than the Reference design due to the reduced core height.

The Denatured and Transmuter designs both have sodium void worths below $3.00. The result is due to replacing Pu-239 with U-233 in the Denatured design and U-238 with Th-232 in the Transmuter design, as described in Section 1.3. In addition, in the Transmuter design, the mass of heavy metal is about 25% lower than that in the Reference design thereby enhancing the impact of switching the Th-232.

1.5 Conclusions

A. The Reference U/Pu design developed in this study has performance similar to the design previously developed as discussed in Section 2.0. Notable differences in design are a 13% larger linear power, 17% smaller reactor power and a 20% longer fuel residence time. The effect of these differences, plus those of control rod modeling, is competing and results in a negligible net change in doubling time performance.

B. The concept of a core which does not require fissile replenishment during reprocessing (coprocessing) is practical in homogeneous carbide designs. Designs have been developed in which compound system doubling times in the core are less than 40 years. A variety of possibilities exist for Coprocessing designs. Two were developed in this study: a low cost version and a low sodium void worth version. In addition to being proliferation resistant, these designs are good producers of U-233.

C. The performance of four U-233 producing concepts was investigated. The Reference design with Th blankets, the low void Coprocessing and the low cost Coprocessing designs consume less than 20 kg/yr of plutonium. The net fissile gains of these designs are capable of supporting a growing FBR/LWR symbiotic system.

The Transmuter net fissile gain is only 117 kg/yr while it consumes 574 kg/yr of plutonium. It can only support system growth when used in conjunction with a Denatured FBR which has a large plutonium gain.

D. The uranium carbide fueled "Denatured" FBR has quite low fuel cycle costs and consequently, might compete economically with Denatured LWR's provided FBR/LWR capital cost differentials are not large. The FBR fueled with U-233, however, is no match for the LWR with U-233 so far as fissile inventory is concerned.

E. The economics of certain proliferation resistant fuel cycles compare favorably with all plutonium fuel cucles. Specifically, the calculated power cost of an equilibrium U-233/plutonium economy using Transmuter FBR's and Denatured LWR's is equal to or less than the power cost from an equilibrium all plutonium economy using conventional FBR's and LWR's.

F. The 1000 MWe power specified in the Ground Rules does not allow for optimum performance of the Denatured and Coprocessing concepts. This is primarily due to the limits on fissile enrichment for those designs.

The Ground Rules specify a 12% maximum enrichment for the Denatured design. The Coprocessing design is limited to a 9.9% enrichment for self-regeneration. To attain these enrichments, large fissile inventories are required, hence large system specific inventories. Both concepts would have much smaller system specific inventories and better performance in reactors with larger (1500 MWe to 2000 MWe) reactor power.

2.0 Study Approach and Ground Rules

2.1 Study Approach

The study was done in two phases. In the first phase, parametric evaluations of design options were done. The effects of the design options on sodium void effect, fuel cycle cost, fissile inventory and doubling time were established. Also, a generic study of the Coprocessing reactor concept was done. The basic requirements of self-regeneration were evaluated along with some solutions to problems unique to Coprocessing designs. The core designs were identified which best fulfill the design objectives of the five final designs.

In the second phase of the work, assembly and core designs for the five reactors were completed. Detailed neutronics, economics, thermal, hydraulic and mechanical calculations were done to establish the performance characteristics of the designs. Additionally, a side study was done to assess the economics of an international symbiotic system of reactors. The cost of a reference LWR/LMFBR system was compared to that of a denatured LWR/transmuter LMFBR system of comparable power output. A summary of the results is presented in Section 8.0. A detailed report is published under separate cover[10].

Due to time constraints, the study is limited to sodium bonded fuel. For similar assembly designs, helium bonded carbide fuel has slightly poorer performance characteristics. In this study, however, the sodium bonded fuel is designed somewhat more conservatively than allowed by the Ground Rules. For comparison, a 0.370" O.D. pin, helium bonded assembly was designed using the 82% smear density and 0.020" thick cladding allowed by the Ground Rules. The result is a core heavy metal mass which is nearly identical to that calculated for the sodium bonded carbide fuel. Therefore, the neutronic results reported here are quite representative of both helium bonded and sodium bonded carbide fuel. However, the pin designs for which this is true are not equally agressive.

Also due to time constraints, a fuel pin lifetime stress analysis was not done for any of the final designs. An analysis was done by W-ARD[6], based on preliminary data. It indicates that sodium bonded carbide fuel with 2σ midwall temperatures under $677^{o}C$ ($1250^{o}F$) at end of life has low cladding damage. Also, helium bonded carbide fuel does have execessive cladding damage above $649^{o}C$ ($1200^{o}F$) for the same fluence. End if life cladding temperatures for the five final designs lie between $649^{o}C$ and $677^{o}C$. The lifetimes used in this study for sodium-bonded carbide designs should not be limited by cladding damage. Helium bonded carbide designs would require either shorter lifetimes or a slightly different pin design.

2.2 Study Ground Rules

Ground Rules were established for the study to ensure that all designs are developed in a consistent manner and that the final designs are comparable. A summary of the Ground Rules for carbide fuel is given in Table 2.1. They are based on Ground Rules used for the Large Heterogeneous Reference Fuel Design Study (LHRFDS)[11]. The primary differences are slightly more agressive assumptions regarding duct and cladding structural performance, a 25% smaller core size and more flexibility regarding fuel pin design. Also, economic parameters are updated and result in much larger fuel cycle costs.

Oxide, carbide and metal fuel in both homogeneous and heterogeneous configurations all have a Reference design. There are some differences between previous homogeneous carbide designs developed by Combustion Engineering and that done for this study. A comparison of the previous Reference and the current PRLCDS design is shown in Table 2.2.

Table 2.1

Summary of PRLCDS Ground Rules for Carbide Fuel

General Parameters	
Reactor Power, MWe	1000
Thermal Efficiency, %	36.5
Reactor Inlet Temperature, °F	650
Reactor Temperature Rise, °F	280
Plant Capacity Factor	70%
Cladding and Duct Material	advanced alloy similar to D9
Fuel Assembly Parameters	
Minimum Cladding Thickness, mils	12
Minimum Cladding Thickness/diameter ratio*	
Sodium bonded carbide	0.15/0.370
Helium Bonded carbide	0.20/0.370
Maximum Peak Linear Power (3σ + 15% O.P.) kW/ft*	38
Maximum Nominal Assembly Outlet Temp., °F	1075
Smear Density, % T.D.	82
Maximum 2σ Peak Cladding* Midwall Temperature, °F	1250
Flow Parameters	
Hot Channel Factors	slightly modified CRBR
Maximum Pin Bundle Coolant Velocity, ft/sec	35
Maximum Pin Bundle Pressure Drop, psi	90
Bypass Flow, %	5
Limiting Conditions	
Fuel Pin Limit, CDF	0.75
Maximum Duct-Duct Interaction	0
Maximum Duct Wall Stress	$0.55\sigma_{allowable}$
Duct-Bundle Interaction, Wire Wraps 169 and 127 Pin Bundles	4
Other Parameters	
Cross Section Set	ENDF/B-IV
Fission Gas Release, %	
Helium Bonded Carbide	60
Sodium Bonded Carbide	40

909 030

Table 2.1 (Continued)

Other Parameters (Continued)	
Fission Energy, MeV/fission	207
Minimum k_{eff} Over Equilibrium Cycle	1.000
Control	CRBR Volume Fractions
Control Enrichment, % B_{10}	92
Economics Parameters	
Out of Reactor Time, yrs.	
Pu Fissile	1.0
U Fissile	1.33
Combined Process Losses, %	1.0
Inflation, %	0
Cost of Money	7.5%
Reprocessing Costs (Including Shipping & Waste Disposal), $/kg_{HM}$	523
Fissile Value, $/gm	
Pu	100
U	80

Table 2.2

Differences Between Previous C-E Reference Design
and Current PRLCDS Reference Design

	Previous Reference Design	PRLCDS Reference Design
Peak Linear Power (3 +15% O.P.), kW/ft	33.5	38
Core Height, in.	36	42
Residence Time, full power days	511	621
Reactor Power, MWt	3333 1200	3000 1095
Control Rod Modeling	empty channel	inserted to core/blanket interface
Structural Material	316SS (core/nominal properties)	adv. alloy (similar to D-9)
Radial Blanket Height, in	48	78
Reactor Breeding Ratio (MOEC)	1.48	1.42
Peak Fast Flux (E>0.1 MeV), 10^{15} n/cm^2/sec)	4.2	4.9
Fissile Gain, kg/yr	387	320
Driver Fissile Inventory	3372	2709
Compound System Doubling Time, years	9.8	9.7
Peak 2σ Cladding Midwall Temperature (Inner Zone), ^{o}F	1222	1216

909 032

It should be noted that peak linear power, core height, and residence time have all been increased. Total reactor power has been decreased by 9%. Also, an important difference is the treatment of control rods. The burnup calculations have been modeled with the rods parked at the core/axial blanket interface. The breeding is thereby reduced significantly. The doubling times, however, are very similar because of the lower fissile inventory and longer fuel residence time.

3.0 Design Optimization

Design options were studied parametrically in the initial stages of this study to determine their impact on fuel cycle cost, doubling time and fissile inventory. Denatured, Coprocessing and Transmuter designs were studied. Extensive work has been done previously for the Reference core and was used to establish the Reference design.(2,3,4) The design parameters studied are shown in Table 1.1.

A fuel assembly design was established for each design option based on preliminary neutronic calculations. A single option was varied with each new design. One dimensional neutronic calculations were used to investigate the burnup behavior of the fuel. Limited two-dimensional static calculations were used to approximate axial and corner blanket performance.

A summary of the results for each variation is given below. A detailed discussion of the methods and results is given in Appendix A and in other reports.(12,13,14)

3.1 Enrichment

The variation of enrichment with core design was studied for the Coprocessing and Denatured concepts. The objective for the Denatured concept was to establish the design with a maximum enrichment of 12%. For the Coprocessing designs, the objective is to establish the maximum enrichment that allowed self-regeneration (gains equal to losses).

The variation of the outer zone fissile enrichment with pin diameter is shown in Figure 3.1 for the Denatured concept. The designs all have a smear density of 82% and an inner zone/outer zone volume split of 54%/46%. (Maximum enrichment can be varied independently of pin diameter by varying either of these two parameters.) Based on these assumptions, a pin diameter of 0.35" O.D. is the smallest with a maximum enrichment of 12%. For the lower smear density,

FIGURE 3.1

Variation of Outer Zone Fissile Enrichment

and System Specific Inventory

with Pin Diameter for the Denatured Concept

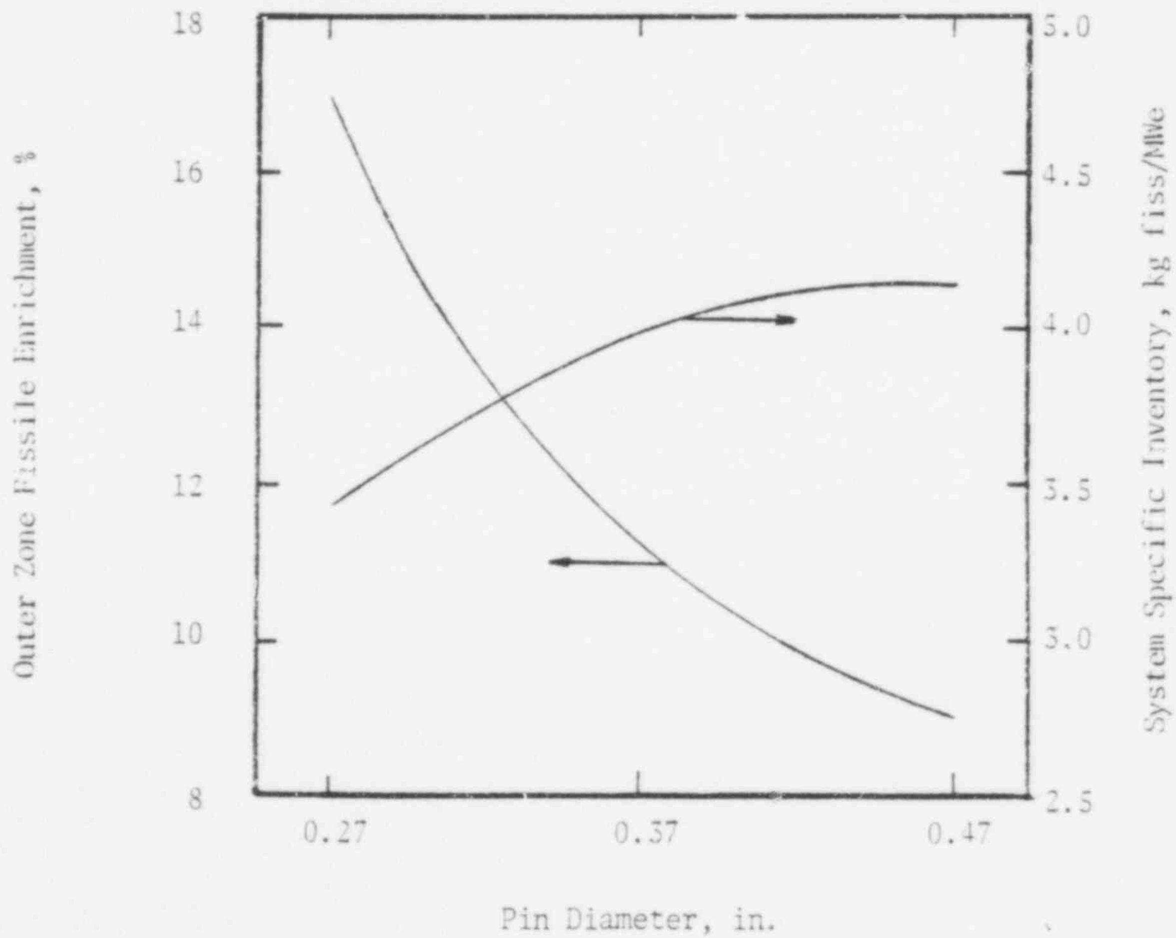

909 035

required in the final design, the same pin diameter is maintained by decreasing the size of the inner enrichment zone.

Self-regeneration in a Coprocessing design is a function of enrichment, conversion ratio and heavy metal mass. There is a minimum conversion ratio which will support self-regeneration. Conversion ratio is inversely proportional to enrichment, so there is a maximum enrichment that will support self-regeneration. Furthermore, enrichment decreases with increasing heavy metal mass so that a maximum heavy metal mass can be established which still supports self-regeneration. Based on a maximum enrichment of 9.9% for U/Pu fuel, the minimum pin diameter (for 82% smear density) which has sufficient heavy metal mass to support self-regeneration is 0.30 O.D.. This design can have only one enrichment zone and, therefore, has excessive radial peaking. The maximum enrichment, 9.5%, for self-regeneration is also determined for Th/U fuel.

3.2 Pin Diameter

The effect of pin diameter on design performance was studied for the Denatured, Coprocessing and Transmuter concepts. The pin diameter for the Reference design was chosen based on previous parametric studies.

Pin diameters vary from 0.27" O.D. to 0.47" O.D. for the Denatured and Transmuter concepts and from 0.30" O.D. to 0.47" O.D. for the Coprocessing concept. The largest pin diameter of interest in this study is 0.47" O.D.. For larger diameters, the fuel pin pitch/diameter ratio approaches 1.05. This value is established as the limit in an assembly at end of life to prevent hot spots. If the pin pitch/diameter ratio is fixed, very little increase in fuel volume fraction and, therefore, breeding, can be obtained.

The variation of fuel cycle cost and system specific power with pin diameter for the Coprocessing concept is shown in Figure 3.2. The minimum fuel cycle cost occurs in the range of 0.36" to 0.40".

FIGURE 3.2

Variation of System Specific Inventory and Normalized Fuel Cycle Cost with Pin Diameter for the Low Cost Coprocessing Design

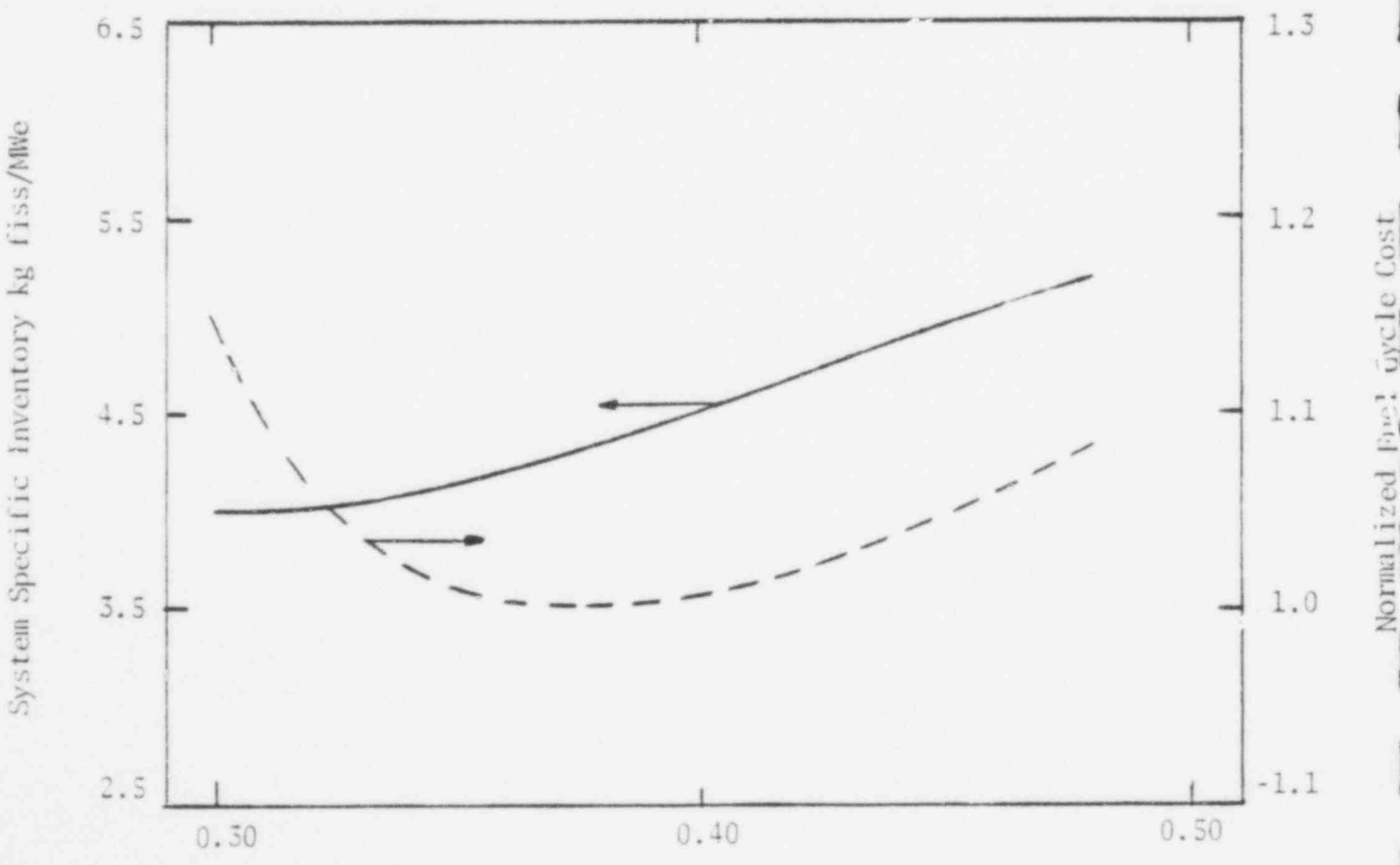

909 037

The minimum inventory occurs at 0.3". A pin diameter of 0.37" O.D. was chosen for the low cost design. It has the minimum cost and only an 8% penalty in inventory compared to the low inventory design. Additionally, the radial power peaking is much lower than that in the low inventory design. A pin diameter of 0.47" O.D. was chosen for the low sodium void worth design. It allows the lowest enrichment of the designs studied and, therefore, the largest number of Th/U assemblies. As discussed above, the Th/U fuel has a lower self-regenerating enrichment than does the Pu/U fuel and also a lower sodium void worth. The lower the critical enrichment of a design, the more Th/U assemblies at their self-regenerating enrichment, can be inserted. This will result in a lower sodium void worth for the design. The low void worth design is self-regenerating in both the U/Pu and Th/U fuel.

The choice of pin diameter for the Denatured design is based on several factors. The design should be competitive with denatured LWR reactors. It must have a fissile enrichment less than 12% and it should have a fuel cycle cost and doubling time near the minimum range.

The 0.35" O.D. pin diameter design is shown above as having the smallest pin diameter (and, therefore, lowest inventory) with a fissile enrichment below 12%. The variation of fuel cycle cost and symbiotic system doubling time with pin diameter is shown in Figure 3.3. The 0.35" design falls within the optimum cost range and has a doubling time only slightly above the minimum.

The components of the power costs are compared for a denatured LWR and three carbide fueled Denatured LMFBRs in Table 3.1. The description of the Denatured LWR is taken from Reference 15. The three LMFBR designs all have lower fabrication and reprocessing costs than the LWR. The LWR has lower capital and operating costs. The total power costs, without fissile credit or inventory costs included, are nearly equal for the LWR and carbide LMFBRs. Because of much larger fissile gains, the LMFBR power costs, including fissile credit, should be lower

FIGURE 3.3

Variation of Symbiotic System Doubling Time and Normalized Fuel Cycle Cost with Pin Diameter for the Denatured Concept

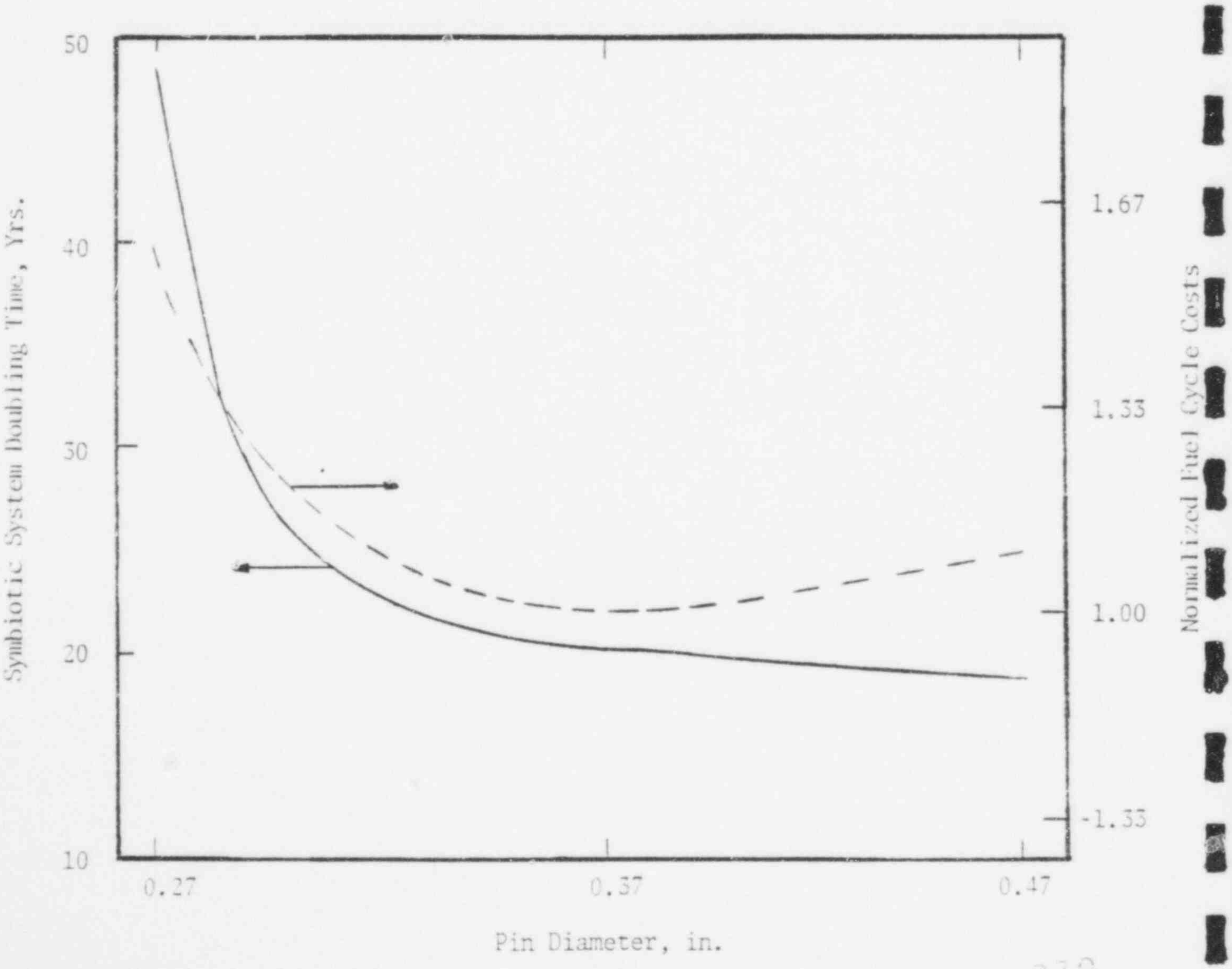

909 039

Table 3.1

Comparison of System Power and Power Cost (Less Fissile)

Between Denatured LWR and LMFBR Designs

	LWR	CARBIDE	LMFBR	
Pin O.D., in.	0.374	0.300	0.350*	0.370
Reactor Power, MWe	1300	1200	1200	1200
Normalized Fabrication and Reprocessing Cost	1.0	-1.37	----	-1.5
Capital and Operating Cost, mills/kWhe	8.6	10.9	----	10.9
Total Power Cost (less fissile), mills/kWhe	12.1	13.1	----	12.6

* Final Design Choice.

(independent of the fissile value used) than those of the denatured LWR. This holds assuming the system fissile inventories are nearly equal.

The system inventory of a System 80(TM) Denatured LWR design[16] has a much lower system inventory than the Denatured LMFBRs studied, 2.5 kg_{fiss}/MWe compared to 3.9 kg_{fiss}/MWe. The lower system inventory is very difficult to achieve in a 1000 MWe Denatured LMFBR with a 12% maximum enrichment. The reason is a much higher worth of U-233 in a thermal spectrum than in a fast spectrum. A system inventory within about 10% to 15% of that of the System 80(TM) design could be achieved with a design operating at 1500 MWe. The Denatured LMFBR design would also require advanced alloys for a long residence and an out of reactor time that is at least one half that used for the System 80(TM) design.

Pin diameter was also varied for the Transmuter concept to determine its optimum in terms of fuel cycle cost and symbiotic system doubling time (Figure 3.4). The minimum fuel cycle cost falls within the range of 0.35" to 0.39". The minimum doubling time occurs with the 0.47" design. The doubling time does not vary much for pin diameters greater than 0.37" O.D.. The 0.37" O.D. design is chosen for minimum cost and low doubling time.

3.3 Residence Time

Several cases with high fluence were studied to determine the effect of fuel residence time on fuel cycle cost and symbiotic system doubling time. The base cases in the parameteric study are designed to a fluence (E > 0.1 MeV) of 2.0×10^{23} n/cm^2. As shown in Table 3.2, both cost and doubling time decrease (16% and 8%, respectively) up to a fluence of 2.6×10^{23} n/cm^2 for the Denatured design. The varation is less pronounced for the larger pin diameter Coprocessing design. Based on these results, the residence time of the Reference, Denatured and Transmuter designs are extented to the limit allowed by duct/bundle interaction. The

FIGURE 3.4

Variation of Symbiotic System Doubling Time and Normalized Fuel Cycle Cost with Pin Diameter for the Transmuter Concept

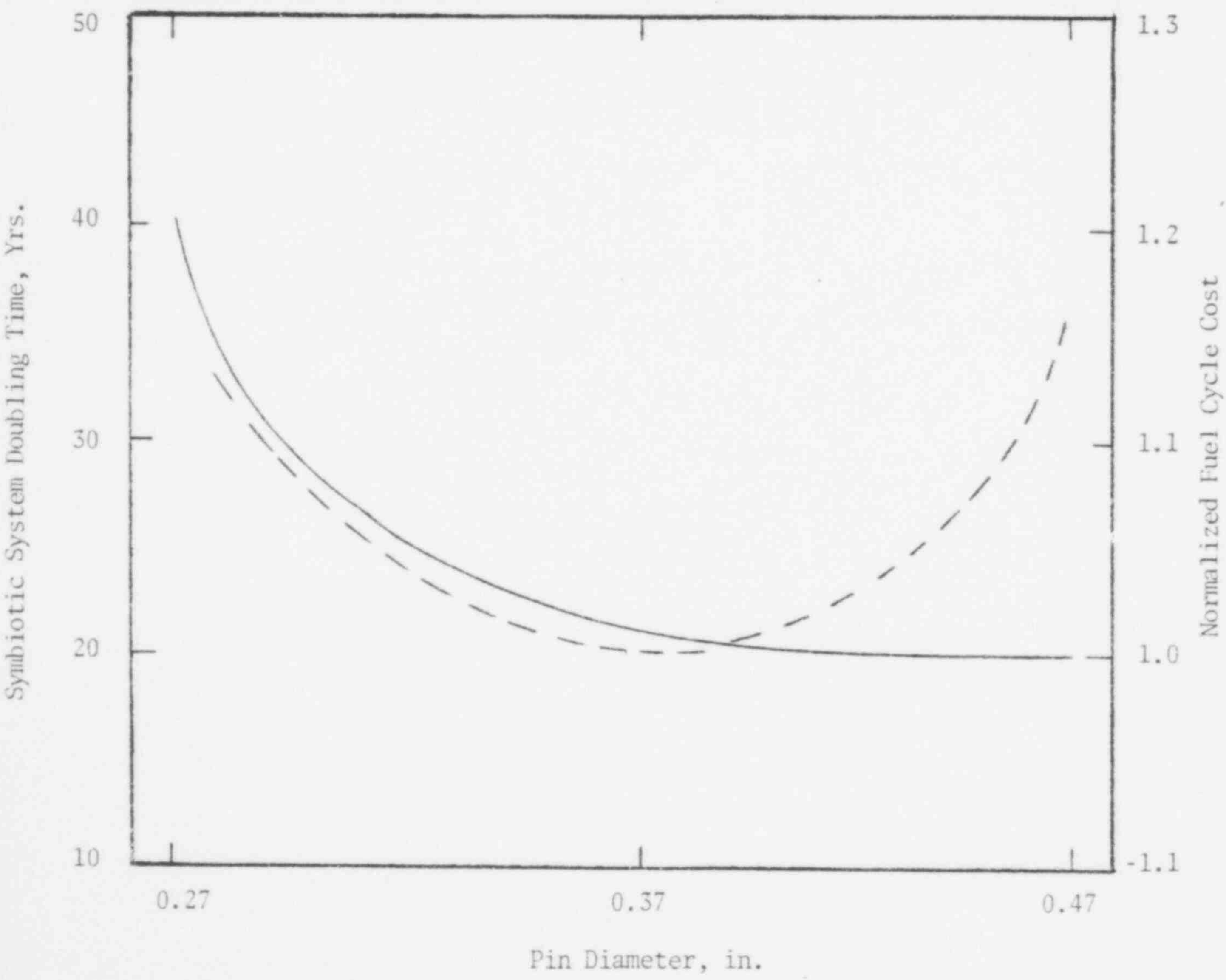

909 042

Table 3.2

Parametric Variations

	Normalized Fuel Cycle Cost	Specific Inventory kg_{fiss}/MWe	Symbiotic System Doubling Time
Denatured Concept			
Base Case			
0.37" O.D. pin 3' core height			
1.9×10^{23} n/cm^2 fluence			
ThC blankets	1.00	2.5	20.1
Height variation, 4'	-1.03	2.5	19.8
Lifetime variation fluence, 2.6	-1.16	2.4	18.6
($\times 10^{23}$ nvt) 3.1	-1.09	2.5	18.8
Reflector	+1.41	2.5	176
Coprocessing Concept			
Base Case (0.47' O.D., 3' core Height, 2.0×10^{23} nvt fluence)	1.00	3.9	12.0
Height, 4'	1.00	3.9	12.1
Lifetime (2.4×10^{23} nvt)	-1.02	3.9	11.7
Low void worth	+1.23	5.7	----
Fuel shims	+1.05	4.2	12.6

909 043

residence time for the Coprocessing designs are limited to fluences of about 2.0 x 10^{23} n/cm^2 to allow for increased smear density which results in better breeding performance.

3.4 Core Height

Core heights of 3' and 4' were examined to determine their effect of fuel cycle cost and symbiotic system doubling time. As shown in Table 3.2 for both the Denatured and Coprocessing designs, this design option has little effect on cost and doubling time.

3.5 Fissile Inventory

Three options were studied to reduce the core fissile inventory. The use of reflectors in place of blankets was tried in the Denatured concept and the use of fuel shims and fuel shuffling to reduce radial peaking were tried in the Coprocessing concept. The use of reflectors reduces the core specific inventory slightly in the Denatured design (Table 3.2), but it also causes a 41% rise in fuel cycle cost. The increase in cost is a result of the loss of fissile credit from the blankets. The small benefit is not considered worth the cost.

Because of the restrictions on fissile enrichment in the Coprocessing concept, designs with enrichments near the maximum for self-regeneration have high radial peaking. The core average power of these designs is lower than that for those designs with lower peaking, thereby, requiring larger core volumes and fissile inventories to produce the same reactor power. For a design with a core average enrichment equal to the maximum (i.e., the 0.300" pin diameter design), the only method available to reduce the high radial peaking is fuel shuffling. The technique is not very effective as it reduces radial peaking only about 1%.

For designs with average enrichments lower than the maximum two methods are available to reduce peaking, the standard enrichment zoning and the use of fuel shims. Fuels shims, here, refer to both internal blankets and low reactivity worth drivers. Of the two options, the use of fuel shims produces a higher cost and doubling time design as shown in Table 3.2. The fuel cycle cost and symbiotic system doubling time are both 5% higher for the design which has internal blankets compared to the base case which has enrichment zoning. If the fuel shims are Th/U drivers, which have a lower reactivity worth compared to U/Pu drivers, another advantage can be obtained. In addition to reducing the radial peaking, the Th/U drivers reduce the sodium void worth of the core. They also increase the fuel cycle cost by over 20%. The sodium void worth, which was minimized in this design, is about $2.00. The fuel cycle cost could be reduced somewhat if the sodium void worth is allowed to increase to the $3.00 limit.

909 045

4.0 Mechanical Design

Driver pin and assembly design, radial blanket assembly design and control assembly volume fractions are detailed in this section. The fuel pin and assembly designs are based on preliminary neutronics estimates. For detailed discussion of performance, refer to Sections 6.0 and 7.0. Radial blanket assembly designs are based on the design of carbide blanket tests (CB-2)[17] in the Fast Test Reactor (FTR). Control assembly volume fractions are based on CRBR data and PRLCDS Ground Rules.

4.1 Driver Pin and Assembly Design

4.1.1 Selection of Pin Design

The selection of the reference pin diameter is based on previous optimization studies[2,3,4]. Fuel cycle costs, reactor doubling time, and fissile inventory are the key parameters considered in the selection process. The 9.40 mm (0.370") O.D. pin with cladding thickness of 0.38 mm and 0.51 mm (15 and 20 mils) for the sodium and helium bonded designs was chosen from these studies as the C-E Reference pin designs. Furthermore, these designs are similar to the proposed carbide driver tests (ACN 1 and 2) in FTR[18]. Both sodium and helium bonded pins are included in ACN-1/2 assembly descriptions. Sodium bonded pin designs exhibit better performance characteristics than similarly designed helium bonded designs. Fuel pin lifetime analyses by W-ARD[6] indicate that the sodium bonded pins can operate at higher temperatures than the helium designs without violating the CDF limits. Due to better performance characteristics and time limitations, only sodium bonded pins were considered in this study. However, at a later date, helium bonded driver pins could be substituted. An aggressive helium bonded pin design of 82% smear density, and 0.51 mm (20 mils) cladding thickness would produce nearly identical heavy metal mass.

The pin diameters for the Transmuter, Denatured and low void worth Coprocessing cores were determined based on PRLCDS optimization studies. Core Height, fissile inventory, pin diameter, residence time, doubling time and fuel cycle costs were examined in this study. For further discussion, refer to Section 3.0. The following parameters, specified by the PRLCDS guidelines, were used in the final pin designs to establish the cladding thickness and fission gas plenum length.

1. Cladding thickness/diameter ratio shall be 0.015/0.370 for sodium bonded and 0.020/0.370 for the helium bonded designs. The minimum cladding thickness for any design shall be greater than 0.30 mm (12 mils).

2. The plenum/fuel volume ratio for pins designed for a peak burnup of 80,000 MWD/MTM shall not be less than 0.75 for the helium bonded pins, 0.50 for the sodium bonded pins. This satisfies the PRLCDS guidelines which require a minimum plenum/fuel volume ratio of 0.25 for any burnup.

Additionally, the fuel pellet is sized to preclude fuel/cladding mechanical interaction. A gross fuel swelling rate of 2.7% $\Delta V/V$ per 10,000 MWD/MTM is used and no credit for cladding swelling is included. This procedure yields conservative pellet sizes and corresponding smear densities with a potential for future improvements. For all cases, a fuel pellet density of 98% of the theoretical density is assumed.

The fuel pin characteristics are listed in Table 4.1.

4.1.2 Assembly design

The Reference design was used to establish the approximate lattice pitch for all designs in order that one reactor design would be appropriate for all core designs. The lattice pitch is obtained

Table 4.1

Assembly Design Description

	Reference	Coprocessing Low Void	Coprocessing Low Cost	Denatured	Transmuter
DRIVER ASSEMBLY					
Pins/Assembly	169	127	169	169	169
Pin Pitch/Diameter Ratio	1.198	1.106	1.174	1.240	1.240
Wire Wrap Diameter, mm	1.81	1.21	1.57	2.07	2.20
Lattice Pitch, cm	16.48	16.58	16.12	16.21	17.09
Duct Wall Thickness, mm	3.81	3.56	3.81	3.81	4.06
Interduct Gap, mm	7.62	7.11	7.11	7.62	7.62
Bundle Porosity, mm/ring	0.100	0.100	0.100	0.100	0.100
FUEL PIN					
Cladding Outside Diameter, mm	9.40	11.94	9.40	8.89	9.40
Cladding Wall Thickness, mm	0.38	0.48	0.38	0.36	0.38
Smear Density, % TD	77	87	83	78	78
Bond Type	Sodium	Sodium	Sodium	Sodium	Sodium
Plenum Volume, cc	31.2	50.4	26.8	28.0	31.2
RADIAL BLANKET ASSEMBLY					
Pins/Assembly	91 →				
Pin Pitch/Diameter Ratio	1.071 →				
Wire Wrap Diameter, mm	0.97	0.97	0.94	.094	0.99
Lattice Pitch, cm	16.51	16.58	16.12	16.21	17.09

Table 4.1 (Cont.)

Assembly Design Description

	Reference	Coprocessing Low Void	Coprocessing Low Cost	Denatured	Transmuter
RADIAL BLANKET ASSEMBLY (CONT.)					
Duct Wall Thickness, mm	2.29 →				
Interduct Gap, mm	6.35	7.11	7.11	7.62	7.62
RADIAL BLANKET PIN					
Cladding Outside Diameter, mm	14.66	14.81	14.35	14.38	15.24
Cladding Wall Thickness, mm	0.508 →				
Smear Density, % TD	96.4 →				
Bond Type	Helium	Helium	Helium	Helium	Helium
Plenum Volume, cc	116.9	102.4	95.8	112.2	127.1
CELL VOLUME FRACTIONS					
Driver Assembly					
Fuel	0.332	0.427	0.373	0.311	0.311
Structure	0.188	0.187	0.191	0.203	0.191
Sodium	0.480	0.386	0.436	0.486	0.497
Radial Blanket Assembly					
Fuel	0.539	0.561	0.555	0.535	0.545
Structure	0.142	0.142	0.146	0.144	0.138
Sodium	0.293	0.287	0.290	0.295	0.291
Gap	0.026	0.009	0.009	0.026	0.026
Control Assembly (rods in)					
Boron	0.312 →				
Structure	0.318 →				
Sodium	0.228 →				

Table 4.1 (Cont.)

Assembly Design Description

	Reference	Coprocessing Low Void	Coprocessing Low Cost	Denatured	Transmuter
CELL VOLUME FRACTIONS (CONT.)					
Control Assembly (rods out)					
Structure	0.312				
Sodium	0.682				

909 050

from the following thermal-hydraulic and mechanical calculations. Thermal/hydraulic calculations provide an initial estimate of the beginning of life (BOL) pin pitch-to-diameter (P/D) ratio based on maximum allowable coolant velocity and pressure drop. Duct/bundle interaction (DBI) calculations are then performed to determine a BOL P/D such that a residence time of 2 years is obtained with 316 stainless steel structural materials and straight start wire wrap configuration. This procedure is described further in Appendix B. With the bundle dimensions determined, the residence time for the design is determined for the advanced stainless steel material properties and locked wire wrap configuration. The duct wall thickness and inter-assembly gaps are set based on duct dilation calculations. These parameters are adjusted until the lattice pitch is near that of the Reference design. The lattice pitch for all designs is nearly equal and could be made to match precisely by adjusting the pin diameters slightly. The results of these calculations are listed in Table 4.1 for the designs considered.

4.2 Radial Blanket Assembly Design

The radial blanket assembly designs are based on the target carbide radial blanket assembly[17] used for the design of the FTR carbide blanket test CB-2. The target is a 36 pin, 16.38 mm (0.645") O.D. helium bonded design with a cladding thickness of 0.51 mm (20 mils) and a P/D of 1.071. The 91 pin PRLCDS radial assemblies possess the same pitch-to-diameter ratio, bundle porosity, smear and pellet densities and cladding thickness as the target assembly. However, the duct wall thicknesses are based on the maximum allowable membrane stress. The inter-assembly gaps correspond with those specified for the fuel assembly designs. These gaps are sufficient for the designated residence times. With the inside duct dimensions, P/D ratio and bundle porosity specified, the pin diameters are calculated. The radial blanket assembly characteristics are displayed in Table 4.1 for the difference designs.

909 051

4.3 Control Assembly Volume Fractions

The control assembly volume fractions are based on CRBR volume fractions[19] and PRLCDS Ground Rules.

4.4 Comparison of Results

The assembly descriptions for the Reference, Transmuter, Denatured and low void worth Coprocessing designs are shown in Table 4.1. The difference among the designs are discussed below.

The Reference and Coprocessing designs possess lower pitch-to-diameter ratios than the Denatured or Transmuter cores. The low P/D ratios of the Reference and low cost Coprocessing designs are primarily the result of the low initial estimate for the neutron flux leading to a low DBI for a residence time of 2 years. The two designs are not DBI limited and, therefore, the P/D ratios are determined from coolant velocity and pressure drop limits. The low void worth Coprocessing design has a low neutron flux and fluence. The lower neutron flux is characteristic of the larger pin diameter and high fissile inventory. The low fluence produced a low BOL P/D.

The smear densities of the Reference, Denatured and Transmuter are similar due to comparable burnups. However, Coprocessing designs have greater smear densities due to lower burnups. The low burnup is largely the result of the shorter lifetimes and an increased pin diameter (greater heavy metal mass) for the low void worth design.

Fuel volume fractions are given for all the designs. The fuel volume fraction is a function of the smear density (fuel pellet sizes) and beginning of life pitch-to-diameter ratio. Therefore, the Coprocessing designs possess the largest fuel volume fractions due to a low BOL P/D ratio and high smear densities. Next largest is the Reference design; it has a tighter P/D though comparable smear densities relative to the Denatured and Transmuter cores. The Denatured and Transmuter volume fractions are similar due to nearly identical smear densities and BOL P/D's.

5.0 Nuclear Analysis

Detailed neutronics calculations were done for all five of the final core designs, the Reference, two Coprocessing, the Denatured, and the Transmuter. A summary of methods and a discussion of results is presented in this section. A detailed discussion of methods is given in Appendix A.

5.1 Methods and Models

A half height R-Z model of the reactor was used for neutronics calculations. Control rods were modeled in their parked position 6" above the core/upper axial blanket interface The Ground Rules were followed for reflector thickness and composition and control rod volume fraction and enrichment.

A starting point for cross sections was a 42 group set supplied by HEDL[20]. They are based on the ENDF/B-IV cross section files. The 42 group set was collapsed to 22 groups for static k_{eff} calculations and to 4 groups for depletion calculations. The k_{eff} calculations were done with F2DB[21]. The minimum k_{eff} during the equilibrium cycle was held to 1.000 ± 0.005.

Core average power was maximized by adjusting the peak linear powers in each enrichment zone so that they were equal at their peak points in life. The number of assemblies for each design was based on preliminary physics and was not adjusted for the final design due to schedule constraints.

5.2 Discussion and Comparison of Results

Detailed neutronics results are presented in Table 5.1. The list of results required by the groundrules in given in Appendix C.

Table 5.1

Detailed Neutronics Results

	Reference	Coprocessing Low Void	Coprocessing Low Cost	Denatured	Transmuter
GENERAL PHYSICS					
Reactor Power MWt	3000.	3000.	2740.	2880.	3000.
MWe	1095.	1095.	1000.	1051.	1095.
Fissile Enrichment (BOL) wt %					
Inner Zone	9.50	9.52	8.97	9.68	14.10
Outer Zone	11.68	9.86	9.95	11.84	17.36
Average	10.56	9.74	9.75	10.86	15.70
Residence Time (yrs)					
Driver	2.43	3.00	2.16	2.85	2.70
Radial Blanket	4.05	5.00	5.40	4.76	4.50
Reactivity Decrement, % Δk/kk'	-0.20	+0.49	+0.96	-4.17	-1.90
Discharge Exposure (MWD/kg)					
Peak Inner Zone	104.2	79.7	97.7	109.4	104.1
Outer Zone	91.3	72.9	104.3	107.1	122.6
Radial Blanket	10.6	7.1	9.3	9.3	11.6
Fast Flux (E>.1 MeV) @ MOEC ($x10^{15}$ n/cm^2-sec)					
Peak	4.96	3.01	4.84	4.18	5.04
Fraction (at peak)	.566	.602	.580	.561	.595
Fluence (E>.1 MeV, $x10^{23}$ n/cm^2)	2.70	1.99	2.31	2.63	3.01

Table 5.1 (Cont.)

Detailed Neutronics Results

	Reference	Coprocessing Low Void	Coprocessing Low Cost	Denatured	Transmuter
PERFORMANCE INDICIES					
Conversion Ratio (MOEC)					
Inner Zone	1.068	1.034	1.121	.930	.867
Outer Zone	.902	1.041	1.052	.749	.694
Core	1.000	1.038	1.071	.842	.794
Breeding Ratio (MOEC)					
Driver	.940	1.004	1.035	.804	.760
Axial Blanket	.216	.232	.263	.168	.187
Radial Blanket	.266	.159	.161	.233	.245
Total	1.422	1.395	1.460	1.21	1.193
System Fissile Inventory (BOEC), kg_{fiss}	4401	6171	4716	4031	5360
System Doubling Time, yrs					
Compound	9.7	16.0	10.6	18.7	23.2
Symbiotic	*13.2	17.1	13.8	15.6	24.7
Support Ratio	0.26*	0.21	0.23	1.72	0.77
Sodium Void Worth ($)	5.02	2.00	4.63	.67	1.85
Doppler Coefficient ($\Delta k/kk'$)	-.0083	-.0079	-.0073	-.0095	-.0066

* for the Reference design with thorium blankets.

Table 5.1 (Cont.)

Detailed Neutronics Results

	Reference	Coprocessing Low Void	Coprocessing Low Cost	Denatured	Transmuter
MATERIAL INVENTORIES					
Fissile Inventory @ BOEC (kg_{fiss})					
Driver U + Pa	0.	1486.	0.	2180.	441.
Pu	2709.	2843.	2949.	434.	2741.
Axial Blanket U + Pa	0.	168.	96.	107.	135.
Pu	130.	0.	0.	0.	0.
Radial Blanket U + Pa	0.	186.	198.	269.	339.
Pu	316.	0.	0.	0.	0.
Fissile Gain (kg/year)					
Driver U + Pa	0.	9.9	0.	-497.8	382.1
Pu	-9.4	11.0	43.0	398.3	-575.5
Axial Blanket U + Pa	0.	157.2	164.0	105.1	133.7
Pu	147.7	0.	0.	0.	0.
Radial Blanket U + Pa	0.	108.5	102.6	145.3	177.1
Pu	182.7	0.	0.	0.	0.
System Specific Inventory @ BOEC (kg_{fiss}/MWe)	3.84	5.63	4.72	3.84	4.90
Heavy Metal @ BOEC (kg)					
Driver	25,971.	44,032.	29,810.	25,122.	21,228.
Axial Blanket	22,292	37,304	23,188	17,127	17,833
Radial Blanket	68,920	60,816	48,776	51,496	53,412

Table 5.1 (Cont.)

Detailed Neutronics Results

	Reference	Coprocessing Low Void	Coprocessing Low Cost	Denatured	Transmuter
POWER					
Power Fraction @ MOEC					
Driver	.927	.967	.966	.956	.936
Axial Blanket	.0322	.0212	.0214	.0188	.0279
Radial Blanket	.0408	.0121	.0124	.0257	.0364
Power Peaking Factors (MOEC)					
Axial (peak assembly)		1.25	1.27	1.25	1.23
Radial (fueled region)		1.23	1.45	1.38	1.45
Peak Power Densities @ MOEC					
Inner Zone (MW/L)	.697	.472	.729	.648	.649
Outer Zone	.662	.541	.769	.646	.602
Peak Linear Power (3σ+15% kW/ft)					
Inner Zone BOL	35.2	33.4	34.0	36.8	36.2
EOL	36.5	32.1	38.1	29.3	35.7
Outer Zone BOL	36.7	37.7	39.7	38.3	37.4
EOL	32.7	37.3	39.1	29.6	32.4

5.2.1 Fissile Enrichment

The average enrichment of the Reference and Denatured designs is similar. The higher worth of the U-233 in the Denatured design compared to that of the Pu-239 in the Reference design offsets its smaller heavy metal mass which would normally lead to a higher enrichment. The enrichment in both designs is less than 12%. The higher fissile enrichment in the Transmuter is due to the low density of the Th-232 and the lower number of fissions in Th-232 relative to U-238.

The low enrichments of the Coprocessing designs are achieved through their relatively large heavy metal masses. The low enrichments in the low void worth Coprocessing design in both U/Pu and Th/U drivers is just low enough to support self-regeneration. The inner zone in the low cost design does support sufficient fissile gain to cause a doubling time for the core of 71 years.

5.2.2 Fuel Residence Time

The lifetimes of the designs were established by a preliminary assessment of duct/bundle interaction (DBI) limitations. The criteria used to set the pin pitch/diameter ratio, which strongly affects DBI, is described in Section 4.0.

5.2.3 Reactivity Decrement

The reactivity decrements reflect the breeding performance of the designs. The Reference and two Coprocessing designs have small decrements because of their excellent breeding performance. The Denatured design has the largest decrement because, in addition to relatively poor breeding, it burns high reactivity worth U-233 and replaces it with low worth Pu-239. In the Transmuter, the opposite is true, thereby reducing the reactivity decrement relative to the Denatured design, even though its breeding performance is poorer. The large

909 059

reactivity decrements account for the larger control rod/driver assembly ratio for the Denatured design. That, in addition to margin added for Pa-233 decay, accounts for the high control ratio in the Transmuter design.

5.2.4 Discharge Exposure

The discharge exposures of the Reference, low cost Coprocessing and Denatured designs are similar due to competing effects of fuel residence and peak power density. The low void worth Coprocessing design has a low exposure even with a long residence time due to the large heavy metal mass allowed by the large pin diameter. The higher discharge exposure for the Transmuter design is caused by the low density of thorium fuel.

5.2.5 Fast Flux and Fluence (E > 0.1 MeV)

The low fast flux of the low void Coprocesssing design is brought about again by the large heavy metal mass. The lower value for the Denatured design is caused by the higher reactivity worth of the U-233 relative to Pu 239.

The fluences of the Reference, low cost Coprocessing and Transmuter designs vary according to their respective fuel residence times. The lower values for the low void worth Coprocessing and Denatured designs is caused by the lower flux levels.

5.2.6 Conversion Ratio and Breeding Ratio

The conversion ratio reflects the breeding performance of the core independently of the blankets. The three designs with U/Pu in the core, the Reference and two Coprocessing designs, have excellent breeding in the core. The two Coprocessing designs have core conversion ratios just large enough to support self-regeneration. The poorer breeding in the Denatured core is due to the smaller number of captures in U-238 compared to the other designs. This is due to both a lower flux level and a larger fission cross section of U-233 compared to Pu-239. The Transmuter has the poorest breeding performance in the core. The low capture cross section of Th-232 along with its lower density account for this result.

The breeding ratio reflects the breeding performance of the whole reactor. The trends in breeding ratio follow the trends in conversion ratio. The reasons for the trends are also the same with one exception. The breeding in uranium blankets of the Reference design is about 15% better than that in the thorium blankets of the other designs.

5.2.7 System Fissile Inventory

The system fissile inventory is a performance index which combines both the in-reactor fissile inventory with the inventory tied up in fabrication and reprocessing. The out-of-reactor inventory is primarily dependent on fuel residence time and in-reactor inventory. The in-reactor inventory is dependent on total power, the ratio of fertile to fissile fissions, heavy metal mass and to a lesser extent, the structure and sodium mass. The Denatured design has the lowest system inventory due to a long fuel residence time, moderate heavy metal mass and the high reactivity worth of U-233 compared to Pu-239. The Reference and low cost Coprocessing designs have larger system inventories due to shorter residence time and the lower worth of Pu-239. The high inventory of the Transmuter is due to the low density of thorium causing greater leakage compared to U-238 and fewer fast fissions in thorium. The low void worth Coprocessing design has the highest system inventory due primarily to its large heavy metal mass.

5.2.8 System Doubling Time and Support Ratio

The system doubling time is a measure of how fast a closed system of reactors can double their number. It is dependent on breeding performand and system fissile inventory. The Reference design has the lowest doubling time due to good breeding performance and a very low system inventory. The low cost Coprocessing design has a slightly higher compound system doubling time (CSDT) due to the somewhat larger system inventory. The symbiotic system doubling time (SSDT) is larger than the CSDT due to a poor performing partner reactor. The CSDT for the low void worth Coprocessing design is significantly larger due to the much larger system inventory and slightly lower breeding performance. Both of these are caused by the additional Th/U drivers used to lower the sodium void worth. The CSDT for the Denatured design is only slightly worse even though it has much poorer breeding. This is due to the 50% lower system inventory. The SSDT is lower than the CSDT because the better performance of the partner reactor. The Transmuter has the largest doubling times due to both poor breeding performance and high system inventory.

The support ratio is the ratio of reactors outside of an energy center that can be supported by partner reactors within the center. Equilibrium is assumed. The partner reactors are specified in the Ground Rules. They are a Denatured breeder for U-233 producing reactors and a Reference breeder with thorium blankets for Denatured designs. Due to difference in partner reactors, the support ratio cannot be used in a comparison of Transmuter and Denatured designs.

The Transmuter design has the largest support ratio of the U-233 producing designs, even though its total gain is less than half that of the Coprocessing designs. This is due to its large U-233 production. The correspondingly large Pu-239 loss is supplied by the Denatured partner. The Transmuter reactors can be best used in symbiosis with partner reactors which can makeup their large Pu-239 losses. The Reference design with thorium blankets has the next largest support ratio. However, it is only one third as large as the Transmuter's support ratio because its U-233 gain is one third lower. This occurs despite the fact that the total gain of the Reference design is twice as large as that of the Transmuter. The same result occurs with the Coprocessing designs. The Pu-239 requirement of those designs is very small. The excess Pu-239 produced by the Denatured partner is used to establish more U-233 producing reactors thereby keeping the support ratio high.

5.2.9 Sodium Void Worth and Doppler Effect

Sodium void worth is one measure of the response a reactor may have during a core disruptive accident (CDA). It has been determined that designs with sodium void worths under $3.00 are much less sensitive to input assumptions used in analyzing a CDA[8]. The sodium void worth is dependent on the Pu-239 mass, the U-238 mass and leakage from the core. The Reference and low cost Coprocessing designs have large inventories of U-238 and Pu-239 and, therefore, have larger sodium void worths. The slightly lower void worth in the low cost Coprocessing design is due to a shorter core which increases leakage to the axial blankets. The lower sodium void worths of the other designs are due to replacing either U-238 or Pu-239 with Th-232 or U-233, respectively. In the low void Coprocessing design, Th/U drivers are concentrated in high worth regions to increase their effectiveness. The sodium void worth calculated for the Reference design is about 25% lower than that calculated by ANL[9]. The difference is believed to come from the different approximations used to account for elastic scattering in the processing of the ENDF/B-IV data[22].

The Doppler coefficient is another reactivity feedback mechanism in the CDA. Its value becomes more negative with a softer spectrum, lower fissile enrichment and larger heavy metal mass. The Transmuter design has the smallest Doppler effect due to the small heavy metal mass, relatively hard spectrum and high fissile enrichment. The two Coprocessing designs have a somewhat larger Doppler effect due to larger fissile masses and lower fissile enrichments. The Reference and Denatured designs have the largest Doppler effect due to low fissile-enrichments and relatively soft spectrums.

909 063

6.0 Thermal-Hydraulic Design

This section provides a description of the PRLCDS thermal and hydraulic design procedures and characteristics. Core orificing strategy, assembly design procedure and the associated temperatures and pressure losses characteristics of these designs are discussed.

6.1 Thermal and Hydraulic Methods

6.1.1 Core Orificing

Flow is allocated to the various regions of the reactor, and with a specific orifice criteria, the flow is distributed among the assemblies within the region. An adiabatic by-pass flow of 5% is assumed. The radial blanket region is allocated flow so that a peak, end-of-life (EOL), 2σ, cladding midwall temperature of $677^{O}C$ ($1250^{O}F$) is not exceeded in each of the blanket orificing zones. This steady state temperature is considered acceptable for meeting transient temperature constraints. The balance of the flow is allocated to the driver assemblies.

Driver region flows are allocated using a criteria of equal EOL, 2σ, peak cladding midwall temperature in each orifice zone. This is thought to be a good approximation to orificing for equal assembly lifetimes. The end of life cladding temperature is a significant parameter relating to the allowable residence time of a fuel pin. Power and temperature history play a secondary role on the cumulative damage of the pin[23].

Detailed core orificing is performed with the comprehensive core physics results generated with the initial assembly designs. Driver assemblies of similar power characteristics are grouped into an orifice zone. The peak powered assembly of each crifice zone is selected as the target assembly. Flow for each zone is allocated in accordance with the target assembly power characteristics. With the total driver region mass flow rate remaining

909 064

constant, orifice zone flows are adjusted to obtain equal EOL peak cladding temperatures.

An approximate orificing scheme is employed in the assembly sizing effort. The gross allocation of flow employs a 5% adiabatic flow, as specified in the PRLCDS Ground Rules, and 100% overcooling of the radial blanket assemblies for the preliminary effort. The balance of the flow is allocated to the driver region. The specific orificing scheme allocates the regional flow to the assemblies in proportion to their power characteristics In particular, assembly-by-assembly orificing for equal mixed mean outlet temperatures at middle of life represents the specific orificing scheme for the assembly design effort. This scheme yields flows to the peak driver assemblies that are within 3% of the recommended criteria described above.

The peak midwall cladding temperatures for the fuel and radial assemblies are calculated using the hot channel factors recommended in the PRLCDS Groundrules. The plant expected operating condition hot channel factors are used in this analysis. Additional uncertainties are applied on the heat flux hot channel factor to reflect nuclear modeling uncertainties. The effect of intra-assembly flow maldistribution is included but no credit for interchannel coolant mixing is taken in the nominal coolant temperature calculations. For additional description of the hot channel methodology, refer to Appendix B.

Following the determination of peak assembly flow rates, subassembly pressure drops and velocities were calculated. With the bundle dimensions, the program ASK(14) was used to calculate the coolant velocity and resulting assembly pressure losses.

Duct temperatures for the design limiting assemblies of the inner and outer enrichment zone were determined using the

909 065

SUPERENERGY[24] computer program which calculates coolant/duct axial and radial temperature distributions. Interchannel coolant mixing and energy redistribution are modeled by an enhanced effective eddy diffusivity, and a swirl flow parallel to the duct wall. The MIT flow split model[25,26] and the MIT-Chiu correlations for eddy diffusivity and swirl flow[27,28] are employed in these calculations.

An evaluation of the W-ARD HT data[29] using SUPERENERGY and the revised MIT flow split mixing parameters indicates flow maldistribution uncertainty factors of 1.05 and 1.03 for radial and fuel assemblies to be appropriate. These values should be used instead of the Ground Rule recommended uncertainties of 1.10 and 1.08 for radial and fuel assemblies obtained from a similar calibration of data with COTEC. Revision of hot channel factors with the recommended values would result in lower cladding temperatures. For further discussion of SUPERENERGY and evaluation of the MIT mixing model, refer to Appendix B.

6.2 Results and Comparisons

The thermal-hydraulic performance characteristics are shown in Table 6.1. The table lists the various parameters for the Reference, Transmuter, Denatured and Low Void Worth Coprocessing designs. Thermal and hydraulic analysis of the low cost Coprocessing design was not done due to time constraints. The significance of each of the thermal-hydraulic parameters is discussed below.

6.2.1 Core Outlet Temperature

The core outlet temperature is dependent on the amount of flow available for the driver region. A high core outlet temperature signifies a greater percentage of the total reactor flow is being allocated to the other regions of the reactor. The amount of flow allocated to the driver regions was determined by the flow allocated for the radial blankets and adiabatic bypass. An adiabatic bypass flow of 5% is specified in the PRLCDS Ground Rules for all designs. The radial blanket flow fraction is dependent on the region power at EOL conditions. Upon examination of the flow fractions and the resultant core outlet temperature, several trends are noted. The low void worth Coprocessing design has the highest core region flow fraction and the lowest core outlet temperature. The Denatured, Reference and Transmuter designs can then be arranged in the order of increasing core outlet temperature and decreasing driver region flow fractions.

Several techniques are suggested for increasing the driver region flow fraction and reducing the core outlet temperature. The radial blanket flow fraction is the only varying factor for all the designs. Since the radial blankets were orificed based on EOL cladding temperature, the EOL powers determine this flow fraction. In the calculation of the radial blanket flow rates, use of a half-wire design and the reduction of the flow maldistribution uncertainty factor for blanket assemblies (refer to Appendix B) results in lower flow requirements needed to obtain the 677^{o}C (1250^{o}F) EOL cladding temperatures. The implementation of a half-wire design contributes to a lower intra-assembly flow maldistribution. Since the intra-assembly flow maldistribution is primarily a function of the number of pins per assembly, it is greater for the radial blankets than for the fuel assemblies. The benefits of the half-wire in reducing flow maldistribution are greater for the radial blanket assemblies than for fuel assemblies. A reduction in the flow maldistribution and the uncertainty factor results in lower cladding temperatures for a given flow rate. Thus, less flow is necessary to obtain the 677^{o}C (1250^{o}F) (2σ) end of life cladding temperatures in the radial blankets; and a higher flow fraction is available for the driver region.

909 067

6.2.2 Coolant Mass Flow Rates

The coolant mass flow rates were determined from a simple enthalpy balance. They are a function of the total core power and the desired reactor temperature rise. The PRCLDS Ground Rules require a reactor inlet temperature of 343°C (650°F) and outlet temperature of 499°C (930°F). A reactor vessel ΔT of 156°C (280°F) was obtained. The mass flow rates reflect the power rating of each design.

6.2.3 Velocity and Pressure Losses

The coolant velocity is a function of bundle flow area and mass flow rate. Bundle dimensions were calculated using duct/bundle interaction, velocity, and pressure drop constraints. In particular, the duct/bundle interaction constraint produces a larger pitch-to-diameter ratio and an increased bundle flow area for most designs than do the thermal-hydraulic limits. Thus, the coolant velocity falls below the limit of 10.7 m/sec (35 ft/sec) for those designs.

The pin bundle pressure losses are a function of the coolant velocity, length of the pin bundle, and the hydraulic diameter of the pin bundle. The coolant velocity and the hydraulic diameter are the predominant factors affecting the magnitude of the pressure losses. Bundle length are nearly the same, 2.51 m (8.25 ft) for the Reference, Denatured and Transmuter designs, and 2.29 m (7.5 ft) for the low void worth Coprocessing designs. The peak powered assembly velocities and associated pressure losses are reported in Table 6.1. The highest pressure loss is for the Reference design. The Reference design is coolant velocity, not pressure drop or duct/bundle interaction (DBI) limited. The Transmuter and Denatured designs are DBI limited and have looser P/D compared to the Reference core. This translates into greater bundle flow areas and lower coolant velocities. The resulting pressure losses are also lower. The low void worth Coprocessing design is pressure drop limited. The Transmuter and low void worth Coprocessing designs have identical velocities but different pin bundle pressure losses. This difference is due to the difference in pin P/D ratio and bundle length. The higher pin bundle pressure loss for the low void worth Coprocessing core can be explained by inspecting the variation in friction factors, hydraulic diameters and bundle lengths. The pin bundle friction losses are computed using the following expression.

$$\Delta P = f \frac{L}{De} \rho \frac{V^2}{2g_c}$$

where: f = friction factor

L = bundle length

De = hydraulic diameter

ρ = sodium density

V = sodium velecity

g_c = gravitational constant.

For the two designs with equivalent velocities, the expression reduces to:

$$\frac{\Delta P_1}{\Delta P_2} = \frac{f_1}{f_2} \times \frac{L_1}{L_2} \times \frac{De_2}{De_1}$$

where $\Delta P_1/\Delta P_2$ is the ratio of the low void worth Coprocessing/ Transmuter pressure losses

subscript 1 denotes LVW Coprocessing

2 denotes Transmuter

Analyzing each of the ratios that are multiplied to yield $\Delta P_1/\Delta P_2$, we obtain:

$$\frac{f_1}{f_2} = 1.04 \quad ; \quad \frac{L_1}{L_2} = 0.91 \quad ; \quad \frac{De_2}{De_1} = 1.28 \quad ;$$

combining:

$$\frac{\Delta P_1}{\Delta P_2} = 1.04 \times 0.91 \times 1.28$$

$$= 1.21$$

The primary factor contributing to the low void worth Coprocessing core's higher pin bundle friction losses is the difference in hydraulic diameters which reflect the P/D ratios. The slightly greater friction factor for the low void worth design is offset somewhat by the smaller bundle length.

6.2.4 Orifice Zones

The relative benefits of lower cladding temperatures are assessed against the higher cost of increasing the number of orifice zones in the selection process. An increase in the number of orifice zones is accompanied by a reduction in the cladding temperatures and an increase in fuel lifetime. This is due, of course, to the increased flow in the peak powered assemblies. The greater flow rate results in increased coolant velocity, assembly pressure loss, and coolant pumping cost. Additionally, higher fabrication and maintenance costs associated with the more complex orificing scheme have to be assessed. The design objective is to minimize the number of orifice zones such that acceptable 2σ cladding midwall temperatures below 677^{o}C (1250^{o}F) are obtained. Six orifice zones are used for the Reference, Denatured and Transmuter designs and five for the Low Void Worth Coprocessing design. The number of orifice zones is well below the limit of 15 suggested in the PRLCDS groundrules. Ample margins exist for core reorificing in future, more detailed analyses.

6.2.5 Coolant Mixed Mean and Duct Temperatures

The coolant mixed mean temperature is indicative of core temperature performance. The coolant mixed mean, duct and cladding temperatures are related. For a low mixed mean temperature design, one would expect correspondingly low cladding and duct temperatures. The duct and cladding temperatures are the primary determinates of assembly lifetime in these designs. Duct dilation and duct/bundle interaction limits are determined from these operating temperatures. The nominal coolant mixed mean temperature of all designs is well below the $579^{O}C$ ($1075^{O}F$) limit stated in the PRLCDS Ground Rules. One observes a difference of approximately $39^{O}C$-$45^{O}C$ ($70^{O}F$-$80^{C}F$) between the nominal duct and bundle temperatures. The difference can be attributed to the energy redistribution in the bundle. The variation between the bundle and duct temperature for each design is due to differences in the competing effect of pins, pins per assembly, pin diameter, and P/Ds.

6.2.6 Peak Cladding Midwall Temperatures

The Reference, Denatured, Transmuter and low void worth Coprocessing designs were orificed such that end of life cladding midwall temperatures (2σ) below $677^{O}C$ ($1250^{O}F$) were obtained tained. EOL, 2σ, cladding midwall temperatures below $677^{O}C$ ($1250^{O}F$) are indicative of greater fuel pin integrity for the desired pin/assembly lifetimes.

The Reference design shows an increase in power over life for the peak inner driver and a decrease in power in the outer zone peak driver over life. Therefore, orificing for equal end of life cladding temperatures benefits the inner zone more than the outer zone. The cladding temperatures of the inner zone gradually increase to $658^{O}C$ (1217^{O} from BOL to EOL. In the outer zone, one observes that the cladding midwall temperatures decrease from $6?4^{O}C$ ($1281^{O}F$) at BOL to $658^{O}C$ ($1217^{O}F$).

The inner and outer enrichment zone peak driver assemblies of the Transmuter design decrease in power over life. This is a result of the low breeding ratio. The radial blanket assemblies markedly increase in power from BOL to EOL showing the power shift from the core to the blankets over life. As a result of the decreasing driver power history, one observes higher cladding midwall temperatures at BOL in the outer and inner enrichment zones. The outer zone experiences a greater change in power than the inner zone, so higher cladding temperatures are observed there.

The Denatured core undergoes the most dramatic reduction in core power over life. The inner and outer enrichment zones see approximately a 26% reduction in power from BOL to EOL. This is due to a low breeding ratio and replacing the high reactivity worth U-233 with the lower worth Pu-239.

For the Low Void Worth Coprocessing design, a conversion ratio above 1.0 in both enrichment zones is observed. Plutonium production is slightly greater than depletion so the power histories are very flat in the two enrichment zones. The radial blanket assemblies and the axial blankets see the most dramatic increase in power of all designs. Reflecting these trends, the cladding temperatures of the driver region remain reasonably constant over life. Orificing of the radial blankets for an end of life temperature of 677°C (1250°C) results in 112% overcooling at MOEC as compared to approximately 60% overcooling for the other designs.

The cladding midwall temperatures for all designs can be reduced significantly by employing a half-wire design for the fuel assemblies and revising the flow maldistribution uncertainty factor from 1.08 to 1.03 as discussed in Section 6.1 to reflect modeling uncertainties. Use of the half-wire design eliminates the intra-assembly flow maldistribution for the fuel assemblies. These changes would result in approximately a 20% reduction in the 2σ coolant temperature. This translates into 2σ end of life cladding temperatures between 632°C (1170°F) and 643°C (1190°F) for the Reference, Transmuter and low void worth designs and approximately 605°C (1120°F) for the Denatured core.

6.2.7 Fuel Centerline Temperature

The 2σ fuel centerline temperatures for the four reactor designs were calculated using the PRLCDS recommended hot channel factors. The values are reported in Table 6.1. Reference design temperatures were calculated for inner and outer enrichment zones at BOL and EOL. A similar trend in fuel centerline temperatures and cladding temperatures is observed. The same power and flow characteristics are used in both calculations and, therefore, equivalent trends are produced. Due to time limitations, only the most limiting fuel temperatures were calculated for the other three designs.

The outer zone beginning of life fuel temperature is the highest for the Reference core. This trend is also observed in the cladding temperatures. Similarly, the greatest fuel centerline temperatures are observed in the outer zone at BOL for the Transmuter, and inner zone at BOL for the Denatured and low void worth cores. The Denatured design's fuel temperature at BOL in the inner zone is the highest in magnitude of all the designs.

The 3σ + 15% overpower fuel centerline temperature should be below the melting point of uranium carbide for all designs. Since, the Denatured design has the highest 2σ fuel centerline temperature, the corresponding 3σ + 15% fuel centerline temperature would be the enveloping value for all designs. That value is 1300°C (2372°F) for the Denatured design. The melting point of uranium carbide is 2742°K[6] or 2469°C. Thie values represents the lower 3σ limit. Since the Denatured design has a much lower fuel centerline temperatre, the limit for all the other designs will also follow the same trend.

909 073

Table 6.1

Detailed Thermal-Hydraulic Performance Results

General Results		Reference	Coprocessing Low Void	Denatured	Transmuter
Reactor Power, MWt		3000	3000	2880	3000
Reactor Inlet Temperature, ^oC		343.	343.	343.	343.
Reactor Outlet Temperature, ^oC		499	499	499	499
Reactor Temperature Rise, ^oC		139	139	139	139
Core Outlet Temperature, ^oC		510	509	510	511
Core Temperature Rise, ^oC		167.	166	167.	168.
Number of Orifice Zones		6	5	6	6
Total Coolant Mass Flow, kg/yr		5.247×10^7	5.240×10^7	4.846×10^7	5.247×10^7
Flow Fractions					
Core		0.8976	0.9312	0.9137	0.8969
Radial Blanket		0.0524	0.0188	0.0363	0.0531
Bypass		0.0500	0.0500	0.0500	0.0500
Peak Powered Assembly Results					
Maximum Coolant Velocity, m/sec		10.7	9.1	8.5	9.1
Bundle Pressure Drop, kPa		628.	515.	397.	423.
Fuel Centerline Temperature, ^oC					
Inner Zone	BOL	1087.	1027.	1156.	----
	EOL	1101.	1025.	986.	----
Outer Zone	BOL	1104.	----	----	1119.
	EOL	1026.	----	----	1025.

Table 6.1 (Cont.)

Detailed Thermal-Hydraulic Performance Results

		Reference	Coprocessing Low Void	Denatured	Transmuter
Peak Cladding Midwall Temperatures (2σ), ^{o}C					
Inner Zone	BOL	652.	674.	712.	663.
	EOL	658.	668.	636.	659.
Outer Zone	BOL	694.	669.	711.	709.
	EOL	658.	668.	637.	663.
Maximum Mixed Mean Outlet Temperature (2σ), ^{o}C					
Inner Zone	BOL	560.	572.	595.	559.
	EOL	565.	568.	547.	558.
Outer Zone	BOL	565.	551.	574.	568.
	EOL	550.	550.	530.	553.
Nominal Duct Temperature, ^{o}C					
Design Limiting Duct, (x/L = 1.0)	BOL	468.	459.	499.	470.
	EOL	473.	460.	468.	471.

7.0 Lifetime Analysis

Duct-duct interaction (DDI) and duct-bundle interaction (DBI) are the primary factors determining assembly lifetime. Cladding stress history measured as cumulative damage function (CDF) is the primary factor governing fuel pin lifetime. Duct-duct interaction and duct-bundle interaction calculations were performed explicitly whereas the CDF analysis was based on the W-ARD study.

7.1 Assembly Lifetime

Duct-duct interaction (DDI) and duct-bundle interaction (DBI) calculations were performed for the PRLCDS designs. The magnitude of DDI and DBI is dependent on the core operating environment. Duct-bundle interaction is the most limiting of the two for the desired assembly residence times of 2-3 years. The mechanical performance results for the Reference, Transmuter, Denatured and low void worth Coprocessing design are listed in Table 7.1. The results are discussed individually below.

7.1.1 Duct-Bundle Interaction

The beginning of life (BOL) pitch-to-diameter (P/D) ratios for the assembly designs are based on preliminary duct/bundle interference calculations such that assembly residence times of 2 years with stainless steel materials are achieved. The BOL pin P/D was selected such that an end of life (EOL) P/D of 1.05 (interior pin-to-pin clearance) would be achieved with straight start wire wrap configuration. This procedure established the bundle dimensions including the wire wrap diameter and is discussed further in Appendix B. An allowable interference associated with the locked wire wrap configuration was then calculated. Table 7.1 lists the allowable interference and its value of an equivalent number of wire wrap for each design. The PRLCDS Ground Rules recommend 4 wire wraps for 169 and 127 pin bundles. These results indicate the 3-4-5 wire wrap criteria to be aggressive for P/Ds lower than 1.20, appropriate for P/Ds of 1.20, and conservative for P/Ds above 1.20. Therefore, the BOL P/D was selected using the procedure described in Appendix B.

A final iteration was performed to verify the preliminary DBI results. It has yielded interference slightly beyond the allowable using the calculated values of nominal duct/bundle interference, and substantially beyond the allowable using the nominal + 1 σ values of duct/bundle interference. The nominal + 1σ values include uncertainties for material properites. The calculation is very conservative, however, in that it ignores irradiation creep in the duct. When credit for duct ballooning due to irradiation creep is taken in the duct/bundle interference calculations, the procedure yields substantially lower values of DBI for the equivalent set of conditions. These DBI values are also reported in Table 7.1. The calculated nominal values for DBI are then well below the allowable. The nominal + 1σ values are close to the allowable DBI limit.

Several techniques can be employed to decrease duct/bundle interference and increase assembly residence time.

1. Use of half-wire wrap spacers for fuel and radial assemblies.
2. Revision of the flow maldistribution uncertainty factors to 1.05 for radial assemblies and 1.03 for fuel assemblies.
3. Use of grid spacers designs.

The half-wire wrap concept can be employed to reduce the effects of intra-assembly flow maldistribution. The main cause of assembly flow maldistribution is the large bypass flow area between the outer row of pins and the duct wall. It can be greatly decreased by reducing the wire wrap diameter between the edge pins and the duct wall.

The coolant mass flow necessary for orificing the radial blanket assemblies can be decreased by using the half-wire design and the revised flow maldistribution uncertainty factor. The intra-assembly flow maldistribution and uncertainty factors are applied directly to obtain the coolant temperature used in the hot channel cladding temperature calculations. Reduction of both factors results in a decrease in the mass flow required for orificing of radial assemblies for an end of life 2σ temperature of 677°C (1250°F). A slightly greater percentage of the total coolant flow rate is then available for the driver region.

Secondly, implementation of the half-wire wrap design and revision of the flow maldistribution uncertainty factor for the fuel assemblies would result in a reduction in driver cladding temperatures. More flow would be allocated for the peak powered assembly. The area reduction between the outer row of pins and the duct wall would also result in an increase in the duct temperature. Overcooling of the edge pins is markedly reduced and the duct wall is estimated to operate 16°C-25°C (30°F-40°F) hotter with the half-wire wrap design. The lower bundle cladding temperatures accompanied by the hotter duct would produce lower duct/bundle interference.

The impact of the higher operating temperature for the half-wire wrap design would have to be assessed. Either larger intra-assembly gaps or thicker walls can be employed to accomodate the larger duct dilation of the half-wire assembly designs. There is adequate margin in the radial assembly gaps to accomodate the half-wire designs, however, the fuel assembly lattice pitch dimensions would have to be altered to reflect these design changes.

The use of a grid spacer removes the wire wrap. The potential exists with advanced grid spacer designs to eliminate duct-bundle interaction as an assembly design concern.

7.1.2 Duct Dilation

Duct temperature, neutron flux and the pressure differential across the duct wall are the primary factors affecting the magnitude of duct dilation. The pressure differential and neutron flux profiles were assumed to remain constant over assembly lifetime. Duct temperatures were varied over life to reflect assembly power history characteristics. Nominal and nominal + 1σ values were calculated for the final designs of the Reference, low void worth Coprocessing, Denatured and Transmuter cores. The nominal + 1σ duct dilation values include uncertainties of the material correlations. Table 7.1 lists the inter-assembly gaps and duct dilation for the different designs. The initial estimate is very close to the nominal value of the inter-assembly gap for the Reference design. The previous estimate for the Transmuter corresponds to a value between the nominal and nominal + 1 sigma values. The initial estimates for the Denatured and low void worth designs are well over the nominal + 1 sigma calculated duct gaps. In all cases, the inter-assembly gap would need to be recalculated for a half-wire wrap assembly design.

7.2 Fuel Pin Lifetime

An evaluation of fuel pin lifetimes for the C-E designs is based on the Westinghouse fuel pin lifetime calculations[6]. W-ARD performed a CDF analysis using the computer code LIFE-3-C. Carbide, helium and sodium bonded, 9.40 mm (0.370") O.D. pin designs were examined. A cladding thickness of 0.51 mm and 0.38 mm (20 and 15 mils) was specified for the helium and sodium bonded pin designs, respectively. An end of life cladding temperature of 677°C (1250°F) and a 12% increase in pin power over life was assumed. The sodium bonded pin results in a CDF of 0.22 and <0.01 for steady-state and U-2b transient behavior. The equivalent

Table 7.1

Mechanical Performance Results

	Reference	Coprocessing Low Void	Denatured	Transmuter
Peak Flux E>0.1 MeV, $n/cm^2/sec$	$4.88x10^{15}$	$3.02x10^{15}$	$4.18x10^{15}$	$4.90x10^{15}$
Assembly Residence Time, FPD	620.	766.5	720.	690.
Peak Fluence, E>.1 MeV, n/cm^2	$2.6x10^{23}$	$2.0x10^{23}$	$2.6x10^{23}$	$2.9x10^{23}$
Duct Bundle Interference				
Allowable DBI, mm	7.22	3.65	8.87	9.35
Equivalent number of wire wraps	4.0	3.0	4.26	4.26
Bundle Porosity, mm/ring	0.1016	0.1016	0.1016	0.1016
Plenum length, cm	53.3	45.7	53.3	53.34
Interassembly Gap, mm	7.62	7.11	7.62	7.62
Maximum Duct/Bundle Interference, (Excludes Ballooning of Duct)				
Nominal, mm	8.89	5.36	8.23	10.34
Number of wire wraps	4.92	4.44	3.95	4.70
Nominal + 1 sigma, mm	10.34	6.45	9.73	12.07
Number of wire wraps	5.73	5.36	4.67	5.50
Maximum Duct/Bundle Interference, (Includes Ballooning of Duct)				
Nominal, mm	5.64	3.09	6.11	7.93
Number of Wire Wraps	3.13	2.56	2.93	3.61
Maximum Duct Dilation, mm				
Nominal	7.75	5.08	6.10	6.70
Nominal + 1 sigma	9.02	5.97	7.37	8.13

helium bonded design accumulated a CDF of 2.61 and 0.02 for steady-state and U-2b transient behavior. However, a reduction of the cladding temperature to 649°C (1200°F), the CDF for the helium bonded pin declined to 0.69 and 0.01, respectively. These results indicate an end of life cladding temperature of 677°C (1250°F) to be acceptable for the sodium bonded design. However, a lower operating temperature, approximately 643°C (1190°F) EOL is recommended for the helium bonded design such that steady state and total CDF limits of 0.50 and 0.75 are not violated.

Based on these results, pin lifetimes are discussed for the C-E sodium bonded pin designs. The Reference design is very similar to the W-ARD carbide sodium bonded pin analyzed. The cladding temperature is 652°C/1206°F (BOL) and 658°C/1216°F (EOL) for the Reference design's inner zone. Explicit calculations should yield comparable values for CDF in the inner zone. The outer zone with declining cladding temperatures of 694°C/1281°F (BOL) to 658°C/1217°F (EOL) and lower flux should result in comparable or lower values for CDF.

A previous analysis[23] indicates the end of life cladding temperature is the primary factor relating to the lifetime of a fuel pin, power and temperature history are secondary factors. Consequently, it is believed that fuel pin lifetime assessments for the other PRLCDS designs can be based on evaluation of W-ARD CDF results by analyzing end of life cladding temperatures. Futher analysis will be required to verify the assessment.

The decreasing cladding temperatures for the inner and outer zones are characteristic of the Transmuter design. The inner zone cladding midwall temperatures of 663°C/1226°F (BOL) and 659°C/1218°F (EOL) are well below the 677°C/1250°F of the W-ARD pin. Lower CDF values should be observed in the inner zone. Similarly, the outer zone with greater power and temperature

909 081

degradation over life should result in CDF values well below the limits.

One observes the most dramatic power and temperature degradation over lifetime in the Denatured core. The power declines approximately 26% over life in both zones, resulting in cladding temperatures of 636^{o}C/1177^{o}F (EOL). Noting the low end of life cladding midwall temperature, one would expect the steady state CDF to be less than 0.22 and negligible for the U-2b transient.

The low void worth Coprocessing design exhibits fairly flat but declining powers and temperatures in the inner and outer enrichment zones. The 2 sigma cladding midwall temperatures are 674^{o}C/1245^{o}F (BOL and 669^{o}C/1236^{o}F (EOL). Therefore, one can expect comparable or lower CDF values than indicated by the W-ARD pin analysis.

For all designs, the CDF limits specified in the PRLCDS Ground Rules are not expected to be violated.

8.0 Economics of Symbiotic, Anti-Proliferation Fuel Cycles

A study of possible economic implications of anti-proliferation fuel cycles was conducted in parallel with PRLCDS core design activities. Details of this study are reported elsewhere[23]. The basic premise of the study is the idea that a non-weapons state faced with future storage of U-235 might elect to forego installation of FBR's and plutonium reprocessing if an assured supply of U-233 were offered at a reasonable price.

The model non-weapons state in the study is Spain which is assumed to be considering either (A) installing FBR's and fuel reprocessing/refabrication capability sufficient to establish an equilibrium FBR/LWR plutonium economy which needs no input of U-235, or (B) foregoing the FBR/LWR plutonium economy in favor of an all U-233/LWR economy with U-233 being supplied from an external supplier nation(s). From an economic point of view, the all U-233/LWR option (B) could be attractive to Spain if the price of U-233 is sufficiently low to make power costs equal to or less than the power costs of the FBR/LWR plutonium option (A).

The supplier nation is also assumed to be faced with a shortage of U-235 and, consequently, to be considering converting to an FBR/LWR pluotnium economy which requires no U-235. Thus, Option A for the supplier is the same as Spain's Option A. However, for Option B, the supplier must set-up a reactor economy which is complementary to Spain's all LWR/U-233 economy but which remains independent of U-235.

Several options for the supplier nation were considered; the most attractive one appears to be FBR Transmuters with thorium blankets, and a mixture of plutonium, uranium and thorium in the driver. The supplier nation's FBRs burn plutonium returned from Spain plus bred plutonium. They produce sufficient U-233 to supply Spain's needs and the combinded economies are in equilibrium.

fuel cycle analysis was conducted in considerable depth to establish correct equilibrium parameters. The following results were obtained using System 80(TM) PWR's and oxide fueled LMFBR's.

Since the supplier nation must operate an all FBR transmuter economy, it will have higher capital costs than it would have if it operated a mixed FBR/LWR economy (Option A). HEDL data on capital and fuel cycle cost components were used to evaluate the cost penalty encountered by the supplier nation. This cost penalty was converted to a break-even selling price for U-233 which would recover all extra costs. The difference between the suppliers break-even selling price for U-233 and the value of U-233 to Spain is either profit for the supplier or a subsidy required to make such an economy work. Results of these calculations are given in Table 8.2.

Results were found to be sensitive to inventory carrying charges on fissile isotopes. Since the analysis considers a closed, equilibrium fissile isotope economy, one view is to consider fissile isotopes to have no value. Column one (Table 8.2) shows the result for this case. If, however, this closed cycle exists in parallel with other fuel cycles which could bid for its fissile isotopes, then carrying charges on Pu and U-233 inventories are appropriate. A typical indifference value for Pu relative to U-235 in a high ore cost situation is 100 $/gm. This is probably the most realistic case to consider.

With higher fissile isotope values, this analysis indicated that the proliferation resistant fuel cycle could be operated at a modest profit to the supplier nation. This result also means that the proliferation resistant cycle has a slightly lower overall cost than the all plutonium cycle. Results are not dependent on the assumed relationship between supplier and non-weapons state; they apply equally to a proliferation resistant fuel cycle established within a single nation.

Table 8.1

	Option A FBR/LWR All Plutonium	Option B FBR/LWR All Plutonium
Installed Capacity required for Equilibrium Gwe/FBR/Gwe/LWR	1.33	1.31

Table 8.2

Subsidy Required for the Anti-Proliferation Fuel Cycle

Pu Fissile Value, \$/gm	0	40	100
U-233 Break-Even Selling Price, \$/gm	35	44	54
U-233 Value to Spain, \$/gm	14	37	71
Subsidy required (Profit), \$/gm	21	7	(17)
Subsidy (Profit), 10^6 \$/yr*	295	98	(239)

*Based on 36.3 Gwe capacity installed in Spain.

909 085

Since the FBR/LWR mix is almost the same whether operating on the all plutonium cycle or the plutonium/U-233 cycle, results are not thought to be sensitive to capital cost assumptions but depend mainly on the balance between fuel fabrication costs (high for U-233) and carrying charges on inventory. Because U-233 is an excellent thermal reactor fuel, the plutonium/U-233 cycle has a lower overall fissile inventory than the all plutonium cycle. This is reflected as a cost advantage when fissile isotopes are highly valued.

9.0 References

1. J.C. Chandler, et al., "The Proliferation Resistant Preconceptual Core Design Study," TC-1082, Hanford Engineering Development, March 1978.

2. M.R. Kulwich and S.A. Caspersson, "Optimization Systems Design Studies for Helium-Bonded Carbide Fuel in 1500 MWe LMFBR's," CE-FBR-76-520 (COO-2426-84), Combustion Engineering, December 1976.

3. R.C. Noyes, et al., "Optimum Pin Diameter for LMFBR (Sodium-Bonded) Carbide Fuels," Nuclear Technology, 26, 4, August 1975, pp. 460-471.

4. S.A. Caspersson, et al., "Optimum Systems Design Studies of Advanced Carbide Fuel," TIS-5240, Combustion Engineering, Presented at International Meeting on Advanced LMFBR Fuels, October 10-13, 1977, Tucson, Arizona.

5. Letter from L.E. Minnick (EPRI) to AI, GE-FBRD and Bechtel, "Guidelines for PLBR Pool Design," August 3, 1977.

6. A. Biancheria, et al., "Contribution to Meeting on Proliferation Resistant LMFBR Core Design Studies," Handout at PRLCDS meeting at ANL in Chicago, Illinois, April 25-26, 1978.

7. Letter from A. Boltax (W-ARD) to V.W. Lowery (RTT), FMT-AB-1164, October 18, 1977.

8. V.W. Lowery, et al., "Performance Potential of Reference Fuel in Large 1200 MWe LMFBR's," U.S. Department of Energy, to be published.

9. S.F. Su, "Sodium Void and Doppler Reactivities in 3000 MWth

Oxide and Carbide LMFBRs," FRA-TM-99, Argonne National Laboratory, April 7, 1977.

10. J.J. Prabulos, "Economics of an Anti-Proliferation Fuel Cycle," Combustion Engineering, to be published.

11. R.H. Klinetob, "Ground Rules, Large Heterogeneous Reference Fuel Design Study, Revision II," Combustion Engineering, November 24, 1978.

12. R.J. Calkins, et al., "Optimization Systems Design Study of Denatured and Transmuter Carbide Fuel in 1000 MWe Homogeneous LMFBR's," Combustion Engineering, to be published.

13. M.R. Kulwich, et al., "Optimization Systems Design of Coprocessed Carbide Fuel in 1000 MWe LMFBR's," Combustion Engineering, to be published.

14. V. Sehgal, "Thermal/Hydraulic and Mechanical Design Calculations for the Proliferation Resistant LMFBR Core Design Study," FBR-78-45/21096, Combustion Engineering, February 28, 1978.

15. D.A. Marr and D.A. Cantley, "Performance Characteristics for a Symbiotic System of Reactors," Hanford Engineering Development Laboratory, September 1977.

16. G.U. Singco, "Plutonium Loadings as a Function of Isotopic Composition," PHD-78-71, Combustion Engineering, June 15, 1978.

17. Letter from S.A. Caspersson (C-E) to D.C. Corrigan (HEDL), CE-FBR-78-24, Combustion Engineering, February 10, 1978.

18. ANL-AFP-51, Advanced Fuels Development Program, Quarterly Progress Report, January-March 1978.

19. Project Management Corporation, "Clinch River Breeder Reactor

Plant Preliminary Safety Analysis Report,' 1975.

20. R.E. Schenter, et al., Nuclear Science and Engineering, Volume 57, Number 3, pp. 222-238, July 1975.

21. P.K. Doherty and D.A. Trumpler, "F2DB, A C-E Version of the 2DB Two-Dimensional Diffusion - Burnup Code for Fast Reactor Analysis," FBR-78-102, Combustion Engineering, January 1978.

22. D. Marr, Personal Communication, July 1978.

23. R.C. Noyes, et al., "Effect of Operating Temperature on LMFBR Core Performance," FBR-77-26/21080, Combustion Engineering, April 1977.

24. B. Chen and N. Todreas, "Prediction of Coolant Temperature Field in a Breeder Reactor Including Interassembly Heat Transfer," COO-2245-20TR, Revision 1, MIT, December 1976.

25. C. Chiu, W.M. Rohsenow, and N.E. Todreas, "Flow Split Measurement in LMFBR Blanket Assemblies," COO-2245-41TR, MIT, April 1978.

26. C. Chiu, W.M. Rohsenow, and N.E. Todreas, "Flow Split Model for LMFBR Wire Wrapped Assemblies," COO-2245-56TR, MIT, April 1978.

27. C. Chiu, W.M. Rohsenow, and N.E. Todreas, "Turbulent Sweeping Flow Mixing Model for Wire Wrapped LMFBR Assemblies," COO-2245-55TR, MIT, April 1978.

28. C. Chiu, W.M. Rohsenow, and N.E. Todreas, "Mixing Experiments in LMFBR Wire Wrapped Blanket Assemblies," COO-2245-437R MIT, April 1978.

29. R.A. Markley, et al., "Preliminary Results from the First

Radial Blanket Heat Transfer Test," Handout, Rod Bundle Thermal-Hydraulics adhoc Working Group Meeting, February 28-March 1, 1978.

30. T.R. Stauffer, et al., "Breeder Reactor Economics," Prepared for Breeder Reactor Corporation, July 1, 1975.

31. P.K. Doherty, "FIDB, A One-Dimensional Diffusion - Burnup Code for Fast Reactor Analysis," CE-FBR-74-102, Combustion Engineering, January 1974.

32. R.W. Hardie and W.W. Little, Jr., "1DX, A One-Dimensional Diffusion Code for Generating Effect Nuclear Cross Sections," BNWL-954, March 1969.

33. P.K. Doherty, "FSIG, A Cross Section Compatibility Code for Multigroup Cross Sections," CEND-102, June 1973.

34. N.R. Bhatt and R.J. Bergeron," Analysis of Protected Accidents in Advanced Core Reloads," FBR-77-88, Combustion Engineering, September 1977.

35. V. Sehgal, "Improvement of Core Orificing Design for the PRLCDS Study," FBR-78-99/21096, Combustion Engineering, Inter-Office Correspondence, March 1978.

36. Letter from P.W. Dickson (W-ARD) to V.W. Lowery (RRT), "Generic Transient Curves for Core Design Guidance," W-ARD, April 1978.

37. G.F. di Lauro and V. Sehgal, "ORIFICE-II, A Computer Program for Reactor Flow Orificing," Unpublished.

38. E.H. Novendstern, "Pressure Drop Predictions for Fuel Assemblies with Wire Wrap Spacer Systems," CONF-711009-16, October 1977.

39. D.P. Johnson, "Large Heterogeneous Reference Fuel Design

909 090

Study," GEFR-00110, GE-FBR, May 1977.

40. V. Sehgal, "A Procedure for Calculation of Beginning of Life Pitch-to-Diameter Ratio," FBR-78-07/21096, Combustion Engineering, January 1978.

41. D.A. Cantley and C.M. Cox, et al., "HEDL Steady State Irradiation Testing Program-Status Report-Thru February 1975," HEDL-TME-75-48, December 1975.

42. E. Khan, W.M. Rohsenow, A. Souin, and N. Todreas, "A Porous Body Model for Predicting Temperature Distribution in Wire-Wrapped Rod Assemblies Operating in Combined Forced and Free Convection," Nuclear Engineering and Design, 35, pp. 199-211, 1975.

43. E.H. Novendstern, "Turbulent Flow Pressure Drop Model for Fuel Rod Assemblies Utilizing a Helical Wire-Wrap Spacer System," Nuclear Engineering and Design, 22, pp. 19-27, 1972.

44. K.W. Fretz, "Impact of MIT/Chiu Flow Split and Mixing Model on Internal Blanket Thermal-Hydraulic Analysis," FBR-78-270/21270, Combustion Engineering, June 1978.

45. P.K. Doherty, et al., "Irradiation Environment and Performance of Carbide Fuel Tests in FTR," CE-FBR-77-342/21280, July 1977.

46. GEFR-10028-62, Sixty-Second Quarterly Report, "Core Engineering," February-April 1977.

47. P. O'Brien, "A Procedure for Determining the Effects of Duct-Bundle Interaction on Advanced Carbide FTR Test Assembly Design," FBR-78-12/21280, Combustion Engineering, February 1977.

Appendix A

Physics Methods and Models

The physics effort for PRLCDS was done in 2 phases. The methods and models for both are described here.

A.1 Introduction

C-E's contribution to PRLCDS was developed as a two phase effort. Phase I work dealt with analyzing several design variations. The intent of this phase was to define general trends in reactor performance as a function of varying fuel pin diameter, core height, blanket type and fuel residence time for the proliferation resistant fuel cycles being considered. This analysis provided a foundation for the selection of reactor designs that merited further investigation. The Phase II effort was a detailed analysis of those designs chosen for further investigation from Phase I.

Due to the differences in scope between the two phases, the tools used to model reactor designs are different. In Phase I, where numerous designs were considered, the one dimensional diffusion theory code F1DB[32] was used. Use of F1DB in conjunction with axial and radial blanket approximations (discussed later in this Appendix) gave a consistent set of results which allowed inter-comparison of designs of a similar fuel type. The designs selected for further analysis from the Phase I work were studied in more detail. This was accomplished through the use of the two dimensional diffusion theory code F2DB[21]. The use of F2DB in concert with a detailed core model resulted in the generation of extensive data for the designs analyzed.

This appendix highlights the reactor physics methods and core models used. It is divided into the following areas:

- computer codes used
- cross section operation and use
- description of core models
- fuel management
- control rod considerations
- material compositions

A.2 Computer Codes

As stated earlier, F1DB was used for the Phase I analysis. In addition, axial peaking factors and bucklings were based on representative 2D calculations (developed using F2DB) for the reactor design types under consideration. The Phase II work was done using F2DB. For cross-section generation and group collapsing the computer codes 1DX[32] and FSIG[33] were used.

A.3 Cross Sections

The cross-sections used in the study are based on ENDF/B-IV data. For Phase I designs, information from preliminary core designs and compositions were used to generate self-shielded cross-sections. They were collapsed from a 42 energy group set provided by HEDL[20] to 22 energy groups using the 1DX code. For the Reference, low cost Coprocessing and Denatured designs the Phase I modeling provided the spectral data necessary to collapse the 22 group structure to 4 groups using the FSIG code. These 4 group cross-section sets were used for Phase II burnup studies.

To obtain 4 group cross-sections for the Transmuter and low void worth Coprocessing designs, it was necessary to develop a preliminary two dimensional model, using F2DB, to obtain the spectral data necessary for collapsing from 22 groups using the FSIG code. Table A.1 shows the 42, 22 and 4 group energy structures. In addition, 22 group cross-sections were prepared for sodium void and Doppler coefficient calculations for each of the Phase II designs. Cross sections for the sodium void calculations were generated for both sodium in and sodium out configurations. The cross-sections for the Doppler calculation included U-238 elevated to 2100°K for all designs.

A.4 Modeling

A.4.1 Phase I

The Phase I calculations were performed with a one-dimensional radial model. For the 36" high cores an axial buckling of 0.0005713 was used. This corresponds to a reflector savings of 20 cm. The axial buckling was varied for the different core heights considered. Appropriate BOL fuel compositions were used to burn to an equilibrium cycle. Approximations were made for the axial and corner blankets with regard to breeding ratio and fissile gain over the equilibrium cycle. A detailed description of the Phase I effort is given in (10).

A.4.2 Phase II

Core Model

Phase II calculations were performed using a half-height core model in conjunction with F2DB (and employing the appropriate reflective boundary conditions). The PRLCDS Groundrules require 92% enriched B_4C control rods be parked in the upper axial blanket during equilibrium cycle burnup. Since half-height modeling was used, it was necessary to approximate control rod effects. This was accomplished by averaging the number densities of the B_4C, Na and SS in the upper axial blanket control rod positions with the number densities of the Na and SS in the lower axial blanket empty channel positions. These averaged number densities were then used as input to the F2DB burnup studies.

For the purposes of modeling, the driver region was divided into 9 zones. The first 8 are on a row by row basis. An effort was made to cylindricize the core models. This resulted in the 9th driver zone being larger than a single row of fuel, but less than two complete rows. Thus, only one zone was employed in this area. (See Figure C.1-C.5 for core layout and control rod positions).

The axial blanket follows the core zone assignments. However, in the axial direction, the blanket is broken down into two regions of 6 and 12 inches, respectively. This allows more detail with regard to the core-axial blanket interface. The radial blanket was modeled on a row by row basis. Two rows of radial reflectors, with the composition specified in the PRLCDS Groundrules, were used. An axial reflector 15" thick was used. Again its composition was specified in the PRLCDS Groundrules. Figure A.1 shows the R-Z core model for the Reference, Denatured and Transmuter Phase II designs. The model used for the Coprocessing designs is shown in Figure A.2. It includes the zone assignments used as well as the F2DB material assignments. The material assignments are described in Tables A.2 and A.3.

Fuel Management

To represent an equilibrium cycle the following were done:

- the core was managed using 1/3 refueling and a 3 cycle residence time;
- axial blanket and radial blanket managed to give representative compositions over the equilibrium cycle.

This model was used to generate BOL/EOL peak linear pin powers and charge/discharge fissile and heavy metal inventories.

Control Rods

The PRLCDS Groundrules required that 92% enriched B_4C control rods be parked in the upper axial blanket during equilibrium cycle burnup. In addition, guidelines are provided for assessing control rod requirements. Table A.4 lists these requirements. An appropriate method for determining control rod worth would be

Δk_{eff} calculations using discrete hex assembly modeling with proper boundary conditions. However, this approach was felt to be beyond the scope of this study. Therefore, the following, more approximate, method was used:

1. Use F1DB to determine the central control rod worth with Phase I final designs.
2. Determine the flux as a function of the distance from the core centerline as a function of,

$$\frac{\phi(r)^2}{\phi_{\mathrm{C\!\!\!L}}} .$$

3. Calculate the number of control rods needed from the requirements given in Table A.2 and information gained in Step 2.

A second evaluation of control rod worth was done using essentially the same methodology as stated above, with the following exceptions:

- central control rod worth calculated using F2DB;
- B_4C number densities input at 80% of full strength to stimulate self-shielding effects;
- more refined Phase II designs used in the evaluation.

This resulted in a more accurate assessment of control rod needs due to the increase flux assessment with the Phase II designs as compared to Phase I designs. Table A.5 lists the control system requirements and worths for the Reference, Denatured and Transmuter designs. Due to time constraints, simplifying assumptions were made to determine the number of control rods required in the Coprocessing designs.

A.5 Material Compositions

The volume fractions for the final designs were used in concert with the material densities presented in Table A.6 to calculate number densities used in the F2DB model. The control assembly volume fractions and material densities used are given in Table A.8. As stated earlier, the radial reflector composition was defined in the PRLCDS groundrules and is given in Table A.9. Axial reflector composition was defined by the groundrules to be the core volume fractions for the Na and SS. The feed heavy metal compositions are defined in the Groundrules and are listed in Table A.7.

Table A.1

Energy Group Structure

Lower Energy Boundary (eV)	42 Group	22 Group	4 Group
6.065×10^6	1		
3.679×10^6	2	1	
2.231×10^6	3	2	
1.353×10^6	4	3	
8.208×10^5	5	4	
4.979×10^5	6	5	1
3.877×10^5	7		
3.020×10^5	8	6	
1.832×10^5	9	7	
1.111×10^5	10	8	2
6.738×10^4	11	9	
4.087×10^4	12	10	
2.554×10^4	13	11	
1.989×10^4	14		
1.503×10^4	15	12	
9.119×10^3	16	13	3
5.531×10^3	17		
3.355×10^3	18	14	
2.840×10^3	19	15	
2.404×10^3	20		
2.035×10^3	21	16	
1.234×10^3	22	17	
7.485×10^2	23	18	
4.540×10^2	24	19	
2.754×10^2	25	20	
1.670×10^2	26		
1.013×10^2	27	21	
6.144×10^1	28		
3.727×10^1	29		

Table A.1 (Cont.)

Energy Group Structure

Lower Energy Boundary (eV)	42 Groups	22 Groups	4 Groups
2.260×10^{1}	30		
1.371×10^{1}	31		
8.315×10^{0}	32		
5.043×10^{0}	33		
3.059×10^{0}	34		
1.855×10^{0}	35		
1.125×10^{0}	36		
6.826×10^{-1}	37		
4.140×10^{-1}	38		
2.511×10^{-1}	39		
1.523×10^{-1}	40		
9.237×10^{-2}	41		
2.521×10^{-2}	42	22	4

Table A.2

Material Description for Reference, Transmuter and Denatured Designs

Material Number	Composition*
41, 86, 104	Control
42, 43, 45, 47	Inner Zone Driver
44, 46	Inner Core Driver and Control
69, 70	Outer Zone Driver
87, 88, 90, 92, 93, 94, 105, 106, 108, 110, 111, 112	Axial Blanket
89, 91, 107, 109	Axial Blanket and Control
113-118	Radial Blanket
119	Radial Reflector
120	Axial Reflector

* Volume fractions of driver, blanket, control and reflector assemblies are specified in Appendix C.

Table A.3

Material Description for Low Cost and Low Void Designs

Material Number	Composition* Low Cost	Composition* Low Void
35, 43, 50	Control	Control
36	Inner Zone Driver	Driver (Th/U)
37	Inner Zone Driver and Control	Driver and Control+
38, 39	Outer Zone Driver	Driver (U,Pu)
40, 41, 48, 49	Radial Blanket	Radial Blanket
42	Radial Reflector	Radial Reflector
44, 51	Axial Blanket	Axial Blanket (Th,U)
45, 52	Axial Blanket and Control	Axial Blanket and Control+
46, 47, 53, 54	Axial Blanket	Axial Blanket (U,Pu)
55	Axial Reflector	Axial Reflector

* Volume fractions of driver, blanket, control and reflector assemblies are specified in Appendix C.

\+ 150 (Th/U) + 63 (U,Pu) + 21 Control

909 102

Table A.4

Control System Requirements

(as defined in PRLCDS Phase II Groundrules)

I. Primary System	
	% ΔK
Hot-to-Cold Shift (to refueling)	0.94+
Reactivity Fault	0.94+
Criticality Uncertainty	0.30+
Fissile Tolerance	0.30+
Excess Reactivity at BOEC	Calculate
Stuck Rod*	Calculate
II. Secondary System	
Hot-to-Cold Shift (to standby)	0.94
Reactivity Fault	0.94
Stuck Rod*	Calculate

* Defined as 1.785 times the average worth of a single withdrawn absorber.

\+ Defined in PRLCDS Groundrules.

Table A.5

Control System Requirements and Worths

	Reference	Tranmsuter	Denatured
Requirements, %ΔK			
Primary System	4.60	7.39	8.67
Secondary System	3.18	4.38	3.36
Total Requirements	7.83	11.77	12.03
Total Worth	9.13	12.81	14.39

Table A.6

Densities and Molecular Weights

	g/cc	g/mole
SS 316 @ 70^{o}F	7.962	56.035
Na @ 800^{o}F	0.8498	22.990
UC	13.61	250.041
ThC	10.6	244.049
PuC	13.49	251.163
(Th,Pu)C	11.08	245.473

Pellet Density: 0.98 T.D.

Table A.7

Isotopic Compositions
(from PRLCDS Groundrules)

Feed	Pu	wt%
	Pu 38	0.997
	Pu 39	67.272
	Pu 40	19.209
	Pu 41	10.127
	Pu 42	2.395
Feed	U	
	U 33	75.2
	U 34	21.1
	U 35	3.0
	U 36	0.7
Fertile	U	
	U 35	0.2
	U 38	99.8
Fertile	Th	
	Th 32	100.0

Table A.8

Control Assembly Volume Fractions*

Inserted Control Assembly Volume Fractions	
B_4C	0.3120
Sodium	0.2282
Structure	0.3180
Gap	0.1418
Empty Channel Volume Fractions	
Sodium	0.905
Structure	0.095
B_4C Density	2.52 g/cm^3
Mass	52.382 g/mole

* Based on CRBR Primary Control Assembly Design specifications.

Table A.9

Radial Reflector Composition

Fe	2.16295×10^{-2} atoms/barn-cm
Ni	4.16394×10^{-2} atoms/barn-cm
Cr	1.39364×10^{-2} atoms/barn-cm
Na	2.03549×10^{-2} atoms/barn-cm

FIG. A.1

CORE LAYOUT FOR REFERENCE, TRANSMUTER, AND DENATURED DESIGN

1 (41)	1=ZONE # (41)=Mat'l.#

AXIAL REFL.	35 (120)												
AXIAL BLNKT.	19 (104)	20 (105)	21 (106)	22 (107)	23 (108)	24 (109)	25 (110)	26 (111)	27 (112)	31 (116)	32 (117)	33 (118)	34 (119)
	10 (86)	11 (87)	12 (88)	13 (89)	14 (90)	15 (91)	16 (92)	17 (93)	18 (94)				
DRIVERS	1 (41)	2 (42)	3 (43)	4 (44)	5 (45)	6 (46)	7 (47)	8 (69)	9 (70)	28 (113)	29 (114)	30 (115)	
	INNER DRIVERS							OUTER DRIVERS		RADIAL BLANKET			RADIAL REFLECTOR

FIG. A.2

CORE LAYOUT FOR HIGH INTERNAL CONVERSION/LOW COST-LOW VOID DESIGNS

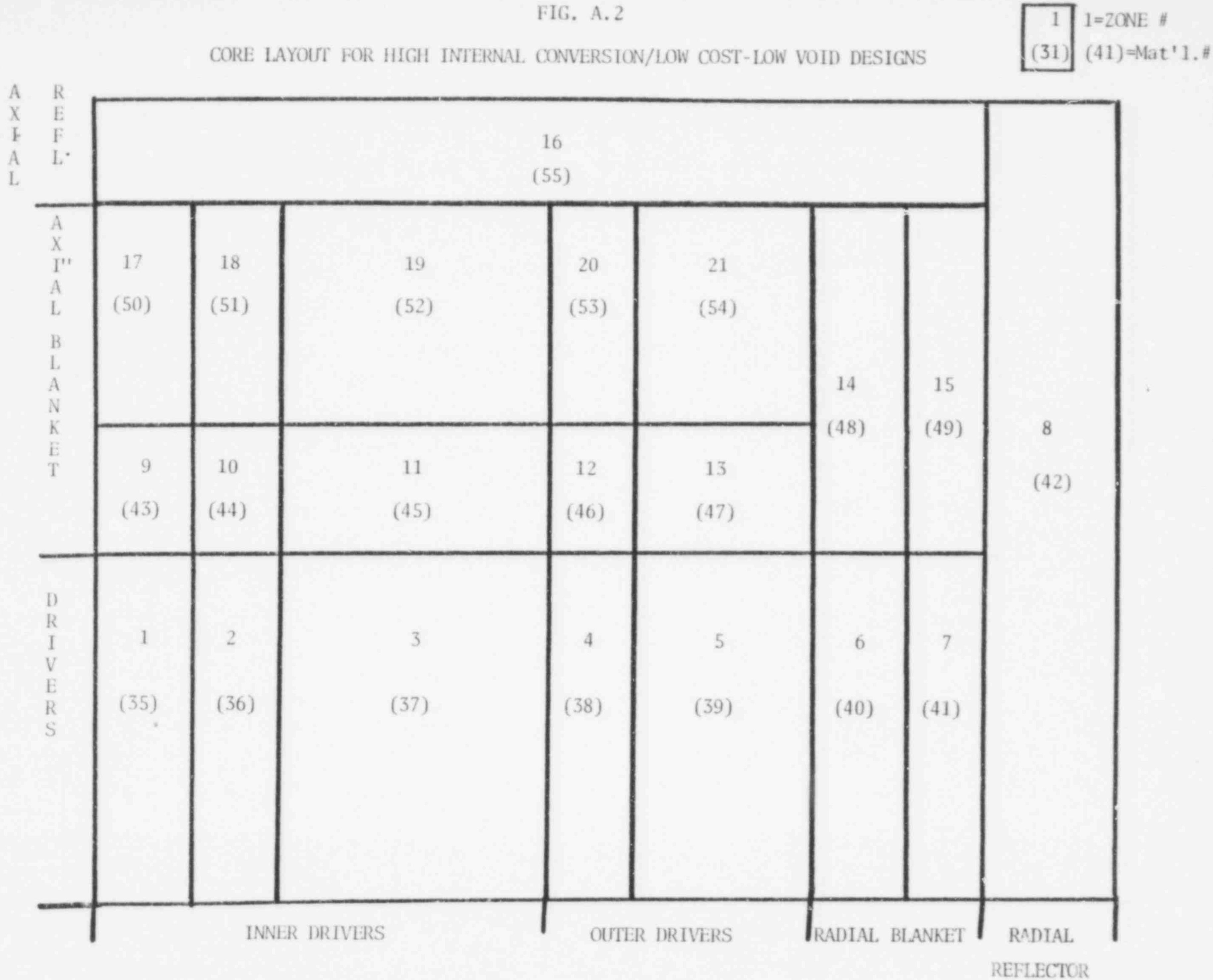

909 110

Appendix B

Thermal, Hydraulic and Mechanical Design Methods

The procedures and assumptions used in the thermal, hydraulic and mechanical design and performance analysis are described here.

909 111

B.1 Introduction

The mechanical and thermal-hydraulic design of the PRLCDS cores is a multi-step process. The reactor coolant mass flow rate is calculated on the basis of the desired reactor vessel coolant temperature rise. Flow is then allocated to the various regions of the reactor based on performance constraints and cooling requirements. Orificing for equal end of life cladding temperatures is used for approximating equal driver assembly lifetimes. The radial blanket assemblies are orificed for an end of life 2σ cladding midwall temperature of $677^{O}C$ ($1250^{O}F$) ; an operating temperature demonstrated below to be compatible with transient temperature limits. Following the determination of the peak powered assembly flow rate, assembly sizing calculations are performed. Coolant velocity, pressure drop, and duct/bundle interaction (DBI) constraints dictate the interior pin-to-pin spacing and bundle dimensions. The driver assemblies are designed for a two year lifetime with stainless steel materials and straight-start wire wrap configuration. With the bundle dimensions determined, advanced stainless steel material and locked wire wrap configuration are then substituted, and a new residence time based on DBI is calculated. The duct wall thickness and inter-assembly gaps are accordingly adjusted to be similar to the reference designs lattice pitch. An exact match can be obtained with a slight adjustment of the pin diameter. The design limiting assembly temperatures are obtained by employing hot channel methodology specified in the PRLCDS Groundrules for cladding temperature calculations. The program, SUPERENERGY, is used to predict nominal duct temperatures.

B.2 Core Orificing

The following constraints as specified in the PRLCDS Groundrules are satisfied:

1. An adiabatic bypass flow of 5%. The remaining 95% of the total

909 112

reactor flow is allocated for fuel and blanket cooling.

2. Maximum nominal mixed mean coolant temperature of 579°C (1075°F).

3. Maximum 2σ cladding midwall temperature of 677°C (1250°F) at end of life condtions.

Based on engineering judgement for appropriate design margin, the following additional constraints are also imposed.

4. Radial blanket assemblies overcooling of 100% for the preliminary design effort. In the final design effort, the radial blanket assemblies are orificed for 2σ temperatures of 677°C (1250°F) at end of life conditions.

5. Minimize the number of discriminator zones.

The behavior of carbide blankets during transients was assessed to obtain an acceptable steady state temperature limit. The E-16 transient was found to be the most limiting. A steady-state 2σ cladding midwall temperature of 677°C (1250°F) was determined to be limiting. The three transient events evaluated in the assessment are defined in Table B.1. The C-E analysis included examination of the U-2b and E-16 transients. These two transients are the most severe upset and emergency events for the CRBRP advanced reload cores. The peak cladding midwall temperature limits for the different transients, obtained from the CRBRP PSAR[19] are given in Table B.2. These are conservative limits such that incremental damage to the cladding is acceptable. Using the E-16 and U-2b transient cladding temperature limits shown in Table B.2, a representative transient power-to-flow ratio of 1.5[34], and a reactor inlet temperature of 352°C (666°F), allowable steady state peak cladding temperatures were calculated[35]. The results are shown in Table B.2 under C-E analysis.

To verify the transient temperature constraints, an assessment of the transient limitation for the radial blanket assemblies based on extrapolation of W-ARD Generic Transient Curves[36] was also made. In the W-ARD analysis, sets of curves for fuel and radial blanket pin behavior are presented for the three transients, the U-2b (rod withdrawal at 100% power), E-16 (natural circulation event) and F-1 (safe shutdown earthquake). The 14.48 mm (0.570") O.D. pin was selected to be representative of the PRLCDS radial blanket assembly designs. The transient curves were extrapolated with blanket operating conditions to yield steady-state operating limits. The temperature limits are given in Table B.1. Once again, the E-16 transient and its associated steady-state cladding temperature is most limiting.

The variance between the W-ARD and C-E transient results is primarily due to computer modeling. Somewhat different power and flow characteristics account for the differences in magnitude. The resulting trends are notably similar. In both cases, the E-16 transient provides the limiting steady state temperature. Since, the W-ARD results provide the lower allowable temperature, an EOL steady state 2σ cladding midwall operating temperature of $677^{o}C$ ($1250^{o}F$) is selected.

Design objectives included minimizing the number of discriminator zones in the orificing effort. The potential benefits of lower cladding temperatures and greater assembly lifetimes were compared to the disadvantages of increasing the number of orifice zones. Associated with an increased number of discriminator zones are higher pumping, fabrication, plant refueling and maintenance expenditures. The number of zones was kept well below the PRLCDS Ground Rules limit of fifteen, allowing ample margin for core reorificing and optimization in future, more detailed analyses.

Orificing the peak driver assembly of each zone for equal end of life cladding temperatures is the criteria used for approximating equal lifetimes. The end of life cladding temperature is the most significant parameter relating to fuel pin lifetime. Previous CDF analysis performed by HEDL[23] for the LHRFDS study indicates the cladding temperature history has greater impact on lifetime if the beginning of life cladding temperature is selected to be the point of reference. However, when pin lifetime was calculated as a function of end of life temperature; the results indicate that end of life cladding temperature has the greatest impact on lifetime, temperature and power history are secondary factors. Hence, the justification of orificing for equal end of life cladding temperatures.

The computer program, ORIFICE-II[37] is used to allocate flows to the driver region based on the concept of equal end of life cladding temperatures in the final design effort. In order to perform core orificing, the end of life peak assembly power characteristics are determined. Assemblies with nearly the same power characteristics are grouped into an orifice zone. Generally, assemblies with large power peaking, characteristic of the outer enrichment zone need to be modeled more discretely. The peak powered assembly is the target assembly of each orifice zone. Orifice zone flow is assigned in proportion to the power characteristics of the target assemblies. Initially, orifice zone flows are calculated such that equal core exit cladding midwall temperatures are obtained. The peak cladding temperatures and relative axial locations are also calculated. ORIFICE-II revises the flow into the orifice zones while keeping the total flow rate constant. The iterations on flow continue till the peak end of life cladding midwall temperatures are nearly equal.

An approximate orificing scheme was used for assembly sizing and peak assembly temperature characterization of the preliminary reactor design. Peak driver assemblies orificed for equal mixed mean outlet temperature at middle of life (MOL) conditions is an approximation to the recommended criteria. This approximation yields flows within 3% of the allocation from the recommended criteria of equal end-of-life cladding temperatures. Contingent upon available core power characteristics and/or time constraints, the approximate orificing scheme can be employed.

B.3 Methodology for Hot Channel Analysis

The peak midwall cladding temperatures for the driver and radial blanket regions were calculated using the hot channel factors(1) listed in Tables B-3 and B-4. The statistical hot channel factors are given for plant thermal and hydraulic design conditions and plant expected operating conditions. For cladding temperature calculations, the plant expected operating conditions hot channel factors are used. The effect of intra-assembly flow maldistribution is included in the nominal coolant temperature calculation. To reflect design conservation, no credit for inter-channel coolant mixing is included in the nominal coolant temperature calculation. The heat flux factor was modified to reflect nuclear modeling uncertainties. The Reference, Transmuter and Denatured designs include direct uncertainty factors of 1.01 and 1.05 for the inner and outer enrichment zones. Similiarly, for the low void worth Coprocessing core, the modified direct heat flux factor includes 1.01 and 1.05 design uncertainty reflecting the Th-U and Pu-U region material compositions. The heat flux factor is applied in calculating the 2 sigma temperature increase between the coolant and cladding midwall.

B.4 Assembly Sizing Calculations

Following the determination of the peak powered assembly mass flow rate using the AOS method, assembly sizing calculations are performed. The computer program ASK(14), Assembly Sizing Kalculations, calculates the bundle dimensions and pressure losses given the assembly mass flow rate, coolant velocity, and coolant properties. Friction and momentum losses due to sudden area expansion and contraction are included in the pin bundle model. The pressure loss enhancement due to wire wraps is not explicitly included in the model. The Novendstern's friction factor multiplier[38] is used to calculate the effect of the wire wrap on pin bundle friction losses. In accordance with the accuracy estimate of the Novendstern's friction factor multiplier, pin bundle friction losses included a 14% uncertainty factor. An additional 6% design margin for helical pitch selection is imposed. A total uncertainty of 20% is attached to the pin bundle friction losses. Therefore, substantial margin exists for assembly redesign with advanced spacer concepts. The inlet/orifice/shield module losses were computed using GE LHRFDS homogeneous reactor core data[39]. The effects of bundle free flow area and mass flow rates are included in the extrapolations. Exit losses are simply caused by the sudden expansion of the coolant into the upper plenum region.

The assembly design procedure included allowances for duct/bundle interaction. The pin pitch-to-diameter (P/D) ratio is evaluated using assembly pressure loss, coolant velocity, and duct/bundle interference constraints. The pin pitch to diameter ratio is then the calculated maximum P/D. The beginning of life (BOL) P/D calculation procedure[40] is described in Section B.6. Briefly, the BOL P/D ratio is selected such that duct/bundle interference does not restrict assembly residence time for a specified operating environment. The BOL P/D can be calculated knowing the duct/bundle interference, bundle size, and wire wrap configuration. If the duct/bundle interference calculations indicate a looser P/D than the thermal-hydraulic constraints, the coolant velocity and pressure losses are recalculated using the new bundle dimensions. A bundle porosity of 4.0 mils/ring is used for the fuel assembly duct/bundle interference calculations. This porosity is based on vibrational test data[41] and represents an aggressive design limit.

B.5 Duct Temperatures

Duct temperatures are calculated for the design limiting assemblies of the inner and outer enrichment zones. High power, burnup and flux are characteristic of the design limiting assembly. Temperatures are calculated for BOL and EOL conditions. The SUPERENERGY[24] computer program calculates coolant and duct temperature distributions. SUPERENERGY employs a subchannel model of the fuel bundle and provides for energy exchange between each of the pins and surrounding coolant. Inter-assembly heat transfer or heat transfer within the cladding is not considered in this study. Axial and within assembly radial power distributions are explicitly included in the calculations. Inter-channel coolant mixing and energy redistribution are modeled by an enhanced effective eddy diffusivity and a swirl flow parallel to the duct wall.

The MIT mixing model[25,26,27,28] and the revised correlations for eddy diffusivity and swirl flow were employed in conjunction with SUPERENERGY. The flow split model and the correlations were developed from calibrations of the available test data for wire wrapped LMFBR assemblies. The MIT-Chiu correlation[27] for eddy diffusivity has an expanded range of applicability (P/D ratio $\geq$ 1.067). The previously available correlation proposed by Khan[42] was inapplicable for P/D's lower than 1.14. For P/D's greater than 1.14, MIT-Chiu and Khan correlations are in agreement. The MIT-Chiu flow split model also provides better agreement with the test data than the Novendstern-Sangster model[43]. The Novendstern-Sangster model was evaluated against the MIT-Chiu flow split model. The interior subchannel-to-average velocity ratio, X_1, indicative of magnitude of the intra-assembly flow maldistribution factor, was computed as a function of bundle size, pitch-to-diameter (P/D) ratio, and helical pitch to diameter (H/D) ratio[44]. The MIT-Chiu model predicts X_1 to be strongly dependent on H/D and P/D, whereas the Novendstern-Sangster model predicts X_1 to be only dependent on P/D for a given bundle size. The MIT-Chiu model indicates the flow maldistribution for fuel bundles could be reduced by selection of an optimum P/D and H/D combination. Predictions of the WARD-HT data[29] using SUPERENERGY and the revised flow split and mixing parameters were compared with COTEC results. SUPERENERGY over-predicts the coolant temperature distribution while COTEC under-estimates the peak coolant temperature. The W-ARD recommended flow maldistribution uncertainty factors of 1.08 and 1.10 for fuel and radial assemblies are obtained from a similar calibration analysis. Based on our analysis, flow maldistribution uncertainty factors of 1.03 and 1.05 for fuel and blanket assemblies are recommended. These uncertainties are consistent with our analytical methods. Application of the W-ARD recommended values for our hot channel analysis imposes additional conservation in our cladding temperatures. Revision of the CRBR hot channel factors would result in lower cladding temperatures.

B.6 Duct/Bundle Interaction and BOL P/D Calculational Procedure

The calculation of duct/bundle interference and a BOL P/D based on duct/bundle interference calculations will be described in this section. The larger growth of the pin bundle relative to the duct results in the dispersion of the pins within the duct with the consequence of reduced pin-to-pin clearances. The calculated growth of the pin bundle relative to the duct is defined as the duct/bundle interference (DBI). This differential growth of the pin relative to the duct is calculated at one inch intervals along the fueled region of the assembly. To be conservative, the minimum value of duct dilation is assumed in the duct/bundle interference calculations. Duct dilation due to irradiation creep is neglected. However, duct dilation due to thermal expansion is included in the calculations.

The C-E Simplified Procedure for Bundle Dilation[45] assumes that the integral behavior of the pin bundle may be predicted by analysis of a single pin at nominal operating conditions. he dilation of the pin and wire wrap is then expanded geometrically to yield the total across-corners bundle dilation. The pin dilation includes stress free swelling and thermal expansion of the pin and wire, and irradiation creep and stress-affected swelling of the pin alone. Irradiation creep of the pin is primarily due to stress caused by fission gas pressure buildup in the pin. The gas pressure is calculated incrementally over life using the perfect gas law. A fission gas release rate of 25% is assumed for the sodium bonded pins. The total across-corners bundle dilation is subtracted from the duct dilation to yield duct/bundle interaction. Initial porosity is accounted for in the duct/bundle interference calculations. The initial clearance between the pin bundle and inside duct wall is subtracted from the duct/bundle interaction to yield the duct/bundle interference.

The minimum allowable BOL P/D can be calculated based on duct/bundle interference calculations. General Electric's mechanical compression testing results[46] indicate the interior pin-to-pin clearance to be a function of duct/bundle interference. The compression testing data was extrapolated for bundle sizes other than 217 pins[47]. An expression relating the allowable across-corners interference as a function of assembly design and operating parameters was derived[35]. Using expression (1) and by performing one duct/bundle interference calculation for an approximate bundle size and operating conditions, the wire wrap diameter can be determined. The wire diameter is given by:

$$D_W = \frac{I}{A_5(A_1N_p^2 + A_2N_p + A_3)} + A_4D_p \qquad (1)$$

I: Across-corners Interference, the differential bundle growth after assembly clearance (initial porosity) has closed, inches (cm).

$A_1 = 6.7527 \times 10^{-6}$

$A_2 = -5.5880 \times 10^{-3}$

$A_3 = 2.3882$

$A_4 = (P/D)_{EOL} - 1$

Desired Wire Wrap Configuration

A_5 = 2.5119 in. (6.3802 cm) Straight Start

3.3492 in. (8.5069 cm) Locked Wire

N_p = Number of pins/assembly

D_p = Pin diameter, inches (cm)

D_w = Wire wrap diameter, inches (cm)

The beginning of life pitch-to-diameter ratio can then be calculated using the following equation.

$$\text{BOL P/D} = 1 + \frac{D_w + C_w}{Dp} \qquad (2)$$

where C_w is the clearance between the wire wrap and the adjacent pins. This clearance per pin is simply related to the assembly porosity by

$$C_{db} = \left\{ \sqrt{3}\,(N_R - 1) + 2 \quad C_w \right\} \qquad (3)$$

and

C_{db}: Duct/bundle clearance, the diametral clearance between the tight packed bundle outer flat-to-flat and the duct inner flat-to-flat.

N_R: Number of rows of pins, center pin is first row.

C_{db}/N_R: Porosity per ring.

This BOL P/D calculation technique was applied to in the selection of the preliminary assembly designs.

B.7 Duct Dilation Procedures

Duct dilation calculations are performed for the design limiting duct. The design limiting duct is located in the high flux and temperature region of the core and possess the greatest pressure differential across the duct wall. These factors produce the maximum dilation of the duct and are conservative for assembly design. The flat-to-flat duct dilation due to irradiation induced swelling and creep is calculated at one inch axial intervals along the fuel region. The greatest of these values is the maximum duct dilation. Nominal and nominal + 1σ values for duct dilation are calculated. The nominal + 1σ values include material property uncertainties. Inter-assembly gaps are set equal to the maximum dilation for a specified residence time.

Table B.1

Definition of Umbrella Transients

Upset Event: U-2b Uncontrolled Rod Withdrawal from 100% Power

An instantaneous withdrawal of one control rod while the reactor is at full power is assumed. The reactor power increases from 100% to 115% instantaneously. This setting, with full sodium flow, is held for five minutes at which time a manual scram is assumed.

Emergency Event: E-16 Tree-Loop Natural Circulation

From intial conditions of full power, this transient involves the loss of all (i.e., preferred, reserved, and standby) power supplies. All sodium pumps coastdown simulataneously, and natural circulation is established in all circulation loops. Feedwater is supplied to the steam generators after a 30 second delay through a turbine driver auxiliary pump.

Faulted Event: F-1 (SSE) Safe Shutdown Earthquakes

The F-1 event results from an 60¢ reactivity insertion following core compaction. Loss of off-site power and pump coastdown is assumed to occur due to the seismic disturbance.

Table B.2

Limiting Cladding Temperatures for Radial Assemblies Based on Transients

Allowable E-16 Transient Peak Cladding Midwall Temperature 3σ, °C (°F)	871 (1600)	
U-2b Transient (115% Overpower) Allowable Transient Peak Cladding Midwall Temperature, 3σ, °C (°F)	788 (1450)	
F-1 (SSE) Allowable Transient Peak Cladding Midwall Temperature, 3σ, °C (°F)	871 (1600)	
	C-E Analysis	W-ARD Transient Analysis
Calculated Allowable Steady-State Peak Cladding Midwall Temperature, °C (°F)		
E-16 Transient		
3σ	698.3 (1298)	687.8 (1270)
2σ	686.7 (1268)	676.7 (1250)
U-2b Transient		
3σ	748.9 (1380)	742.2 (1368)
2σ		
F-1 (SSE)		
3σ	----	798.9 (1470)
2σ		

TABLE B-3

FUEL ASSEMBLIES ROD TEMPERATURES HOT CHANNEL/SPOT FACTORS

		Coolant	Film	Cladding	Gap	Fuel	Heat Flux
DIRECT$^{(+)}$							
Power Level Measurement and Control System Dead Band		1.03					1.03
Inlet Flow Maldistribution		1.05					
Subassembly Flow Maldistribution			1.035				
Calculational Uncertainties		1.08					
Cladding Circumferential Temperature Variation			$1.0^{(\Diamond)}$ $1.7^{(*)}$	$1.0^{(\Diamond)}$			
STATISTICAL $(3\sigma)^{(o)}$							
Inlet Temperature Variation		$1.02^{(\phi)}$ $1.0^{(\dagger)}$					
Reactor ΔT Variation		$1.04^{(\phi)}$ $1.0^{(\dagger)}$					
Nuclear Data		1.06					1.065
Fissile Fuel Maldistribution		1.01					1.035
Wire Wrap Orientation		1.01					
Subchannel Flow Area		1.028	1.0				
Film Heat Transfer Coefficient			1.12				
Pellet-Cladding Eccentricity			1.15	1.15			
Cladding Thickness & Conductivity				1.12			
Gap Conductance					$1.48^{(1)}$		
Fuel Conductivity						1.10	
Coolant Properties		1.01					
TOTAL	2σ	$1.232^{(\phi)}$ $1.221^{(\dagger)}$	1.168 $1.986^{(*)}$	1.128			1.081
	3σ	$1.264^{(\phi)}$ $1.248^{(\dagger)}$	1.234 $2.101^{(*)}$	1.192	1.48	1.10	1.106

(+) Uncertainties due to physics analysis calculational methods and control rod effects (4% on coolant enthalpy rise is applied directly on nuclear radial peaking factors.

(*) For cladding midwall temperature calculations. Applies to nominal temperature drop between cladding midwall and bulk coolant.

(◊) For fuel temperature calculations.

(o) In addition, the assembly inlet temperature will be increased by 16°F. to account for primary loop temperature control uncertainties.

(1) Applies to BOL conditions.

(φ) Applies to Plant Expected Operating Conditions.

(†) Applies to Plant T&H Design Conditions.

909 125

TABLE B.4

RADIAL BLANKET ASSEMBLY ROD TEMPERATURE HOT CHANNEL/SPOT FACTORS

	Coolant	Film	Cladding	Gap	Fuel	Heat Flux
DIRECT(+)						
Power Level Measurement and Control System Dead Band	1.03					1.03
Inlet Flow Maldistribution	1.07					
Assembly Flow Maldistribution		1.05				
Calculational Uncertainties	1.1					
Cladding Circumferential Temperature Variation		1.0(Δ) 2.2(*)	1.0(Δ)			
STATISTICAL (3σ)(o)						
Inlet Temperature Variation	1.02(ϕ) 1.0(†)					
Reactor Δ Variation	1.04(ϕ) 1.0(†)					
Nuclear Data	1.08					1.09
Fissile Fuel Maldistribution	1.01					1.01
Wire Wrap Orientation	1.01					
Subchannel Flow Area	1.035	1.0				
Film Heat Transfer Coefficient		1.21				
Pellet-Cladding Eccentricity		1.15	1.15			
Cladding Thickness & Conductivity			1.12			
Gap Conductance				1.48		
Fuel Conductivity					1.10	
Coolant Properties	1.01					
TOTAL 2σ	1.292(ϕ) 1.284(†)	1.231 2.708(*)	1.128			1.092
TOTAL 3σ	1.332(ϕ) 1.320(†)	1.321 2.906(*)	1.192	1.48	1.10	1.123

(+) Uncertainties due to physics analysis calculational methods and control rod effects are applied directly on nuclear radial peaking factors. These uncertainty factors are as follows. On coolant enthalpy rise: 1.13 for row 10 at BOC; 1.03 for row 10 at EOC; 1.05 for rows 11 & 12 at BOC; 1.0 for rows 11 & 12 at EOC. On heat flux: 1.19 for row 10 at BOC; 1.08 for row 10 at EOC; 1.10 for rows 11 & 12 at BOC; 1.00 for rows 11 & 12 at EOC.

(o) In addition, the assembly inlet temperature will be increased by 16°F, to account for primary loop temperature control uncertainties.

(*) For cladding midwall temp. calculations. Applies to nominal temp. drop between cladding midwall and bulk coolant.

(Δ) For fuel temperature calculations.

(ϕ) Applies to Plant Expected Operating Conditions.

(†) Applies to Plant T&H Design Conditions.

Appendix C

Breeder Reactor Design and Performance Data

The attached documentation details the physical configuration and performance of the five C-E PRLCDS homogeneous carbide designs. Core maps, fuel isotopic inventories, neutron balances, flux and power distributions are provided for each.

Table C.1

Breeder Reactor Design and Performance Data

Reactor Designation	Ref.	Low Void	Low Cost	Den.	Trans.			
1.0 <u>Core and Reactor Data</u>								
1.1 Power Information								
Plant Thermal Power, MWt	3000	3000	2740	2880	3000			
Plant Electric Power, MWe	1095	1095	1000	1051	1095			
Core Power Density, MWt/l (MOEC)	.428	.325	.399	.402	.393			
Net Electric Power								
Plant Capacity Factor %	70.	70.	70.	70.	70.			
Power Split, Fraction of Total (MOEC)								
Core Fuel	.9270	.9667	.9662	.9555	.9357			
Axial Blanket	.0322	.0212	.0214	.0188	.0279			
Radial Blanket	.0408	.0121	.0124	.0257	.0364			
Internal Fertile Assembly . . . . (including axial extension)	.0	.0	.0	.0	.0			
Other	.0	.0	.0	.0	.0			
Average Linear Power (MOEC)								
Core Fuel, kW/m	62.70	64.53	55.98	57.82	63.29			
Axial Blanket, kW/m	2.54	1.42	1.24	1.33	2.20			
Radial Blanket, kW/m	3.14	.87	.88	1.90	3.06			
Internal Fertile Assembly, kW/m	----	----	----	----	----			
Fission Energy and Deposition, MeV/fission .	207.	207.	207.	207.	207.			
1.2 Temperature Information								
Core Inlet Temperature, ^{o}C	343.3	343.3	343.3	343.3	343.3			
Core Average Outlet Temperature, ^{o}C	510.5	508.9	509.4	509.8	511.3			
Core ΔT, ^{o}C.	167.2	165.6	166.1	166.5	168.0			
Reactor Inlet Temperature, ^{o}C	343.3	343.3	343.3	343.3	343.3			
Reactor Outlet Temperature, ^{o}C	498.9	498.9	498.9	498.9	498.9			
Reactor ΔT, ^{o}C	155.6	155.6	155.6	155.6	155.6			

Table C.1 (Cont.)

Reactor Designation	Ref.	Low Void	Low Cost	Den.	Trans.			
Number of Core Orifice Zones	6	5		6	6			
Peak Assembly Mixed Mean Coolant Outlet Temperature (2σ), ^{o}C	565.4	567.7		594.5	559.4			
Nominal Duct Temperature, ^{o}C Design Limiting Duct (X/L = 1.0)	472.9	460.4		498.9	471.1			
Peak Cladding Temperature (2σ, Midwall), ^{o}C								
BOL	694.0	674.0		710.7	701.7			
EOL	658.4	667.6		636.6	662.5			
Fuel Centerline Temperature (2σ), ^{o}C Design Limiting Pin								
Peak	1103.9	1026.5		1155.7	1119.1			
Average	----	----	----	----	----			
1.3 Coolant Information								
Bundle Pressure Drop, kPa (Peak Power Assembly)								
Driver	628.1	515.0		397.1	423.3			
Internal Fertile Assembly	----	----		----	----			
Radial Blanket								
Primary System Pressure Drop, kPa								
Flow Split, Fraction of Total								
Core.	.8976	.9312	.9252	.9137	.8969			
Radial Blanket	.0524	.0188	.0248	.0363	.0531			
Internal Fertile Assembly	----	----	----	----	----			
Other	.0500	.0500	.0500	.0500	.0500			
Total Coolant Mass Flow Rate, kg/hr.	5.25×10^7	5.25×10^7	4.99×10^7	4.85×10^7	5.25×10^7			
Maximum Coolant Velocity, m/sec	10.67	9.14	10.67	8.53	9.14			
1.4 Geometric Information (see Figure II-1)								
Core Height, cm	106.7	91.4	91.4	106.7	106.7			
Equivalent Diameter [(1)], cm	441.0	510.5	451.7	440.8	448.6			

(1) Diameter of the envelope including the outer edge of the core.

909 129

Table C.1 (Cont.)

Reactor Designation	Ref.	Low Void	Low Cost	Den.	Trans.			
Core Volume, L	11,072	14,400	11,073	11,212	11,599			
Axial Blanket Height, cm	45.7 →							
Radial Blanket Height, cm	198.1	182.9	182.9	198.1	198.1			
Axial Shield Height, cm.	38.1	38.1	38.1	38.1	38.1			
Number of Core Enrichment Zones	2	2	2	2	2			
Number of Assemblies								
Drivers by Enrichment Zone.	126/120	156/231	60/246	120/144	126/120			
Internal Fertile Assemblies	----	----	----	----	----			
Radial Blankets	216	252	216	216	198			
Control Rods	13	22	16	19	19			
1.5 Fuel Management								
Refueling Interval, calendar days	296.	365.	395.	347.	329.			
Fuel Residence Time, calendar days	887.	1095.	789.	1041.	986.			
Blanket Residence Time, calendar days . . .	1500.	1825.	1971.	1736.	1743.			
Fraction of Assemblies Replaced at Each Refueling								
Fuel Assemblies by Enrichment Zone . . .	1/3/1/3	1/3/1/3	1/2/1/2	1/3/1/3	1/3/1/3			
Radial Blanket Assemblies	1/5	1/5	1/5	1/5	1/5			
Interior Fertile Assemblies	----	----	----	----	----			
2.0 Fuel Assembly Data(2)								
2.1 Pins per Assembly	169	127	169	169	169			
2.2 Pin Pitch-to-Diameter Ratio.	1.198	1.106	1.174	1.240	1.240			
2.3 Spacer Description								
Wire Wrap Diameter, mm	1.80	1.21	1.57	2.07	2.20			
Spacer Pitch, cm	30.48 →							
Edge Ratio	1.0 →							
2.4 Overall Bundle Length, cm	251.5	228.6	228.6	251.5	251.5			

(2) Only variations from this assembly design are listed for internal fertile, radial blanket and control assemblies.

Reactor Designation	Ref.	Low Void	Low Cost	Den.	Trans.			
2.5 Lattice Pitch, cm	16.48	16.58	16.12	16.21	17.09			
2.6 Duct Inside Flat-to-Flat, cm.	14.96	15.16	14.65	14.69	15.52			
2.7 Bundle Porosity, mm/ring	.102 →							
2.8 Duct Wall Thickness, mm	3.81	3.56	3.81	3.81	4.06			
2.9 Interduct Gap, mm	7.62	7.11	7.11	7.62	7.62			
2.10 Duct Material								
Material Type			Advanced Alloy					
Swelling Properties.			See Ground Rules					
Irradiation Creep Properties								
3.0 Fuel Pin Data								
3.1 Fuel Parameters								
Fuel Type (oxide, carbide, nitride). . . .	Carbide →							
Stoichiometry (O/M, C/N, N/M).	1.044	1.044	1.044	1.042	1.023			
BOL Fissile Enrichment (fiss/HM), w/o . .								
Inner Zone	0.095	0.095	0.090	0.968	0.141			
Outer Zone	0.117	0.099	0.100	0.118	0.174			
Fuel Form (powder or pellet)	pellet →							
Pellet Diameter, mm.	7.67	10.35	7.95	7.29	7.70			
Pellet Density, g/cm (3)	13.22	*	13.22	13.31	10.83			
Fuel Smear Density, % T.D.	77.	87.	83.	78.	78.			
3.2 Cladding Parameters								
Cladding Outside Diameter, mm	9.40	11.94	9.40	8.89	9.40			
Cladding Wall Thickness, mm.	.38	.48	0.38	.36	.38			
Cladding Material (4)								
Material Type			Advanced Alloy					
Swelling Properties								
Irradiation Creep Properties			See Ground Rules					
Stress-Rupture Properties.								
3.3 Bond Type (sodium or helium).	Sodium →							

* 13.22 for Pu/U fuel; 10.65 for Th/U fuel.

(3) If powder fuel is utilized, this should be specified along with smear density.

(4) Information included for internal fertile, radial blanket, and control pins only if different.

Table C.1 (Cont.)

Reactor Designation	Ref.	Low Void	Low Cost	Den.	Trans.			
3.4 Strasser Sleeve Parameters								
Sleeve Outside Diameter, mm	8.31	11.11	8.25	7.92	8.36			
Sleeve Wall Thickness, mm	.076 →							
Fractional Perforation of Sleeve	45% →							
Sleeve Material.			Advanced Alloy					
3.5 Equivalent Plenum Volume, cc								
Top Plenum	31.2	43.2	26.8	28.0	31.2			
Bottom Plenum	----	----	----	----	----			
4.0 <u>Radial Blanket Assembly Data</u>								
4.1 Pins per Assembly	91 →							
4.2 Pin Pitch-to-Diameter Ratio	1.071 →							
4.3 Spacer Description								
Wire Wrap Diameter, mm	.97	.97	.94	.94	.99			
Spacer Pitch, cm	30.48 →							
Edge Ratio	1.0 →							
4.4 Overall Bundle Length, cm	251.5	228.6	228.6	251.5	251.5			
4.5 Duct Inside Flat-to-Flat, cm	15.27	15.42	14.95	14.99	15.88			
4.6 Duct Wall Thickness, mm	2.29 →							
5.0 <u>Radial Blanket Pin Data</u>								
5.1 Fuel Parameters								
Fuel Type (oxide, carbide, nitride). . .	Carbide →							
Stoichiometry (O/M, C/M, N/M).	1.026	1.000 →						
EOL Fissile Enrichment (fiss/HM), w/o .								
Fuel Form (3) (powder or pellet)	pellet →							
Pellet Diameter, mm	13.53	13.68	13.23	13.25	14.11			
Pellet Density, g/cm^3.	13.31	10.39	10.39	10.39	10.39			
Fuel Smear Density, % T.D.	96.4 →							
5.2 Cladding Parameters								
Cladding Outside Diameter, mm	14.66	14.81	14.35	14.38	15.24			
Cladding Wall Thickness, mm	.508 →							

Table C.1 (Cont.)

Reactor Designation	Ref.	Low Void	Low Cost	Den.	Trans.			
5.3 Bond Type (sodium or helium)	Helium →							
5.4 Strasser Sleeve Parameters								
Sleeve Outside Diameter, mm	----	----	----	----	----			
Sleeve Wall Thickness, mm	----	----	----	----	----			
Fractional Perforation of Sleeve.	----	----	----	----	----			
Sleeve Material	----	----	----	----	----			
5.5 Equivalent Plenum Volume, cc								
Top Plenum	116.9	102.4	95.8	112.2	127.1			
Bottom Plenum	----	----	----	----	----			
6.0 Internal Fertile Assembly Data								
6.1 Pins per Assembly.	----	----	----	----	----			
6.2 Pin Pitch-to-Diameter Ratio.	----	----	----	----	----			
6.3 Spacer Description								
Wire Wrap Diameter, mm	----	----	----	----	----			
Spacer Pitch, cm	----	----	----	----	----			
Edge Ratio	----	----	----	----	----			
6.4 Overall Assembly Length, cm.	----	----	----	----	----			
6.5 Duct Inside Flat-to-Flat, cm	----	----	----	----	----			
6.6 Duct Wall Thickness, mm	----	----	----	----	----			
7.0 Internal Fertile Pin Data								
7.1 Fuel Parameters								
Fuel Type (oxide, carbide, nitride) . . .	----	----	----	----	----			
Stoichiometry (O/M, C/M, N/M)	----	----	----	----	----			
EOL Fissile Content (fiss/HM), w/o . . .	----	----	----	----	----			
Fuel Form (3) (powder or pellet).	----	----	----	----	----			
Pellet Diameter, mm	----	----	----	----	----			
Pellet Density, g/cm^3	----	----	----	----	----			
Fuel Smear Density, % T.D.	----	----	----	---	----			
7.2 Cladding Parameters								
Cladding Outside Diameter, mm	----	----	----	----	----			
Cladding Wall Thickness, mm	----	----	----	----	----			

Reactor Designation	Ref.	Low Void	Low Cost	Den.	Trans.			
7.3 Bond Type (sodium or helium).	----	----	----	----	----			
7.4 Strasser Sleeve Parameters								
Sleeve Outside Diameter, mm	----	----	----	----	----			
Sleeve Wall Thickness, mm.	----	----	----	----	----			
Fractional Perforation of Sleeve	----	----	----	----	----			
Sleeve Material.	----	----	----	----	----			
7.5 Equivalent Plenum Volume, cc								
Top Plenum	----	----	----	----	----			
Bottom Plenum.	----	----	----	----	----			
8.0 Control Assembly Data								
8.1 Pins per Assembly								
8.2 Pin Pitch-to-Diameter Ratio								
8.3 Spacer Description								
Wire Wrap Diameter, mm								
Spacer Pitch, cm								
Edge Ratio								
8.4 Overall Assembly Length, cm								
8.5 Duct Inside Flat-to-Flat, cm								
8.6 Duct Wall Thickness, mm								
8.7 Guide Tube Flat-to-Flat Outside Dimension, cm								
8.8 Guide Tube Wall Thickness, mm								
9.0 Control Pin Data								
9.1 Control Parameters								
Control Material	B_4C →							
Enrichment	92% →							
Smear Density (% T.D.)								
9.2 Cladding Parameters								
Cladding Outside Diameter, mm.								

Table C.1 (Cont.)

Reactor Designation	Ref.	Low Void	Low Cost	Den.	Trans.			
Cladding Wall Thickness, mm								
10.0 <u>Performance Characteristics</u>								
10.1 System Doubling Time, yrs								
Compound	9.7	16.0	10.8	18.7	33.2			
Symbiotic	13.2*	17.1	13.8	15.6	24.7			
10.2 Breeding ratio (MOEC)								
Core	.940	1.004	1.035	.804	.760			
Internal Fertile Region	----	----	----	----	----			
Axial Blanket	.216	.232	.263	.168	.187			
Radial Blanket.	.266	.159	.161	.233	.245			
Total	1.422	1.395	1.460	1.205	1.193			
10.3 Driver Conversion Ratio, by zone								
BOEC								
Inner	1.092	1.049	1.177	.906	.867			
Outer	.899	1.058	1.073	.722	.694			
EOEC								
Inner	1.046	1.019	1.078	.949	.855			
Outer	.904	1.037	1.034	.774	.711			
10.4 Breeding Gain, kg/yr								
$U^{233} + U^{235} + Pa^{233}$	0.	273.	266.9	-247.3	690.5			
$Pu^{239} + Pu^{241}$	320.	10.	43.1	398.3	-573.5			
10.5 Fuel Cycle Cost, mills/kWhr								
Fabrication	3.77	5.24	4.51	4.75	3.17			
Reprocessing	3.05	3.29	3.01	2.22	2.18			
Fissile Inventory	4.91	6.58	5.67	3.86	5.32			
Fissile Credit.	-4.19	-2.99	-3.59	-2.75	0.66			
Total	7.55	14.83	9.60	8.36	11.35			
10.6 CDF for Design Limiting Pin (EOL).								
10.7 Specific Power, MWt/kg_{fiss} (BOL)	.347	.177	.313	.352	.301			
10.8 Sodium Void Effect, $\Delta k/kk'$	.0181	.0065	.0160	.0027	.0055			

*for Reference design with ThC blankets.

Table C.1 (Cont.)

	Reactor Designation	Ref.	Low Void	Low Cost	Den.	Trans.
10.9	Doppler Coefficient, Tdk/dt	-.0083	-.0079	-.0073	-.0095	-.0067
10.10	Peak Neutron Flux (E > 0.1 MeV), 10^{15} n/cm^2/sec	4.96	3.01	4.84	4.18	5.04
10.11	Peak Fluence (E > 0.1 MeV), 10^{23} n/cm^2	2.70	1.99	2.31	2.63	3.01
10.12	Peak Linear Power, kW/m					
	Driver					
	Nominal	95.4	98.0	103.2	99.6	97.2
	3σ, 15% op.	120.4	123.7	130.2	125.7	122.7
	Internal Fertile Assembly					
	Nominal	----	----	----	----	----
	3σ, 15% op.	----	----	----	----	----
	Radial Blanket					
	Nominal	31.6	9.2	10.1	18.7	27.3
	3σ, 15% op.	42.8	12.5	13.7	25.3	36.9
10.13	Discharge Exposure, MWD/MT					
	Peak					
	Core	109,600	79,700	97,700	129,600	151,300
	Internal Fertile Assembly	----	----	----	----	----
	Axial Blanket	12,600	11,100	14,300	11,000	15,100
	Radial Blanket	16,200	7,100	9,300	12,300	16,400
	Average					
	Core	66,800	51,800	51,100	80,400	91,700
	Internal Fertile Assembly	----	----	----	----	----
	Axial Blanket	2,400	3,400	2,100	1,900	2,700
	Radial Blanket	1,700	800	500	1,500	2,100
10.14	Core Inventory (BOEC), kg					
	Fertile					
	$^{232}Th + ^{234}U$	0.	13,568.	0.	726.	16,430.
	$^{238}U + ^{238}Pu + ^{240}Pu$	22,523.	25,262.	26,393.	21,056.	898.
	Fissile					
	$^{233}U + ^{235}U + Pa^{233}$	36.	1486.	0.	2180.	441.
	$^{239}Pu + ^{241}Pu$	2709.	2843.	2948.	433.	2722.
	Total Fissile	2745.	4329.	2948.	2613.	3163.
	Total Heavy Metal*	25,971.	44,024.	29,810.	25,121.	21,291.

*Fissile + Fertile + ^{236}U + ^{242}Pu + F.P.

909 136

	Ref.	Low Void	Low Cost	Den.	Trans.			
10.15 30 Year Cummulative Fissile Requirement, kg/GWe								
$^{239}Pu + ^{241}Pu$								
$^{233}U + ^{235}U$								
10.16 Fuel Cycle Cost, mills/kWhe / kg ^{233}U gain /yr	0.037*	0.056	0.045	-0.040	0.019			
10.17 ^{233}U Production / ^{239}Pu Desctruction	15.2*	-25.1	-6.2	----	1.2			
10.18 Discharge Fuel Radiation Level, R/hr @ 1m.								
10.19 Energy Support Ratio	0.26*	0.21	0.23	1.72	0.77			
*For Reference design with thorium blankets.								
11.0 Volume Fractions								
11.1 Driver Cell								
Fuel	.332	.448	.382	.310	.311			
Structure	.188	.186	.180	.190	.191			
Sodium	.480	.366	.438	.500	.497			
11.2 Internal Fertile Cell								
Fuel	----	----	----	----	----			
Structure	----	----	----	----	----			
Sodium	----	----	----	----	----			
11.3 Radial Blanket								
Fuel	.539	.561	.535	.535	.545			
Structure	.142	.142	.146	.144	.138			
Sodium	.293	.287	.294	.295	.291			
Bond	.026	.009	.026	.026	.026			
11.4 Control Cel								
Control Material	.312 →	→	→	→	→			
Structure	.318 →	→	→	→	→			
Sodium	.228 →	→	→	→	→			

FIGURE C.1

REFERENCE CORE ARRANGEMENT

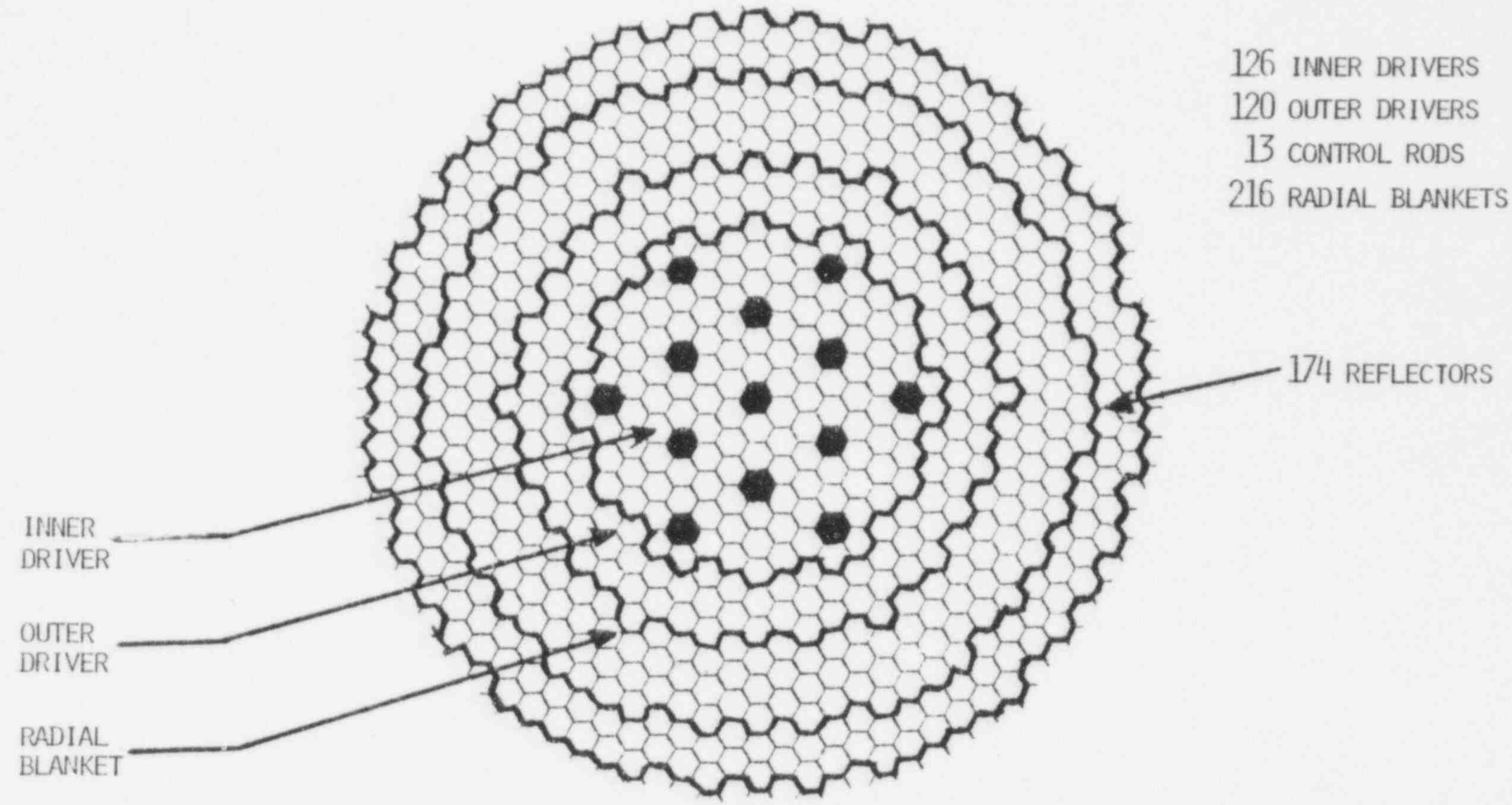

Reference Core

Table C.2

Fuel Inventory (kg)

	Beginning of Equilibrium Cycle					End of Equilibrium Cycle				
Isotope	CZ1	CZ2	AB	IB	RB	CZ1	CZ2	AB	IB	RB
Th-232	----	----	----		----	----	----	----		----
Pa-233	----	----	----		----	----	----	----		----
U-232	----	----	----		----	----	----	----		----
U-233	----	----	----		----	----	----	----		----
U-234	----	----	----		----	----	----	----		----
U-235	18	18	42		131	13	15	40		128
U-236	1	1	----		----	2	1	----		----
U-238	11263	10510	22106		68436	10859	10268	21964		68258
Pu-238	13	17	----		----	11	15	----		----
Pu-239	1145	1268	129		316	1194	1265	251		466
Pu-240	339	381	1		4	368	399	5		9
Pu-241	132	164	<1		<1	109	141	<1		<1
Pu-242	44	50	----		----	49	53	<1		<1
Fission Products	349	258	12		33	694	504	32		59
Fissile	1295	1450	171		447	1316	1421	291		594
Fertile	11615	10908	22107		68440	11238	10682	21969		68267
Total HM	13304	12667	22290		68920	13299	12661	22292		68920

Table C.3

Regional Neutron Balances

10^{18} Reactions/Sec

Reference Design

Reaction Rate	Beginning				End			
	CZ1	CZ2	AB	RB	CZ1	CZ2	AB	RB
Th-232 Capture								
Fission								
Pa-233 Capture								
Fission								
U-232 Capture								
Fission								
U-233 Capture								
Fission								
U-234 Capture								
Fission								
U-235 Capture	.1605	.1013	.0737	.0903	.1201	.0816	.0694	.0864
Fission	.5611	.3622	.2328	.2875	.4208	.2913	.2210	.2748
U-236 Capture	.0103	.0043			.0187	.0076		
Fission	.0018	.0008			.0032	.0015		
U-238 Capture	50.88	30.19	19.19	23.92	48.11	28.52	19.32	23.80
Fission	7.412	4.970	1.127	1.470	7.798	4.659	1.229	1.551
Pu-238 Capture	.0859	.0657			.0712	.0565		
Fission	.2507	.2086			.2100	.1788		
Pu-239 Capture	8.848	6.075	.3864	.5620	9.126	5.862	.7314	.5874
Fission	33.35	24.29	1.018	1.558	34.67	23.41	1.978	2.452
Pu-240 Capture	2.686	1.899	.0087	.0153	2.896	1.925	.0318	.0315
Fission	1.991	1.580	.0018	.0037	2.173	1.592	.0071	.0081
Pu-241 Capture	.9487	.7372	.0001	.0002	.7754	.6132	.0005	.0005
Fission	5.245	4.184	.0003	.0008	4.302	3.478	.0024	.0023
Pu-242 Capture	.2352	.1654			.2576	.1722		
Fission	.1978	.1586			.2197	.1640		
Fuel Fissions								
Fissile	39.15	28.84	1.251	1.844	39.39	27.18	2.201	2.729
Fertile	9.654	6.761	1.129	1.474	10.18	6.43	1.237	1.559
Total Fuel	49.00	35.76	2.380	3.318	49.80	33.77	3.438	4.288
Fuel Capture								
Fissile	9.957	6.914	.4601	.6524	10.02	6.557	.8013	.6742
Fertile	53.65	32.16	19.20	23.94	51.07	30.50	19.35	23.73
Total Fuel	63.85	39.24	19.66	24.59	61.37	37.24	20.15	24.51
Structure Capture	5.627	3.261	1.925	1.076	5.593	3.153	1.953	1.075
Na Capture	.5537	.2731	.1884	.0793	.5484	.2637	.1889	.0786
B_{10} Capture	----		4.360				4.596	
Leakage	23.67	25.87			25.99	24.16		
Source	142.7	104.4	6.653	9.312	143.3	98.59	9.724	11.53

909 140

Figure C.2

REFERENCE DESIGN

TOTAL FLUX RADIAL DISTRIBUTION AT MIDPLANE

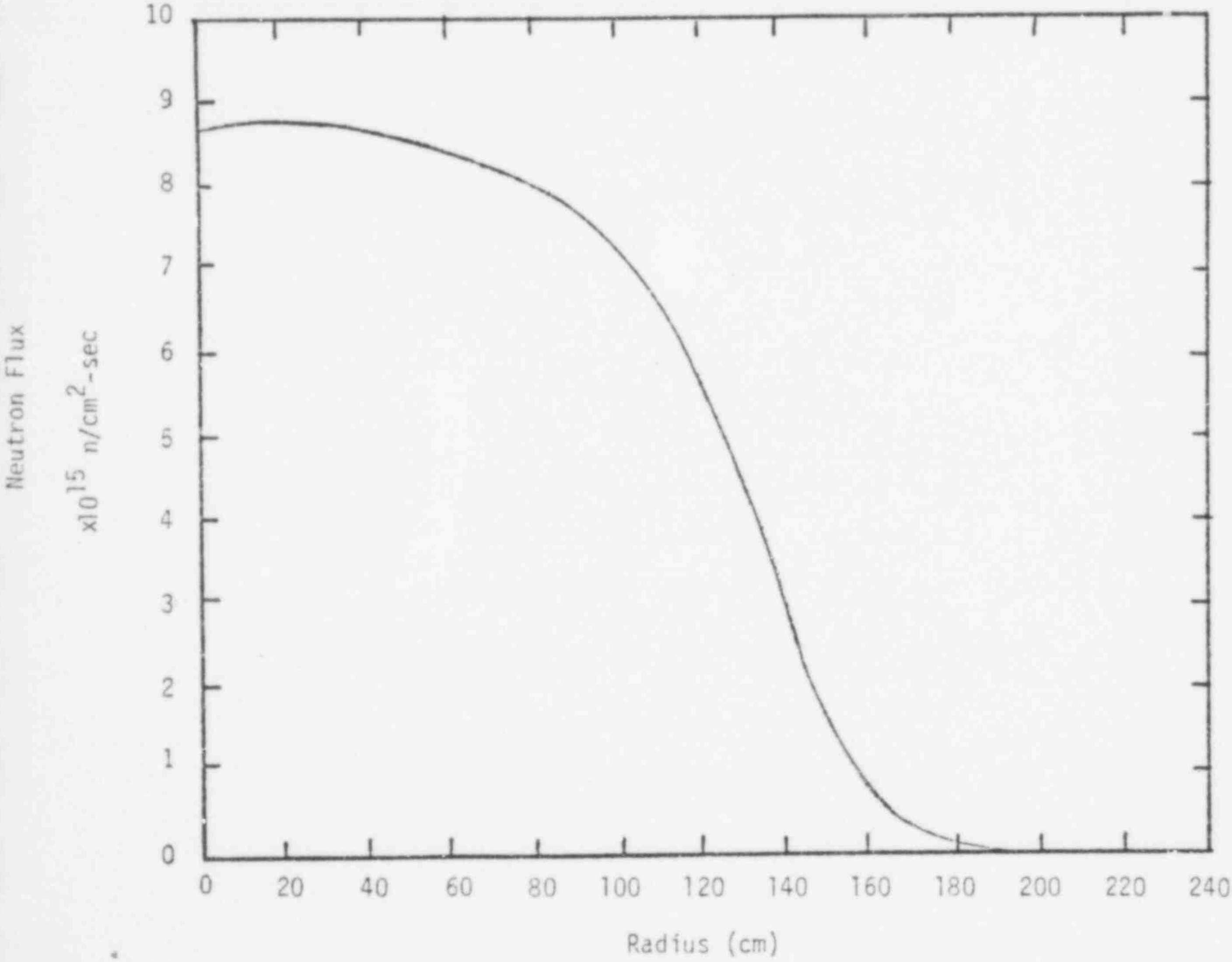

Figure C.3

REFERENCE DESIGN

TOTAL FLUX AXIAL DISTRIBUTION AT POSITION OF PEAK RADIAL FLUX

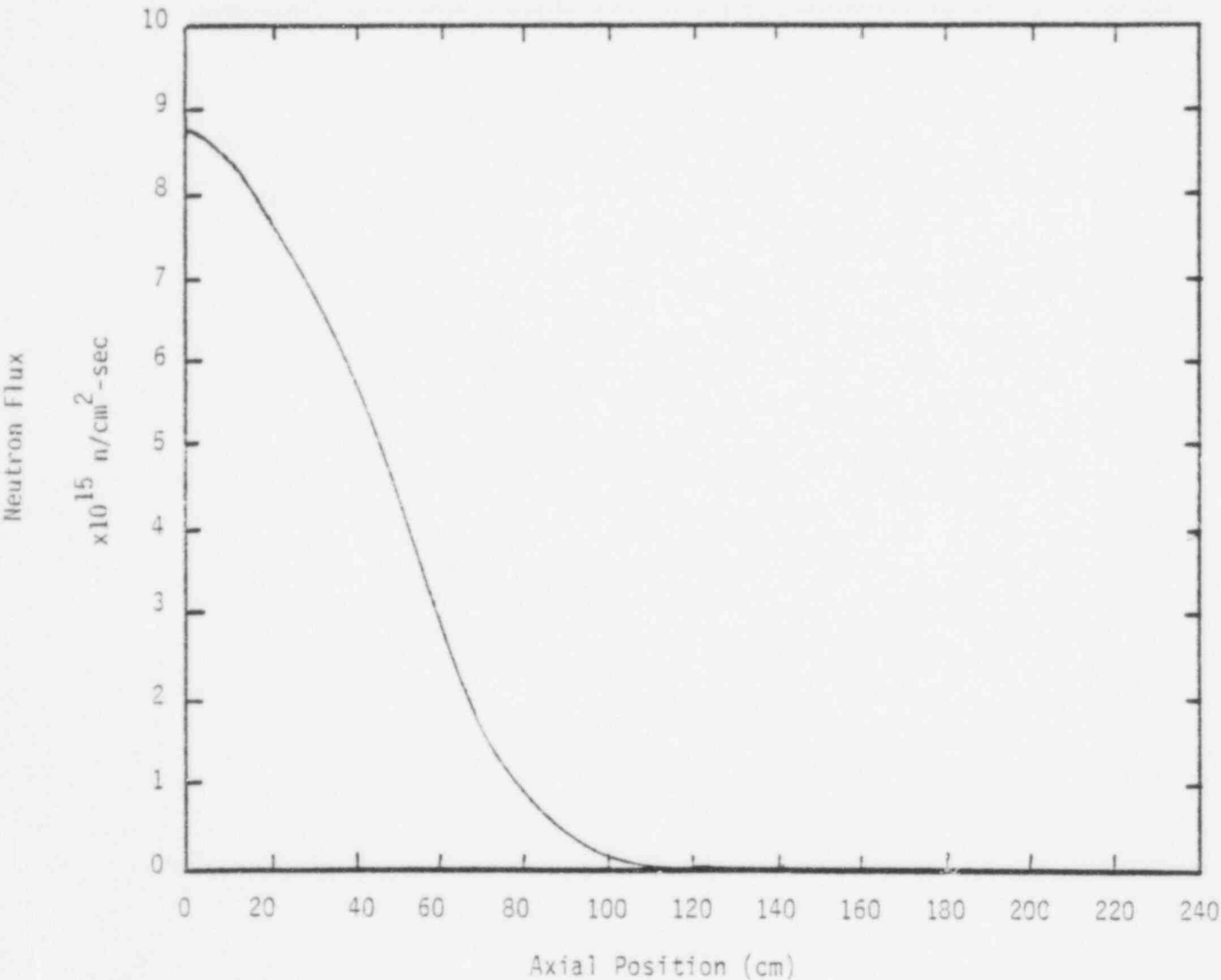

Figure C.4

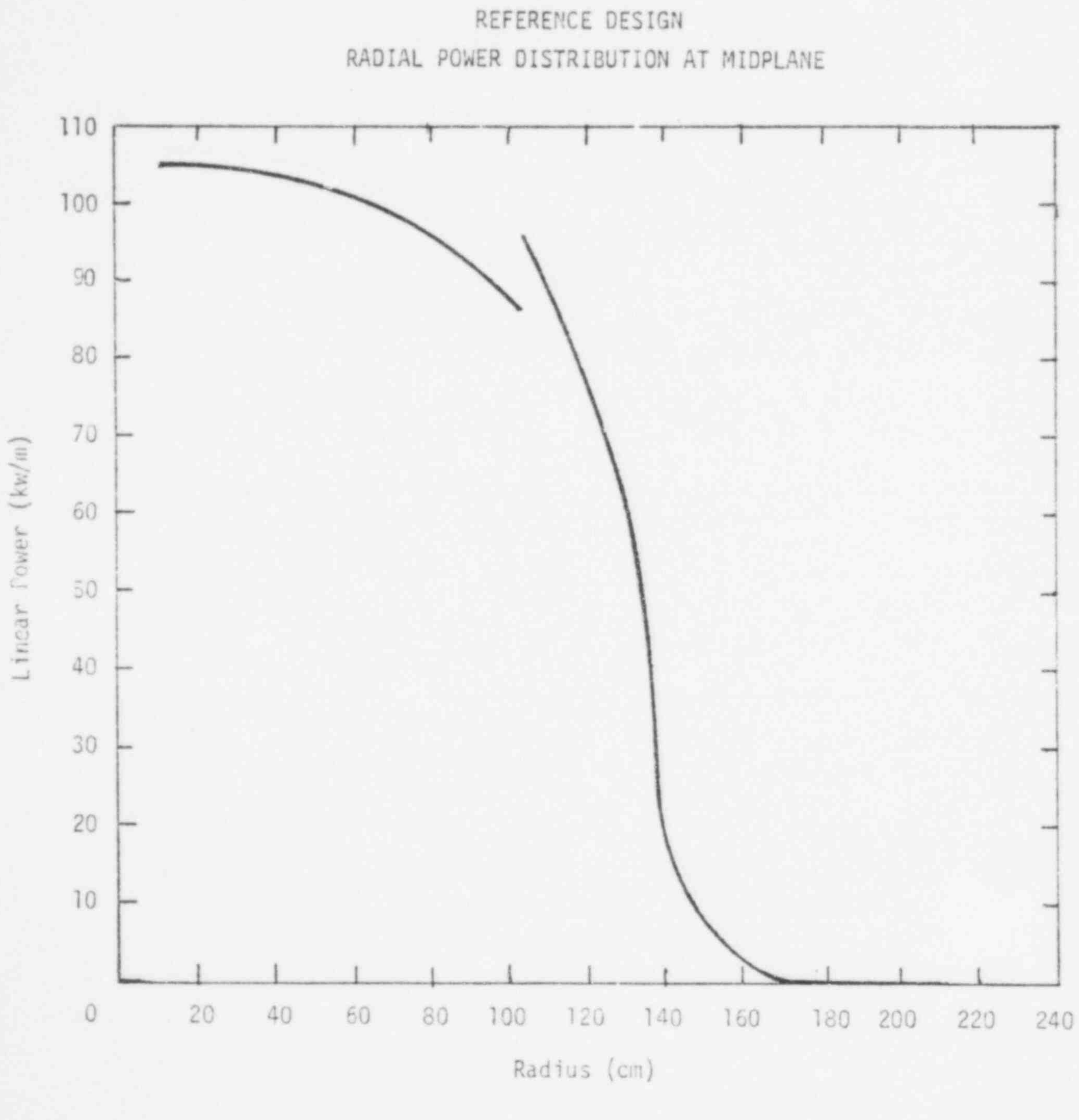

909 143

Figure C.5

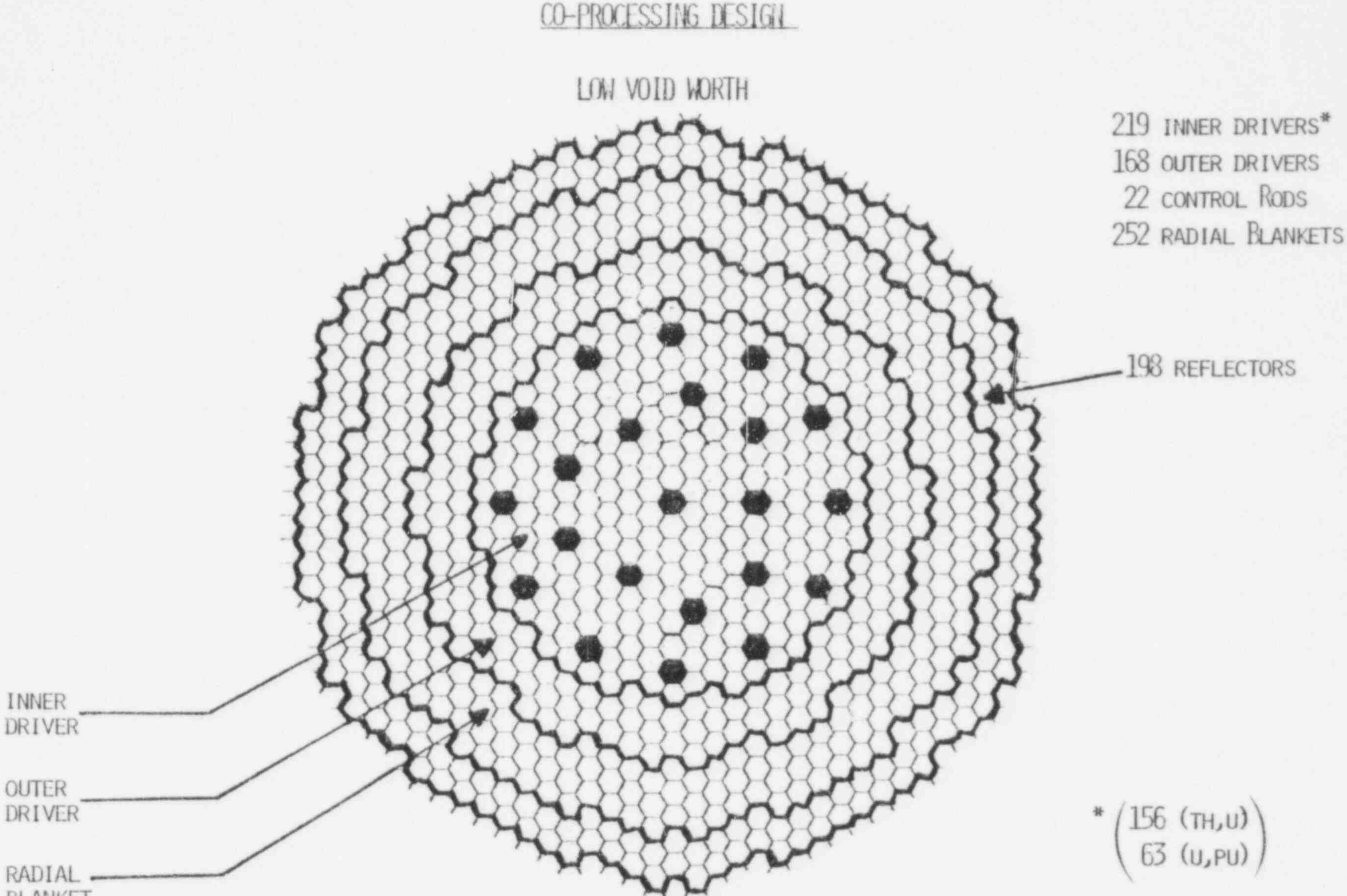

909 144

Low Void Worth Core

Table C.4

Fuel Inventory (kg)

	Beginning of Equilibrium Cycle					End of Equilibrium Cycle				
Isotope	CZ1	CZ2	AB	IB	RB	CZ1	CZ2	AB	IB	RB
Th-232	13168	----	37130		60704	12832		36954		60584
Pa-233	53	----	26		17	49		27		18
U-232	----	----	----		----	----		----		----
U-233	1371	----	142		169	1377		299		277
U-234	400	----	1		1	403		3		2
U-235	62	----	<1		<1	67		<1		<1
U-236	16	----	----		----	18		----		----
U-238	6579	17646	----		----	6421	17337	----		----
Pu-238	----	----	----		----	----	----	----		----
Pu-239	727	1930	----		----	732	1944	----		----
Pu-240	284	753	----		----	289	763	----		----
Pu-241	50	136	----		----	48	129	----		----
Pu-242	23	60	----		----	24	62	----		----
Fission Products	490	276	6		7	960	559	22		16
Fissile	2263	2066	168		186	2273	2073	326		295
Fertile	20431	18399	37131		60705	19945	18100	36957		60586
Total HM	23223	20801	37305		60898	23220	20794	37305		60897

Table C.5

Regional Neutron Balances

10^{18} Reactions/Sec

Low Void Design

Reaction Rate	Beginning				End			
	CZ1	CZ2	AB	RB	CZ1	CZ2	AB	RB
Th-232 Capture	39.14		20.45	13.98	37.39		20.50	14.06
Fission	1.294		.2415	.1423	1.239		.2607	.1523
Pa-233 Capture	.4503		.0946	.0351	.4107		.0924	.0367
Fission	.0354		.0021	.0007	.0324		.0022	.0008
U-232 Capture								
Fission								
U-233 Capture	3.152		1.072	.0753	.3106		.2282	.1205
Fission	34.55		.1105	.7249	34.05		2.229	1.166
U-234 Capture	1.952		.0028	.0014	1.926		.0081	.0031
Fission	1.305		.0007	.0004	1.292		.0023	.0009
U-235 Capture	.2924		<.0001	<.0001	.3076		.0001	<.0001
Fission	1.074		<.0001	<.0001	1.131		.0004	.0001
U-236 Capture	.0727		<.0001	<.0001	.0824		<.0001	<.0001
Fission	.0156		<.0001	<.0001	.0177		<.0001	<.0001
U-238 Capture	15.61	30.54			14.93	29.21		
Fission	2.885	5.506			2.766	5.283		
Pu-238 Capture								
Fission								
Pu-239 Capture	2.760	5.366			2.720	5.258		
Fission	12.01	23.08			11.87	22.69		
Pu-240 Capture	1.134	2.198			1.129	2.168		
Fission	1.076	2.039			1.075	2.018		
Pu-241 Capture	.1854	.3640			.1727	.3379		
Fission	1.093	2.135			1.019	1.984		
Pu-242 Capture	.0607	.1165			.0619	.1172		
Fission	.0673	.1261			.0690	.1275		
Fuel Fissions								
Fissile	48.75	25.21	1.074	.7256	48.10	24.67	2.231	1.167
Fertile	6.560	7.545	.2422	.1427	6.372	7.301	.2631	.1531
Total Fuel	55.40	32.88	1.316	.8683	54.56	32.10	2.494	1.320
Fuel Captures								
Fissile	6.840	5.730	.2052	.1104	6.717	5.596	.3207	.1572
Fertile	57.83	32.73	20.54	13.98	55.37	31.38	20.51	14.06
Total Fuel	64.81	38.58	20.66	14.09	62.23	37.09	20.83	14.22
Structure Capture	4.448	2.370	1.657	.6836	4.359	2.309	1.663	.6868
Na Capture	.3362	.1509	.1245	.0505	.3289	.1467	.1236	.0504
B10 Capture			5.273				5.408	
Leakage	21.31	22.10			22.53	22.17		
Source	146.3	96.08	3.251	2.149	144.0	93.82	6.206	3.282

Figure C.6

CO-PROCESSING DESIGN/LOW COST OPTION

TOTAL FLUX RADIAL DISTRIBUTION AT MIDPLANE

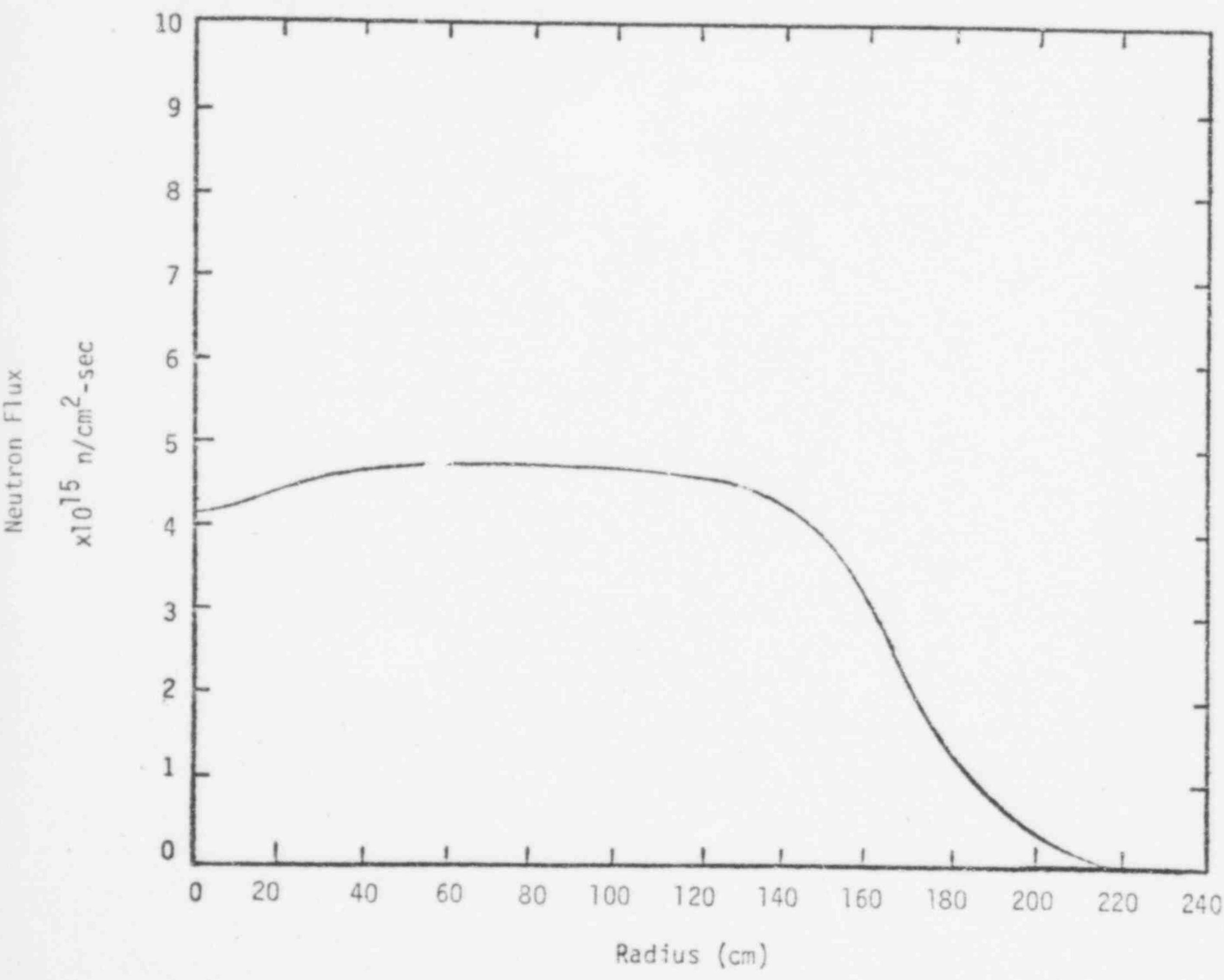

909 147

Figure C.7

CO-PROCESSING DESIGN/LOW VOID OPTION

TOTAL FLUX AXIAL DISTRIBUTION AT POSITION OF PEAK RADIAL FLUX

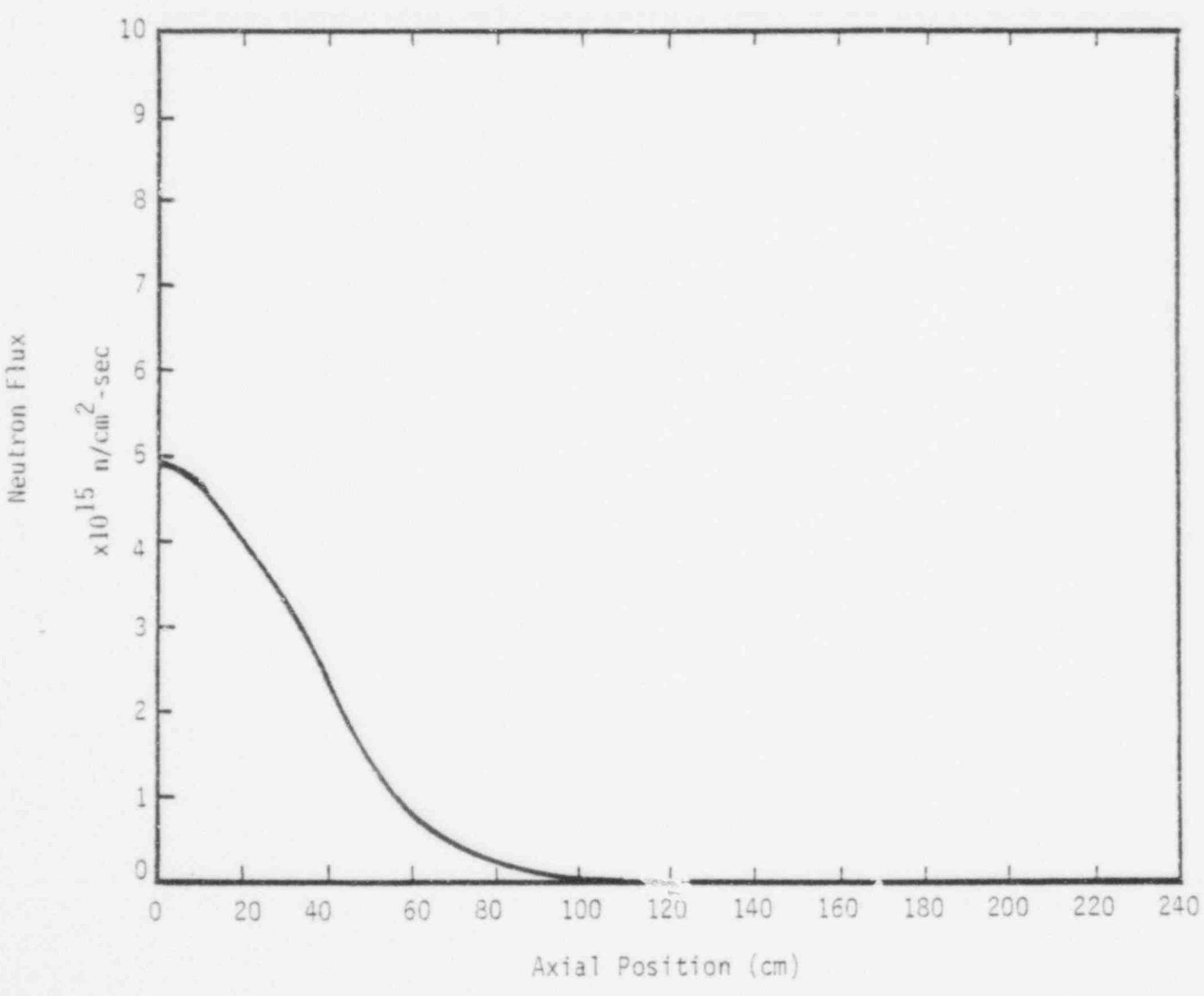

909 148

Figure C.8

CO-PROCESSING DESIGN/LOW VOID OPTION

RADIAL POWER DISTRIBUTION AT MIDPLANE

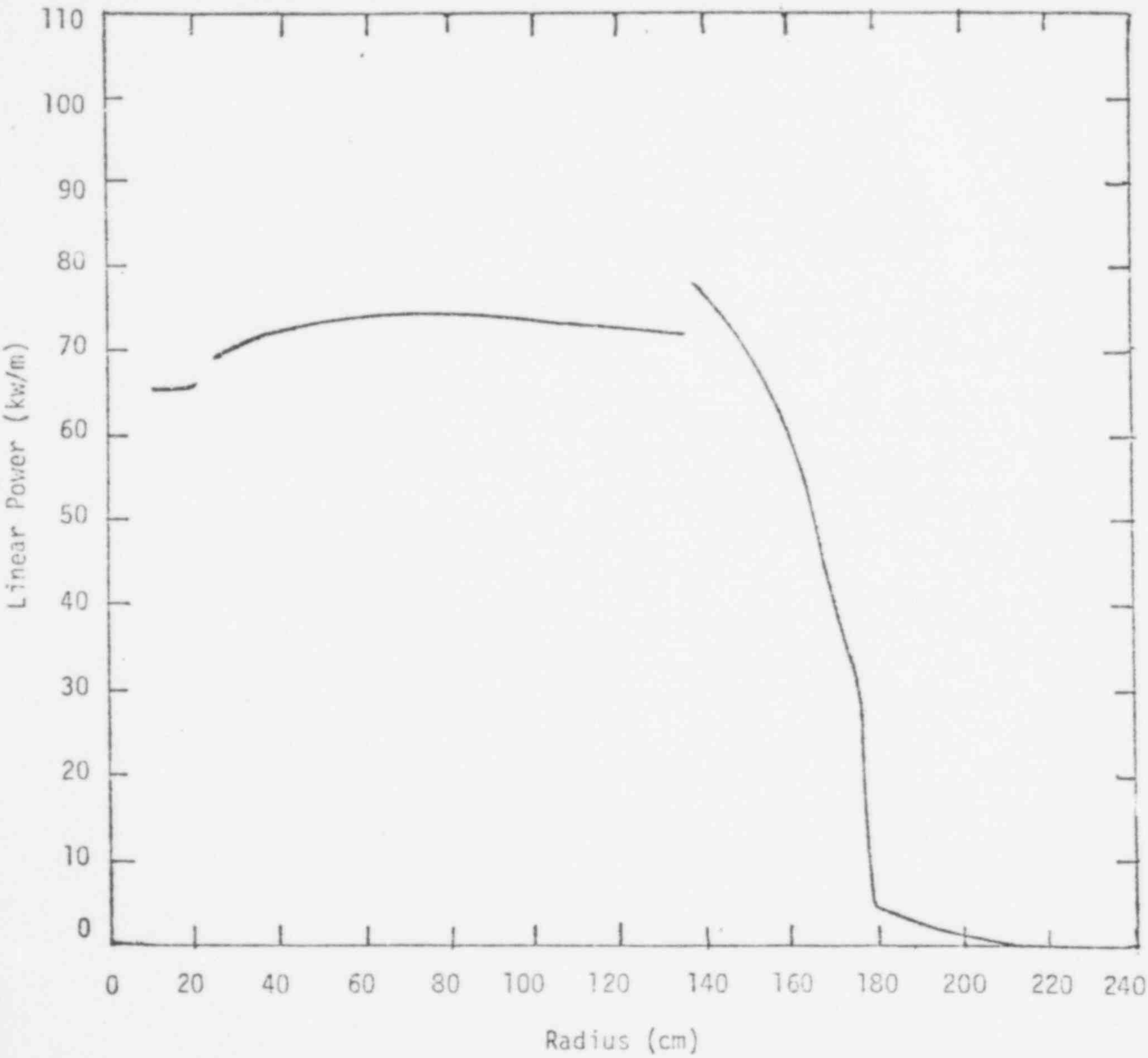

FIGURE C.9

CO-PROCESSING CORE ARRANGEMENT

LOW COST

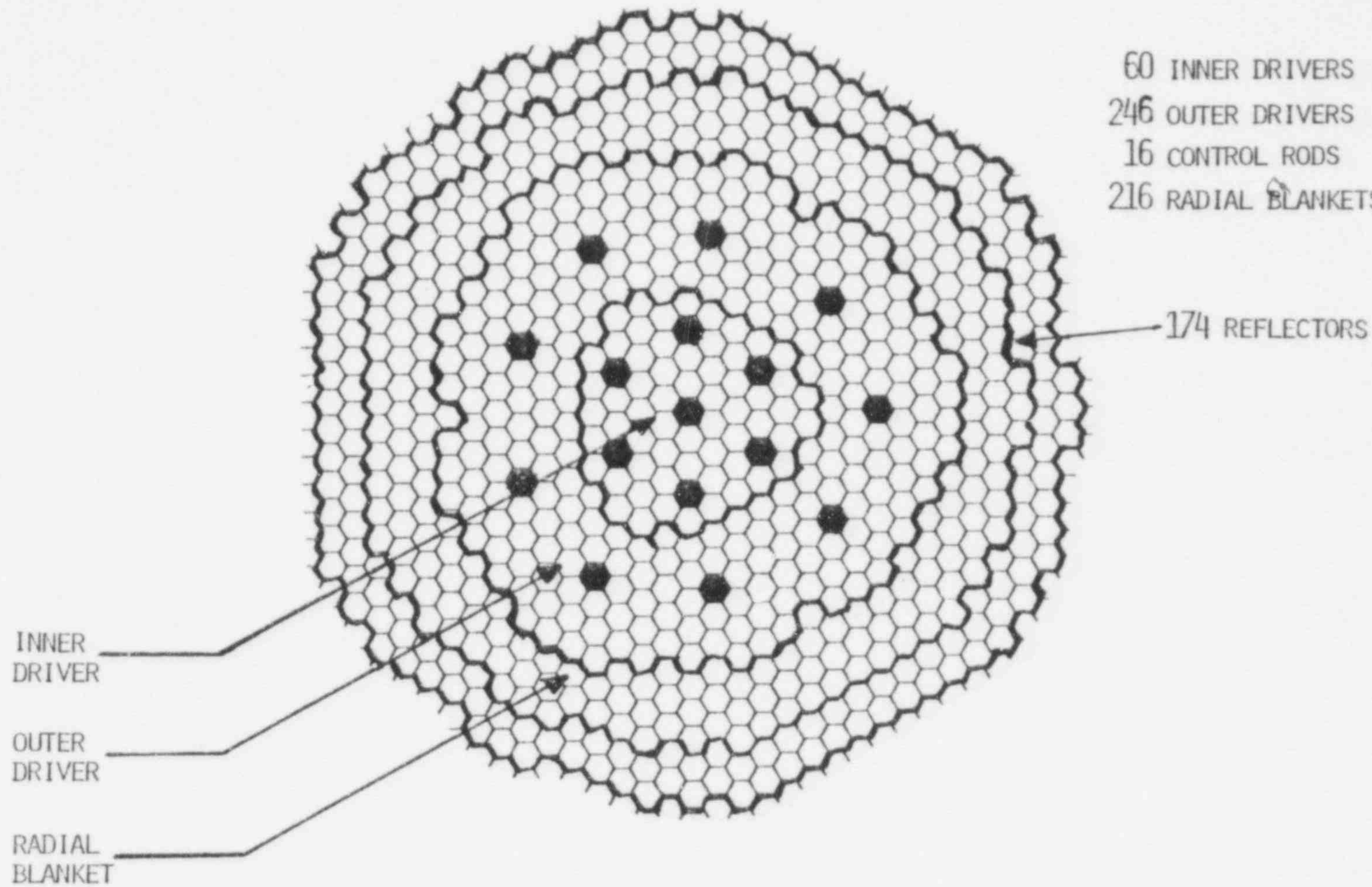

Coprocessing - Low Cost Design

Table C.6

Fuel Inventory (kg)

	Beginning of Equilibrium Cycle					End of Equilibrium Cycle				
Isotope	CZ1	CZ2	AB	IB	RB	CZ1	CZ2	AB	IB	RB
Th-232	----	----	23116		48588	----	----	22922		48466
Pa-233	----	----	27		18	----	----	27		17
U-232	----	----	----		----	----	----	----		----
U-233	----	----	69		181	----	----	246		293
U-234	----	----	<1		1	----	----	3		2
U-235	----	----	<1		<1	----	----	<1		<1
U-236	----	----	<1		<1	----	----	<1		<1
U-238	4996	20324	----		----	4757	19714	----		----
Pu-238	----	----	----		----	----	----	----		----
Pu-239	508	2244	----		----	533	2275	----		----
Pu-240	195	878	----		----	207	903	----		----
Pu-241	35	161	----		----	34	153	----		----
Pu-242	16	70	----		----	17	74	----		----
Fission Products	95	288	2		7	295	837	18		17
Fissile	543	2405	96		199	567	2428	273		310
Fertile	5191	21202	23116		48589	4964	20617	22925		48468
Total HM	5845	23965	23214		48795	5843	29956	23216		48795

Table C.7

Regional Neutron Balances

10^{18} Reactions/Sec

Low Cost Design

Reaction Rate	Beginning				End			
	CZ1	CZ2	AB	RB	CZ1	CZ2	AB	RB
Th-232 Capture			21.23	13.28			21.10	12.88
Fission			.2222	.1379			.2490	.1429
Pa-233 Capture			.1043	.0269			.1050	.0242
Fission			.0031	.0009			.0034	.0008
U-232 Capture								
Fission								
U-233 Capture			.0658	.0694			.2314	.1059
Fission			.6619	.7030			2.350	1.078
U-234 Capture			.0013	.0009			.0074	.0020
Fission			.0004	.0004			.0029	.0008
U-235 Capture			<.0001	<.0001			.0001	<.0001
Fission			.0002	<.0001			.0004	.0001
U-236 Capture								
Fission								
U-238 Capture	22.64	57.99			21.48	53.14		
Fission	3.396	9.391			3.311	8.656		
Pu-238 Capture								
Fission								
Pu-239 Capture	3.896	10.66			4.034	10.19		
Fission	14.98	42.59			15.78	40.96		
Pu-240 Capture	1.545	4.332			1.617	4.211		
Fission	1.182	3.561			1.273	3.488		
Pu-241 Capture	.2531	.7220			.2399	.6470		
Fission	1.411	4.095			1.348	3.680		
Pu-242 Capture	.0829	.2301			.0905	.2315		
Fission	.0724	.2179			.0816	.2211		
Fuel Fissions								
Fissile	16.39	46.68	.6649	.7038	17.13	44.64	2.354	1.079
Fertile	4.578	12.95	.2226	.1383	4.584	12.14	.2519	.1437
Total Fuel	21.04	59.85	.8875	.8421	21.80	5.700	2.606	1.222
Fuel Capture								
Fissile	4.149	11.39	.1701	.0964	4.274	10.84	.3366	.1301
Fertile	24.18	62.32	21.23	13.29	23.06	57.35	21.11	12.88
Total Fuel	28.41	73.94	21.40	13.38	27.43	68.42	21.45	13.01
Structure Capture	2.243	5.596	1.689	.5216	2.281	5.560	1.706	.5112
Na Capture	.2008	.4404	.1374	.0346	.1984	.4148	.1373	.0336
B10 Capture			5.032				5.270	
Leakage	9.486	34.97			11.93	40.67		
Source	61.38	174.8	2.178	2.087	63.64	166.5	6.490	3.042

909 152

Figure C.10

CO-PROCESSING DESIGN/LOW VOID OPTION

TOTAL FLUX RADIAL DISTRIBUTION AT MIDPLANE

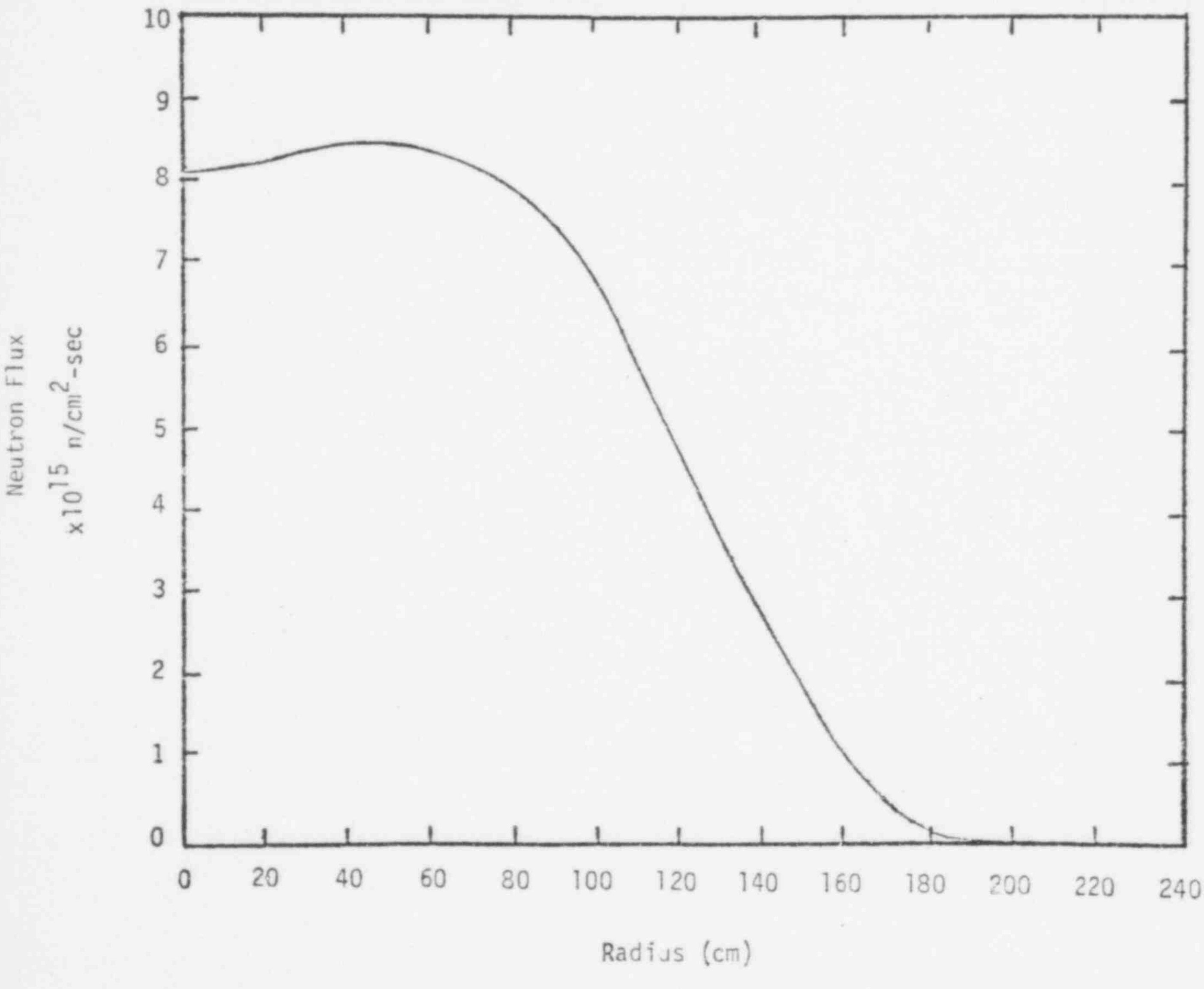

Figure C.11

CO-PROCESSING DESIGN/LOW COST OPTION

TOTAL FLUX AXIAL DISTRIBUTION AT POSITION OF PEAK RADIAL FLUX

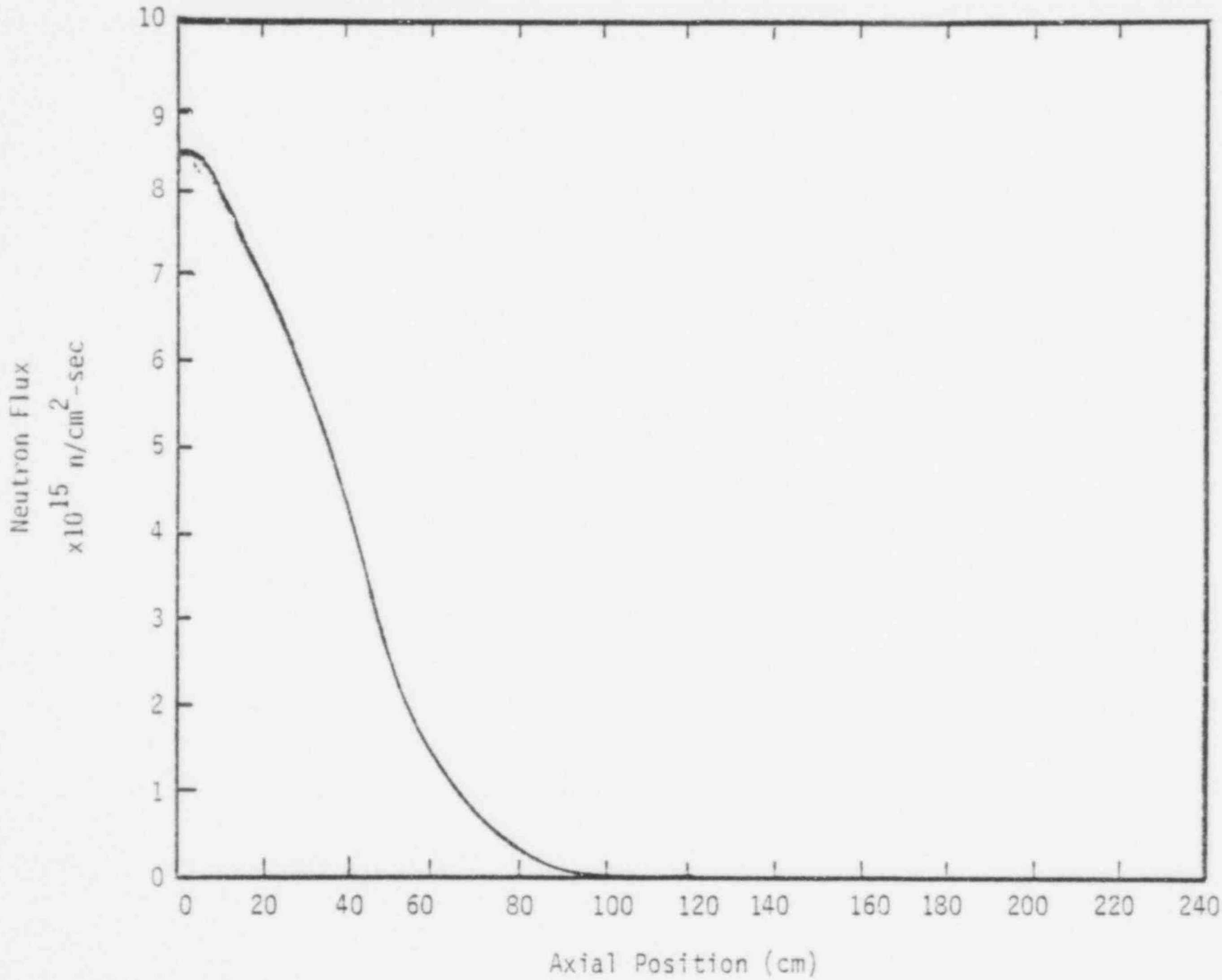

Figure C.12

CO-PROCESSING DESIGN/LOW COST OPTION

RADIAL POWER DISTRIBUTION AT MIDPLANE

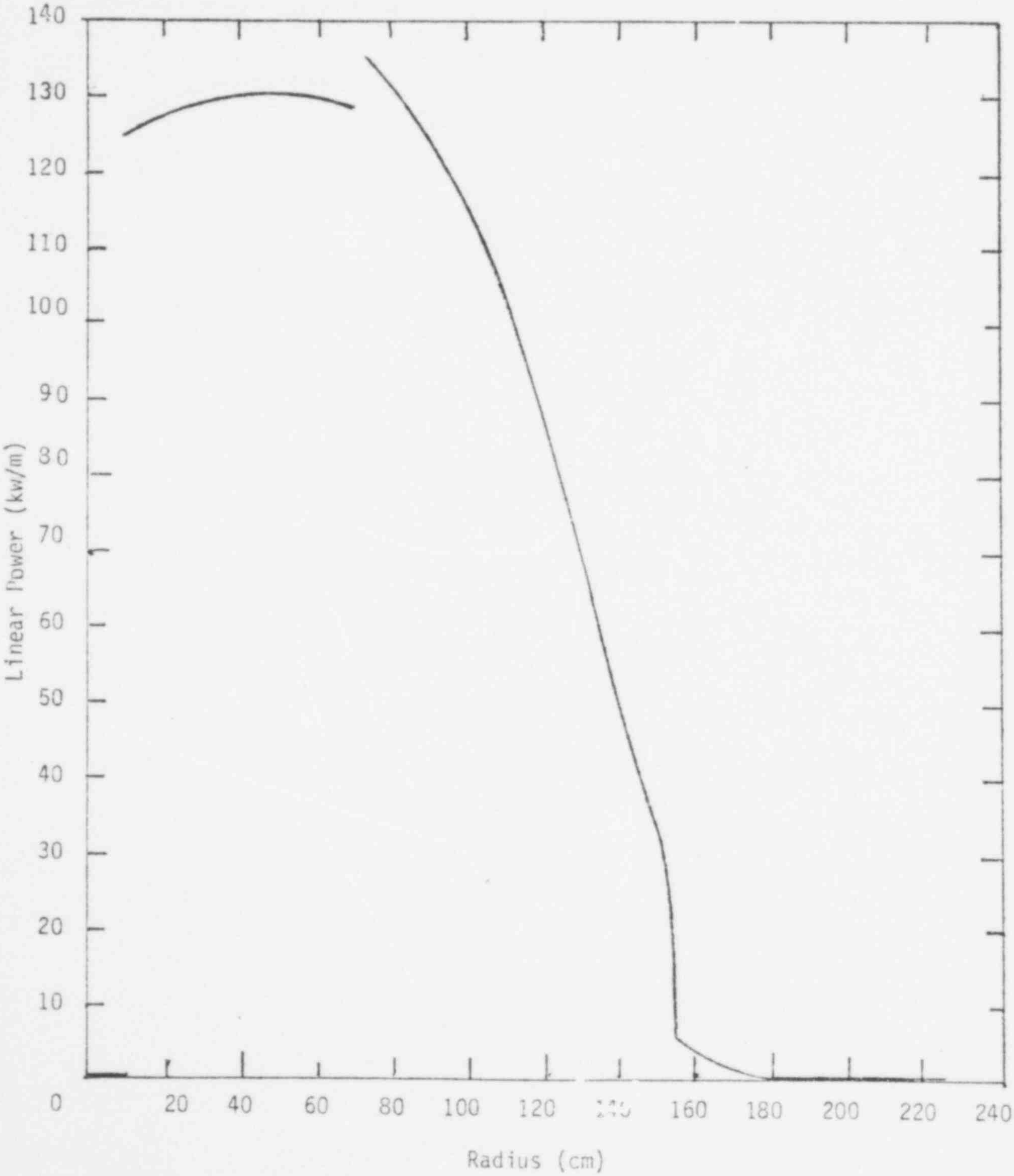

FIGURE C.13

DENATURED CORE ARRANGEMENT

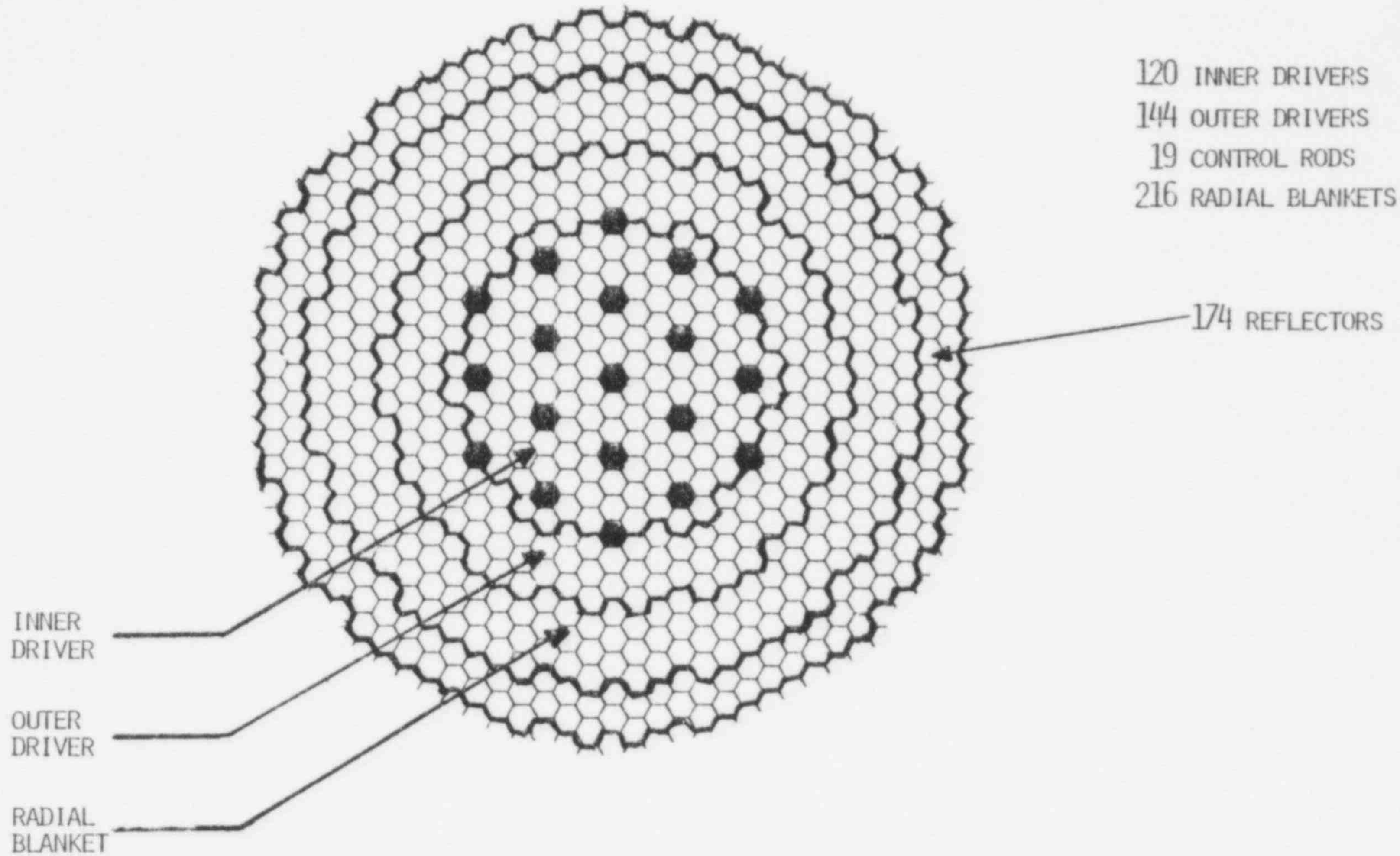

909 156

Denatured Core

Table C.8

Fuel Inventory (kg)

	Beginning of Equilibrium Cycle					End of Equilibrium Cycle				
Isotope	CZ1	CZ2	AB	IB	RB	CZ1	CZ2	AB	IB	RB
Th-232	----		17033		51236	----	----	16918		51080
Pa-233	----		18		24	----	----	19		26
U-232	----		----		----	----	----	----		----
U-233	785	1279	89		244	556	1025	188		381
U-234	293	433	1		2	284	426	3		4
U-235	48	68	<1		<1	53	73	<1		<1
U-236	13	17	<1		----	16	20	<1		<1
U-238	9666	11374	----		----	9326	11115	----		----
Pu-238	----	----	----		----	----	----	----		----
Pu-239	244	189	----		----	449	362	----		----
Pu-240	11	5	----		----	29	15	----		----
Pu-241	<1	<1	----		----	1	<1	----		----
Pu-242	<1	<1	----		----	<1	<1	----		----
Fission Products	361	335	4		14	707	662	18		32
Fissile	1077	1536	107		268	1059	1460	207		407
Fertile	9970	11812	17034		51238	9639	11556	16921		51084
Total HM	11421	13700	17145		51520	11421	13698	17146		51523

Table C.9

Regional Neutron Balances

10^{18} Reactions/Sec

Denatured Design

Reaction Rate	Beginning				End			
	CZ1	CZ2	AB	RB	CZ1	CZ2	AB	RB
Th-232 Capture			13.55	18.43			14.65	20.65
Fission			.1548	.2122			.1796	.2558
Pa-233 Capture			.0888	.0695			.0961	.0804
Fission			.0019	.0017			.0022	.0021
U-232 Capture								
Fission								
U-233 Capture	2.794	2.844	.0931	.1523	2.102	2.444	.2094	.2588
Fission	29.64	30.82	.9014	1.486	22.21	26.39	2.035	2.539
U-234 Capture	2.267	2.086	.0032	.0042	2.340	2.221	.0101	.0094
Fission	1.208	1.298	.0008	.0012	1.216	1.342	.0027	.0029
U-235 Capture	.3612	.3150	<.0001	<.0001	.4211	.3663	.0002	.0002
Fission	1.262	1.136	.0001	.0002	1.464	1.312	.0006	.0005
U-236 Capture	.0943	.0788			.1244	.0990		
Fission	.0158	.0156			.0203	.0190		
U-238 Capture	35.36	26.04			36.32	27.52		
Fission	5.112	4.440			5.114	4.551		
Pu-238 Capture								
Fission								
Pu-239 Capture	1.610	.7756			3.170	1.614		
Fission	5.944	3.109			11.56	6.365		
Pu-240 Capture	.0785	.0241			.2163	.0711		
Fission	.0553	.0201			.1499	.0574		
Pu-241 Capture	.0021	.0005			.0080	.0019		
Fission	.0117	.0026			.0439	.0105		
Pu-242 Capture	<.0001				.0002	<.0001		
Fission	<.0001				.0002	<.0001		
Fuel Fissions								
Fissile	36.86	35.07	.9034	1.487	35.28	34.08	2.038	2.542
Fertile	6.375	5.756	.1556	.2134	6.480	5.951	.1823	.2587
Total Fuel	43.25	40.84	1.059	1.701	41.78	40.05	2.221	2.800
Fuel Capture								
Fissile	4.768	3.935	.1820	.2218	5.701	4.426	.3057	.3393
Fertile	37.71	28.15	13.55	18.44	38.88	29.81	14.66	20.66
Total Fuel	42.57	32.16	13.74	18.65	44.70	34.34	14.96	20.99
Structure Capture	4.694	3.309	1.704	.9379	4.989	3.575	1.852	1.052
Na Capture	.4391	.2483	.1501	.0664	.4682	.2696	.0162	.0739
B10 Capture			5.891				6.474	
Leakage	21.65	28.74			19.26	26.47		
Source	112.6	105.3	2.626	4.223	111.2	104.7	5.532	6.975

909 158

Figure C.14

DENATURED DESIGN

TOTAL FLUX RADIAL DISTRIBUTION AT MIDPLANE

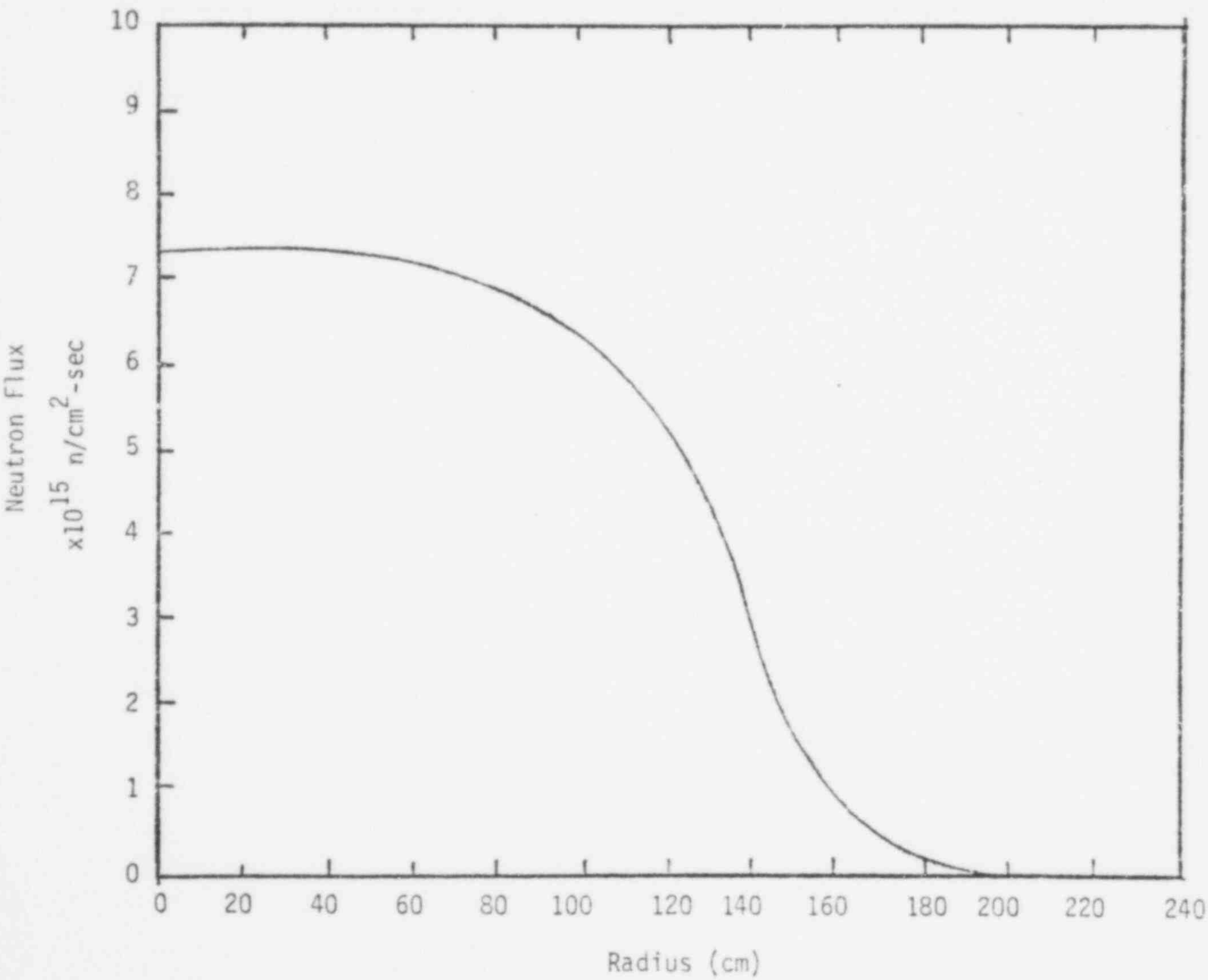

Figure C.15

DENATURED DESIGN

TOTAL FLUX AXIAL DISTRIBUTION AT POSITION OF PEAK RADIAL FLUX

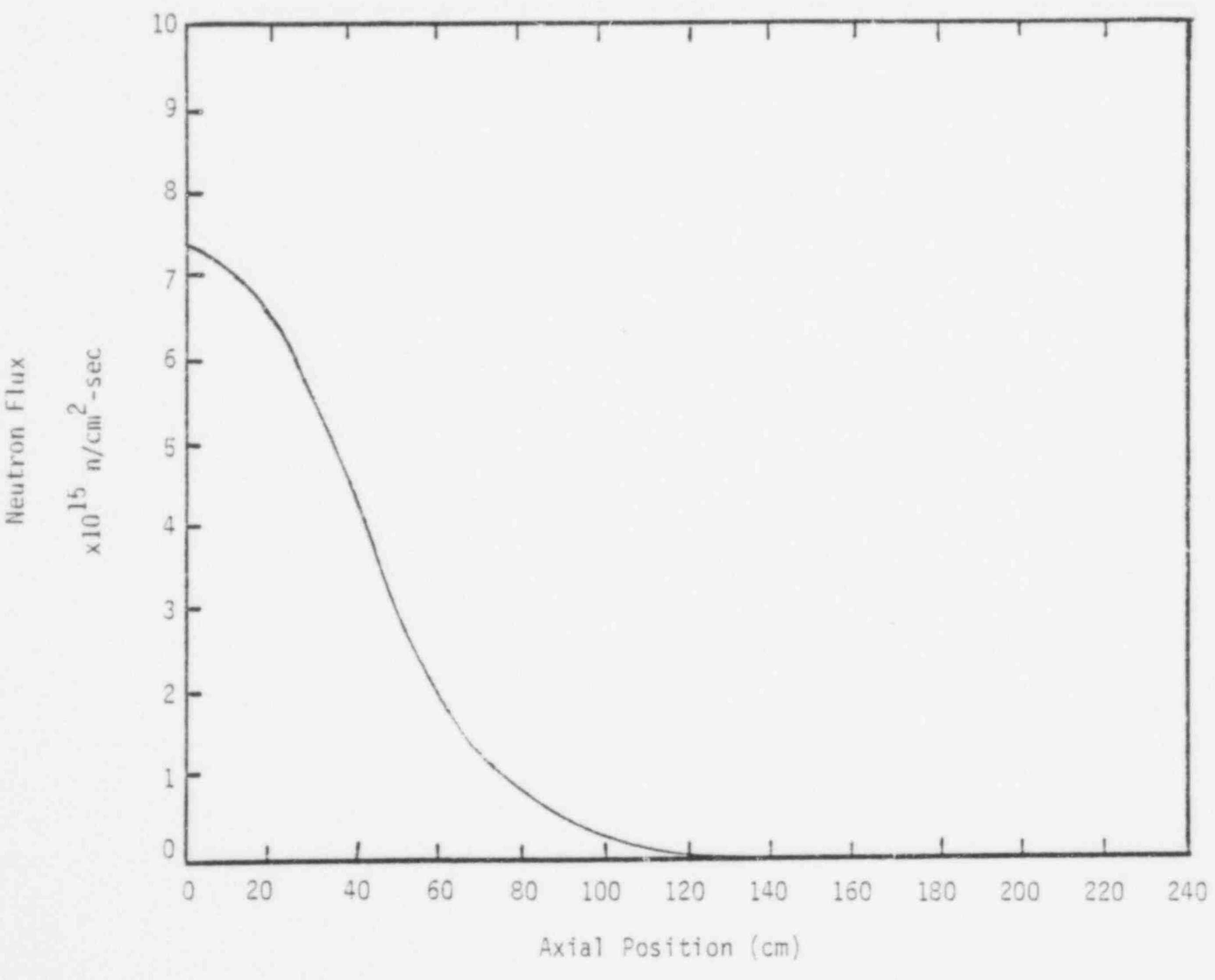

Figure C.16

DENATURED DESIGN

RADIAL POWER DISTRIBUTION AT MIDPLANE

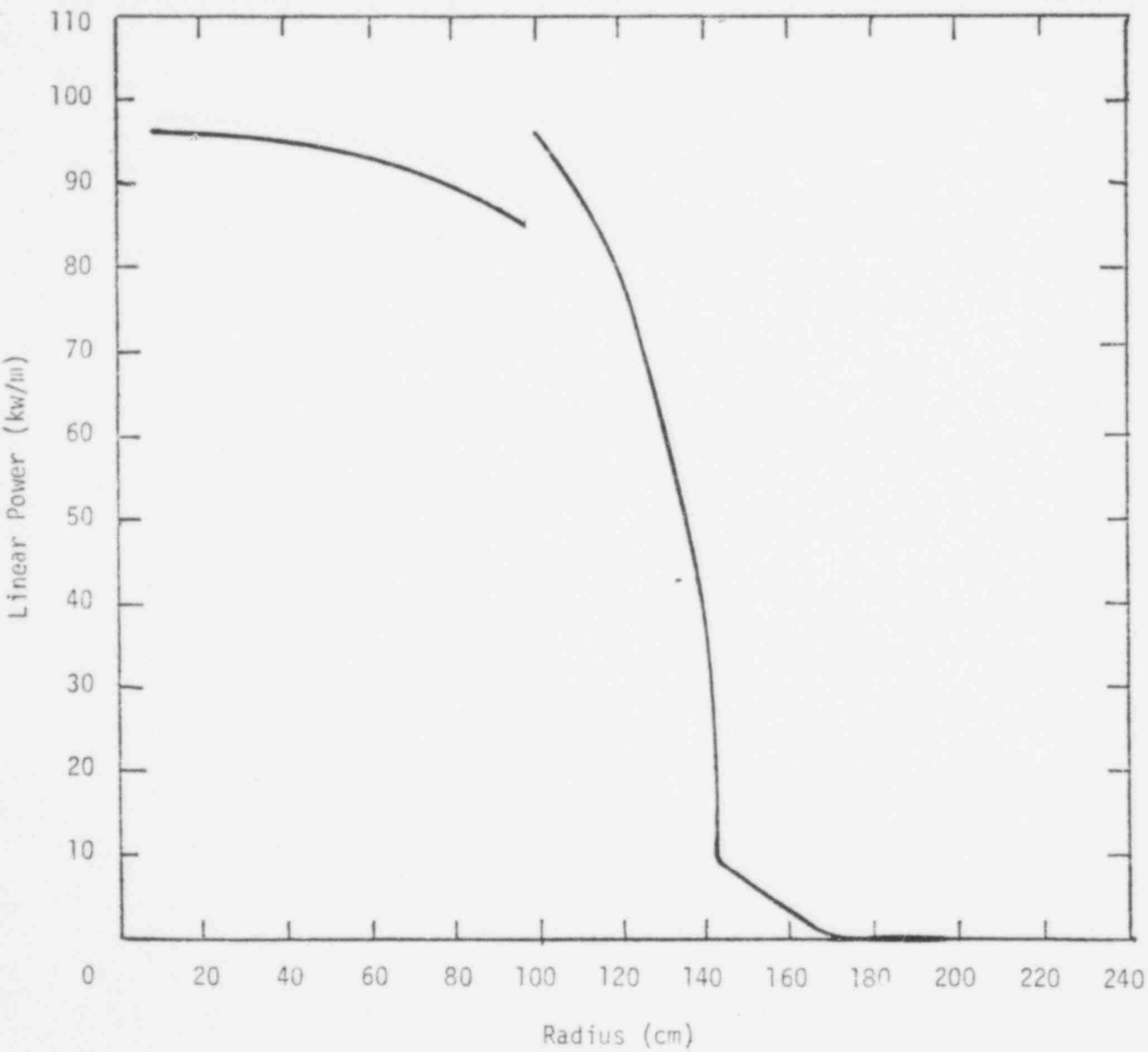

909 161

FIGURE C.17

TRANSMUTER CORE ARRANGEMENT

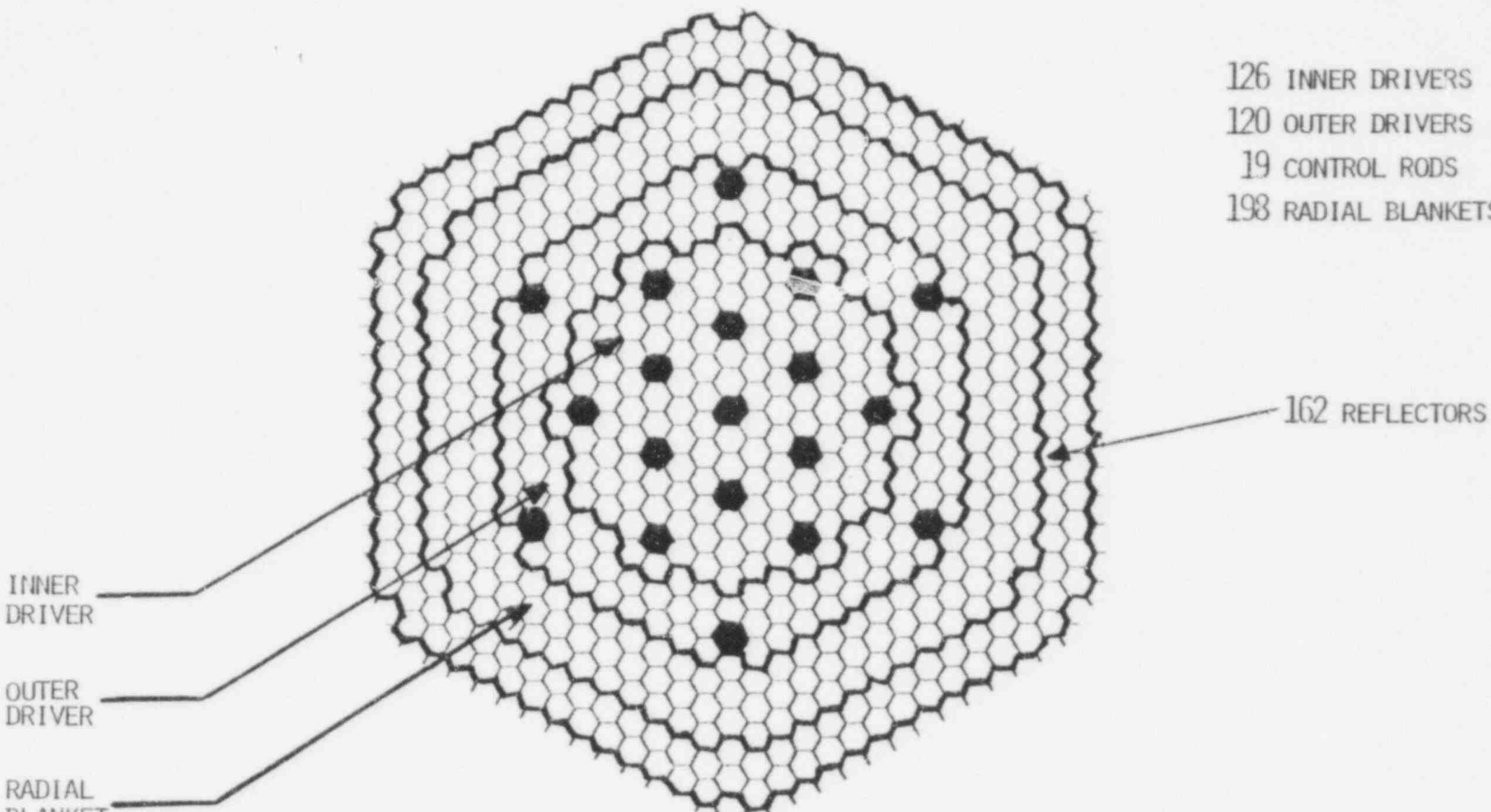

Transmuter Core

Table C.10

Fuel Inventory (kg)

	Beginning of Equilibrium Cycle					End of Equilibrium Cycle				
Isotope	CZ1	CZ2	AB	IB	RB	CZ1	CZ2	AB	IB	RB
Th-232	8526	7886	17713		53078	8189	7688	17572		52892
Pa-233	38	22	24		31	54	32	24		32
U-232										
U-233	233	148	111		308	420	277	232		467
U-234	12	4.5	2		3.2	26	10	4.3		6.2
U-235	<1	<1	<1		<1	1	<1	<1		<1
U-236	<1	<1	<1		<1	<1	<1	<1		<1
U-238	----	----	----		----	----	----	----		----
Pu-238	16	21	----		----	14	18	----		----
Pu-239	1028	1329	----		----	783	1117	----		----
Pu-240	397	464	----		----	403	471	----		----
Pu-241	161	203	----		----	130	173	----		----
Pu-242	55	62	----		----	60	66	----		----
Fission Products	394	291	7		21	776	568	26		46
Fissile	1461	1702	135		339	1388	1444	256		499
Fertile	8951	8377	17715		53081	8631	8187	17576		52898
Total HM	10860	10431	17857		53441	10855	10264	17858		53443

Table C.11

Regional Neutron Balances

10^{18} Reactions/Sec

Transmuter Design

Reaction Rate	Beginning				End			
	CZ1	CZ2	AB	RB	CZ1	CZ2	AB	RB
Th-232 Capture	43.83	25.40	18.35	24.00	41.24	24.19	18.38	24.41
Fission	1.437	.9326	.2324	.3048	1.351	.8786	.2531	.3336
Pa-233 Capture	.5775	.2124	.1471	.1075	.8054	.2996	.1438	.1083
Fission	.0436	.0186	.0034	.0028	.0609	.0259	.0037	.0031
U-232 Capture	----	----	----					
Fission								
U-233 Capture	.9242	.376	.1500	.2386	1.634	.6880	.3058	.3558
Fission	10.09	4.177	1.467	2.353	17.83	7.631	3.013	3.531
U-234 Capture	.1005	.0256	.0062	.0080	.2176	.0573	.0175	.0153
Fission	.0640	.0184	.0018	.0026	.1386	.0408	.0054	.0053
U-235 Capture	.0040	.0059	.0001	.0001	.0116	.0021	.0004	.0003
Fission	.0145	.0026	.0002	.0004	.0420	.0079	.0013	.0010
U-236 Capture	.0001				.0006	.0001		
Fission					.0001			
U-238 Capture	----	----						
Fission								
Pu-238 Capture	.0915	.0703			.7402	.0607		
Fission	.3002	.2506			.2434	.2148		
Pu-239 Capture	7.032	5.514			5.230	4.515		
Fission	28.90	24.01			21.55	19.57		
Pu-240 Capture	2.842	2.044			2.822	2.032		
Fission	2.524	2.034			2.509	2.000		
Pu-241 Capture	1.047	.8128			.8254	.6754		
Fission	6.017	4.791			4.740	3.971		
Pu-242 Capture	.2640	.1835			.2831	.1920		
Fission	.2695	.2126			.2893	.2200		
Fuel Fissions								
Fissile	45.06	32.99	1.471	2.356	44.22	31.21	3.018	3.536
Fertile	4.324	3.235	.2342	.3074	4.242	3.135	.2585	.3389
Total Fuel	49.65	36.44	1.705	2.663	48.75	34.56	3.227	3.874
Fuel Capture								
Fissile	9.586	6.921	.2972	.3462	8.506	6.181	.4500	.4644
Fertile	46.86	27.54	18.35	24.01	45.02	26.34	18.40	24.43
Total Fuel	56.71	34.64	18.65	24.36	53.82	32.71	18.85	24.89
Structure Capture	5.734	3.334	2.185	1.158	5.616	3.257	2.200	1.179
Na Capture	.5342	.2824	.2141	.0878	.5227	.2760	.2128	.0885
B10 Capture			8.166				8.425	
Leakage	28.67	30.70			26.69	27.53		
Source	141.3	105.4	4.225	6.621	135.4	98.34	8.169	9.659

Figure C.18

TRANSMUTER DESIGN

TOTAL FLUX RADIAL DISTRIBUTION AT MIDPLANE

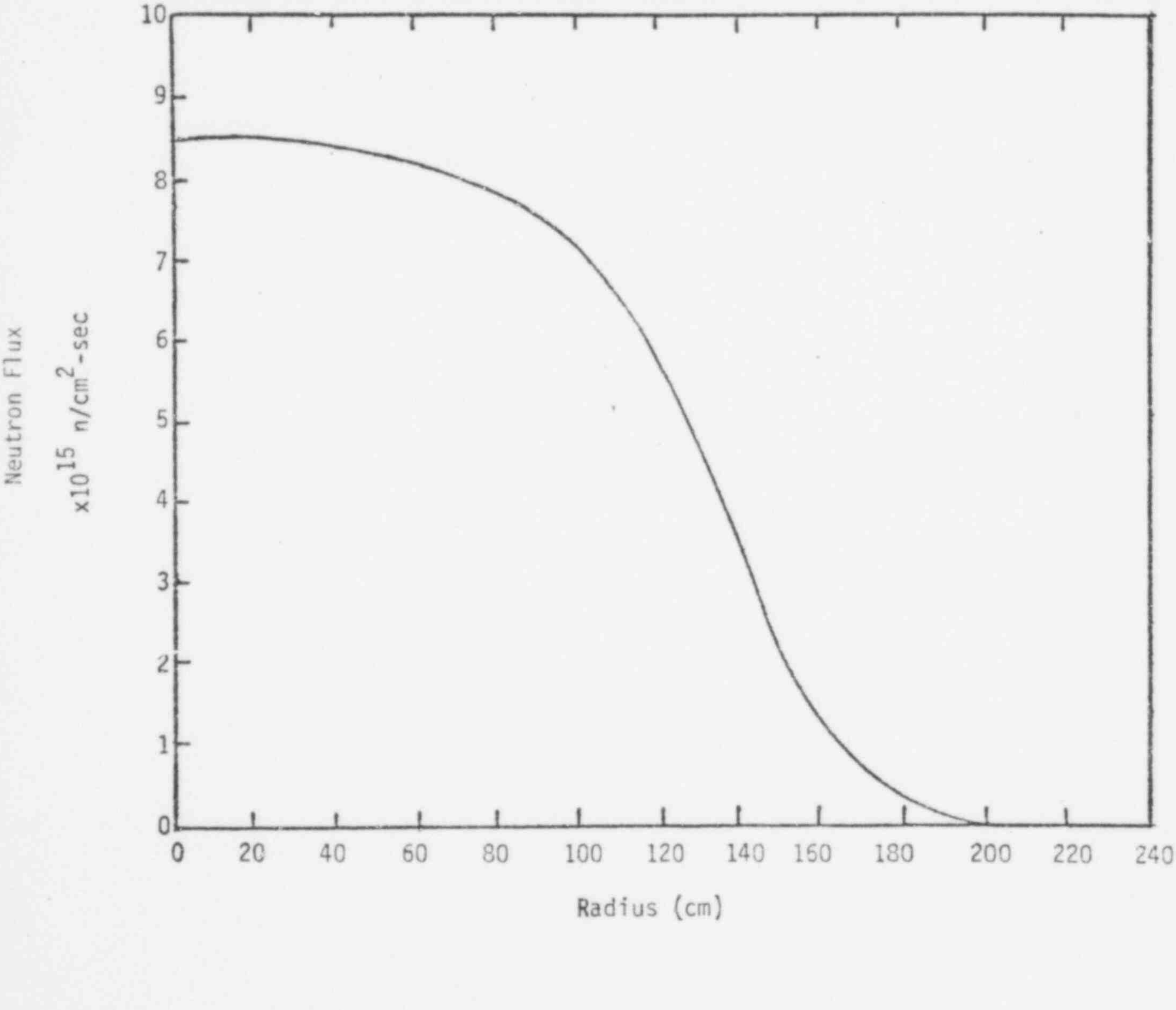

909 165

Figure C.19

TRANSMUTER DESIGN

TOTAL FLUX AXIAL DISTRIBUTION AT POSITION OF PEAK RADIAL FLUX

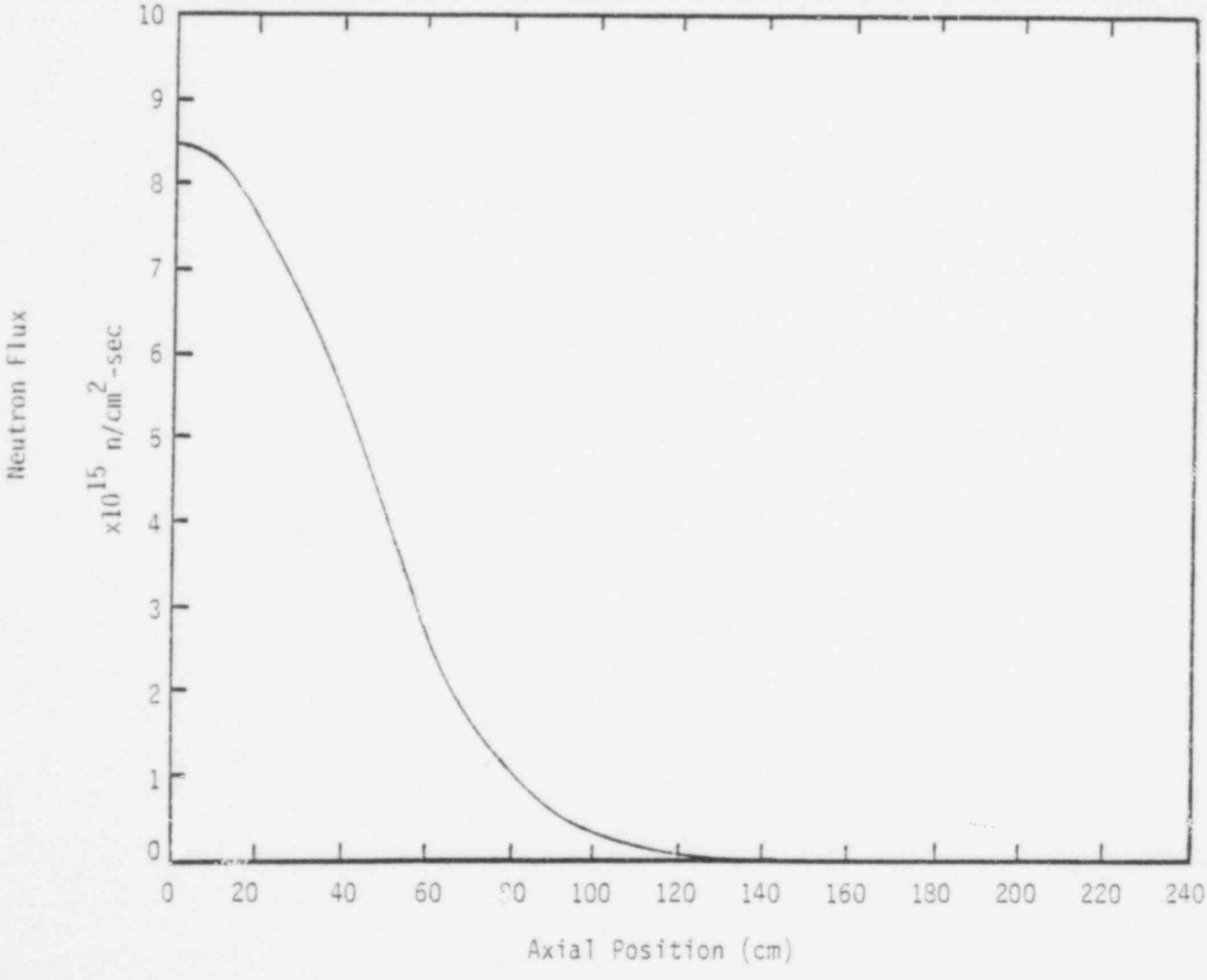

Figure C.20

TRANSMUTER DESIGN

RADIAL POWER DISTRIBUTION AT MIDPLANE

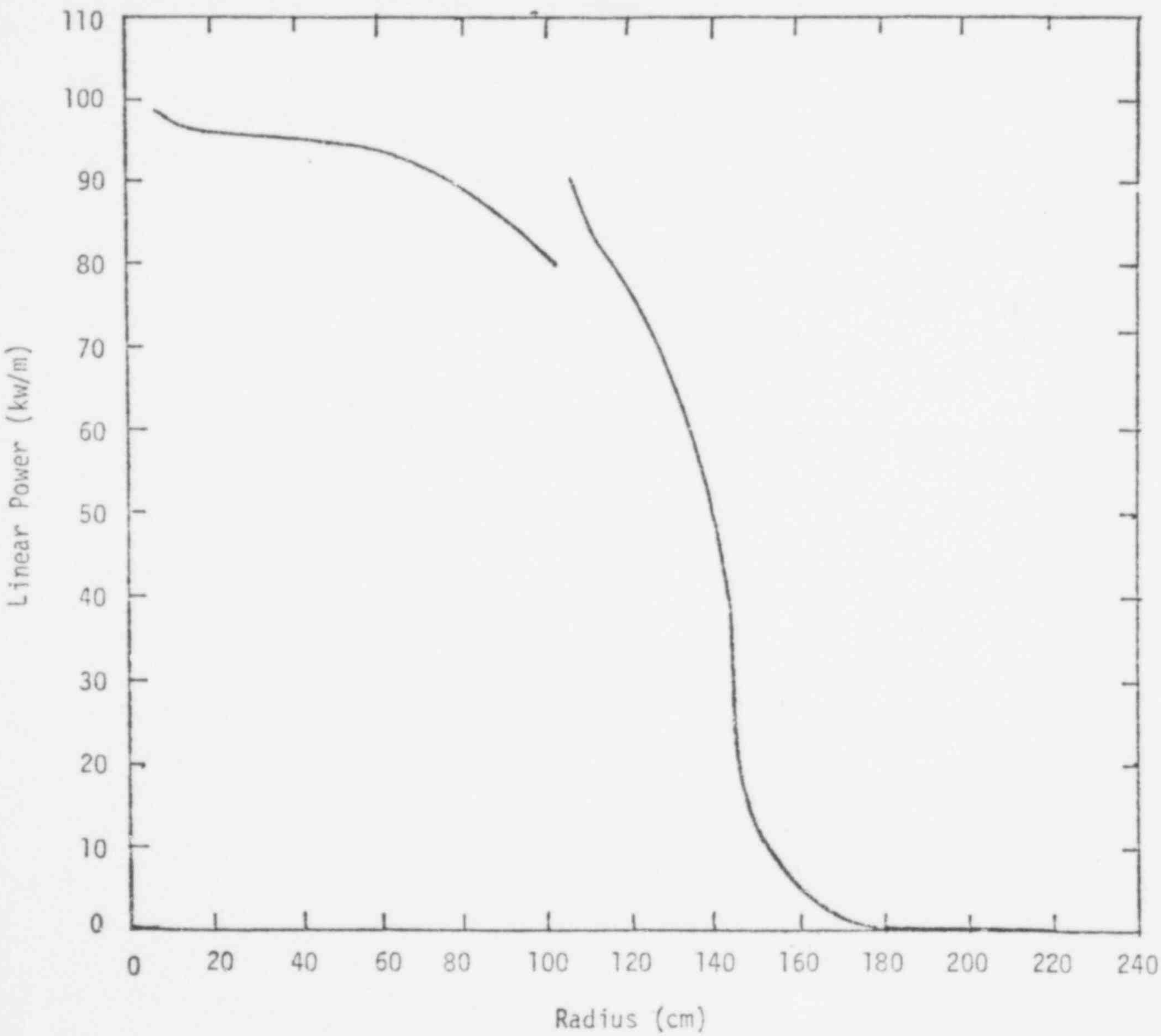

Table C.12
REFERENCE CORES
BATCH INVENTORY (kg)

	CHARGE					DISCHARGE				
Isotope	CZ1	CZ2	AB	IB	RB	CZ1	CZ2	AB	IB	RB
Th-232	----	----	----		----	----	----	----		----
Pa-233	----	----	----		----	----	----	----		----
U-232	----	----	----		----	----	----	----		----
U-233	----	----	----		----	----	----	----		----
U-234	----	----	----		----	----	----	----		----
U-235	8	7	15		27	3	4	13		24
U-236	----	----	----		----	1	< 1	----		----
U-238	3894	3589	7416		13757	3490	3347	7274		13579
Pu-238	5	6	----		----	3	4	----		----
Pu-239	359	423	----		----	408	420	122		150
Pu-240	103	121	----		----	132	139	4		5
Pu-241	54	64	----		----	31	41	< 1		< 1
Pu-242	13	15	----		----	18	18	----		----
Fission Products	----	----	----		----	345	246	20		26
Fissile	421	494	15		27	442	465	135		174
Fertile	4002	3716	7416		13757	3625	3490	7278		13584
Total HM*	4436	4225	7431		13784	4431	4219	7433		13784

* [redacted]rti[redacted] Fi[redacted]e + [redacted]sio[redacted]du[redacted]+ U[redacted] +P[redacted]2

Table C.13
COPROCESSING LOW VOID CORE

BATCH INVENTORY (kg)

	CHARGE					DISCHARGE				
Isotope	CZ1	CZ2	AB	IB	RB	CZ1	CZ2	AB	IB	RB
Th-232	4510	----	12435		12163	4174	----	12259		12043
Pa-233	----	----	----		3	4	----	1		4
U-232	----	----	----		----	----	----	----		----
U-233	470	----	----		14	476	----	157		122
U-234	132	----	----		----	135	----	2		1
U-235	19	----	----		----	24	----	----		----
U-236	4	----	----		----	6	----	----		----
U-238	2249	5984	----		----	2091	5675	----		----
Pu-238	----	[illegible]	----		----	----	----	----		----
Pu-239	239	6[illegible]	----		----	244	650	----		----
Pu-240	93	[illegible]	----		----	98	258	----		----
Pu-241	18	48	----		----	16	41	----		----
Pu-242	7	19	----		----	8	21	----		----
Fission Products	----	----	----		<1	470	283	16		10
Fissile	746	684	----		17	756	691	158		126
Fertile	6984	6232	12435		12163	6498	5933	12261		12044
Total HM	7741	6935	12435		12181	7738	6928	12435		12180

609 169

Table C.14

COPROCESSING LOW COST CORE

BATCH INVENTORY (kg)

	CHARGE					DISCHARGE				
Isotope	CZ1	CZ2	AB	IB	RB	CZ1	CZ2	AB	IB	RB
Th-232	----	----	7739		9730	----	----	7545		9608
Pa-233	----	----	----		3	----	----	----		2
U-232	----	----	----		----	----	----	----		----
U-233	----	----	----		25	----	----	177		137
U-234	----	----	----		<1	----	---	3		2
U-235	----	----	----		----	----	----	----		----
U-236	----	----	----		----	----	----	----		----
U-238	1705	6885	----		----	1466	6275	----		----
Pu-238	----	----	----		----	----	----	----		----
Pu-239	163	739	----		----	188	770	----		----
Pu-240	63	288	----		----	75	313	----		----
Pu-241	12	56	----		----	11	48	----		----
Pu-242	5	22	----		----	6	26	----		----
Fission Products	----	----	----		<1	200	549	16		11
Fissile	175	795	----		28	199	818	177		139
Fertile	1768	7173	7739		9730	1541	6588	7548		9609
Total HM	1948	7990	7739		9758	1946	7981	7741		9759

Table C.15

DENATURED CORE

BATCH INVENTORY (kg)

	CHARGE					DISCHARGE				
Isotope	CZ1	CZ2	AB	IB	RB	CZ1	CZ2	AB	IB	RB
Th-232	----	----	5715		10304	----	----	5600		10148
Pa-233	----	----	----		----	----	----	----		----
U-232	----	----	----		----	----	----	----		----
U-233	354	520	----		----	125	266	99		137
U-234	99	146	----		----	90	139	2		2
U-235	14	21	----		----	19	26	<1		<1
U-236	3	5	----		----	6	8	<1		<1
U-238	3337	3876	----		----	2997	3617	----		----
Pu-238	----	----	----		----	----	----	----		----
Pu-239	----	----	----		----	205	173	----		----
Pu-240	----	----	----		----	18	10	----		----
Pu-241	----	----	----		----	<1	<1	----		----
Pu-242	----	----	----		----	<1	<1	----		----
Fission Products	----	----	----		----	346	327	14		18
Fissile	368	541	----		----	349	465	99		137
Fertile	3436	4022	5715		10304	3105	3766	5602		10150
Total HM	3807	4568	5715		10304	3806	4566	5715		10305

Table C.16

TRANSMUTER CORE

BATCH INVENTORY (kg)

	CHARGE					DISCHARGE				
Isotope	CZ1	CZ2	AB	IB	RB	CZ1	CZ2	AB	IB	RB
Th-232	2962	2698	5952		10688	2625	2500	5811		10502
Pa-233	----	----	----		----	16	10	<1		1
U-232	----	----	----		----	----	----	----		----
U-233	----	----	----		----	187	129	121		159
U-234	----	----	----		----	14	6	2		4
U-235	----	----	----		----	<1	<1	<1		<1
U-236	----	----	----		----	<1	<1	<1		<1
U-238	----	----	----		----	----	----	----		----
Pu-238	6	8	----		----	4	5	----		----
Pu-239	443	524	----		----	198	312	----		----
Pu-240	127	150	----		----	133	157	----		----
Pu-241	67	80	----		----	36	50	----		----
Pu-242	16	19	----		----	21	23	----		----
Fission Products	----	----	----		----	382	277	19		25
Fissile	510	604	----		----	437	501	121		160
Fertile	3095	2855	5952		10688	2776	2666	5813		10506
Total HM	3621	3479	5952		10688	3616	3469	5953		10691